



EUROPEAN
COMMISSION

Community Research



DOPAS

(Contract Number: FP7 - 323273)

Deliverable n°5.11

Status report on ELSA/LASA related laboratory tests (D3.28) and on process modelling activities (D5.5)

Author: *Oliver Czaikowski*

Date of issue of this report: **23.9.2014**

Start date of project: 01/09/2012

Duration: 48 Months

Project co-funded by the European Commission under the Euratom Research and Training Programme on Nuclear Energy within the Seventh Framework Programme

Dissemination Level

PU	Public	
PP	Restricted to other programme participants (including the Commission Services)	x
RE	Restricted to a group specified by the partners of the DOPAS project	
CO	Confidential, only for partners of the DOPAS project	

DOPAS



1/2

Scope	Deliverable n°3.28 (WP3) Deliverable n°5.5 (WP5)	Version:	1.0
Type/No.	Report	Total pages	2+75
		Appendixes	0
Title	D5.11 Status report on ELSA/LASA related laboratory tests and on process modelling activities	Articles:	7

ABSTRACT:

This report presents the work performed by GRS as part of the European project DOPAS under WP3 Task 2 Design and technical construction feasibility of the plugs and seals and WP5 Task 1 Performance assessment of plugs and seals systems. This report is one of three status reports, which combines information from both Work package 3 and Work Package 5 into a new Deliverable D5.11. LASA project stands for long-term stable shaft seal in salt formations.

RESPONSIBLE:

GRS, Oliver Czaikowski

REVIEW/OTHER COMMENTS:

The report has been internally approved by GRS in September 2014. The DOPAS coordinator has reviewed the memorandum and approved for submission.

D5.11 publicity is PP and the report will be available during the project duration on request. This report will be available at the DOPAS web site after the DOPAS project has ended.

APPROVED FOR SUBMISSION:

Johanna Hansen

Full scale demonstration of plugs and seals (DOPAS) Deliverable D3.28 & D5.5

Status report on LASA related
laboratory tests and on process
modelling activities

Oliver Czaikowski
Lothar Hartwig
Uwe Hertes
Kyra Jantschik
Rüdiger Miehe
Jürgen Müller
Peter Schwarzianeck

February 2015

Remark:

The research leading to these results has received funding from the European Union's European Atomic Energy Community's (Euratom) Seventh Framework Programme FP7/2007-2013 under Grant agreement no 323273, the DOPAS project and under contract no. 02E11132 from the German Federal Ministry of Economics and Energy (BMWi).

The work was conducted by the Gesellschaft für Anlagen- und Reaktorsicherheit (GRS) mbH.

The authors are responsible for the content of this report.

Table of contents

1	Introduction.....	7
2	Testing material	9
3	Laboratory experiments	11
3.1	Material stability	11
3.1.1	Experimental layout	11
3.1.2	Testing procedure.....	13
3.1.3	Measurement results and interpretation	17
3.2	Long-term deformation behaviour	19
3.2.1	Experimental layout	19
3.2.2	Testing procedure.....	20
3.2.3	Measurement results and interpretation	22
4	Modelling work.....	26
4.1	Physical Modelling	26
4.2	Numerical simulation	29
4.2.1	Simulation of the triaxial compression test	29
4.2.2	Simulation of the uniaxial creep test.....	44
5	Preliminary conclusions and outlook	75
6	Acknowledgements	76
7	References	77

1 Introduction

This report presents the work performed by GRS as part of the European project DOPAS (Full scale Demonstration of Plugs and Seals) under WP 3 task 2 and WP 5 task 1 on “Design and technical construction feasibility of the plugs and seals” and “Performance assessment of plugs and seals systems”. The work is related to the research and development on plugging and sealing for repositories in salt rock and is of fundamental importance for the salt option which represents one of the three European repository options in addition to the clay rock and the crystalline rock options.

In the German concept for the final disposal of radioactive and hazardous wastes in salt formations cements and cement based systems are proposed as technical barriers (shaft and drift seals). Due to the specific boundary conditions in salt host rock formations these materials (salt and sored concretes) contain crushed salt instead of sand or gravel. The programme aims at providing experimental data needed for the theoretical analysis of the long-term sealing capacity of these sealing materials.

In order to demonstrate hydro-mechanical material stability under representative load scenarios, the long-term deformation material behaviour as well as the sealing capacity of the seal, a comprehensive laboratory testing programme is carried out.

One of the most challenging aspects is the determination of the pre-experimental status of the core material that was provided for laboratory investigations, since the salt concrete was taken from an existing dam that has been loaded in situ by the creeping rock salt for more than 10 years. Therefore, it is obvious that material properties, such as e.g. the initial gas permeability, have to be measured under a load comparable to the in situ minimum stress.

Main work and results achieved in the DOPAS tasks 3.2 and 5.1 during the first 24 months of the project will be presented in this status report as deliverables D3.28 and D5.5. Chapter 2 gives an short overview on the core material that was provided for laboratory investigations. The status of the laboratory experiments performed in task 3.2 on the salt concrete samples is illustrated in chapter 3. The modelling work conducted in task 5.1 is reported in chapter 4. Preliminary conclusions and outlook on the further work programme are summarized in chapter 5.

Remark:

The report at hand is an interim version issued after 24 months of the DOPAS project.
The report will be superseded by a final report to be issued in February 2016.

2 Testing material

Salt concrete is a mass concrete that is used for the construction of dam structures or for backfilling of drifts in rock salt. Backfilling of excavations and construction of dam structures aims to receive the integrity of the geological barrier, to stabilize the disturbed rock zone at the contour and to limit and decelerate inflow of brine.

There are different mixtures of salt concrete, as the salt concrete M1 and M2, used in ERAM (Morsleben repository) or the type “ASSE”, which was used in the ASSE mine. In the context of this work the numerical simulations are conducted on the basis of laboratory tests on specimen from salt concrete type “ASSE”.

The composition of salt concrete consists of a matrix from cement with inclusion of crushed salt. The proportion is defined in Tab. 2.1.

Table 2.1: Composition of salt concrete type „ASSE“ related to 1 m³ [Mül10]

Component of salt concrete	Proportion in [kg/m ³]	Proportion in mass-%
Blast furnace cement	380	18.3
Crushed salt	1.496	72.1
NaCl-brine	198	9.5
Total	2.074	100.0

The specimens for the uniaxial and triaxial tests were extracted from the in situ construction “ASSE-Vordamm”. The drift sealing element was constructed at the 945 m level from November 1991 to January 1992 [Sta94]. Its dimensions are 8.0 m length, 5.5 m width and 3.4 m in height. The “ASSE-Vordamm” constitutes only a part of the whole dam structure, which was constructed in the ASSE as shown in Fig. 2.1.

The sealing element is composed of three devices: the salt concrete itself, the contact zone between concrete and host rock and the excavation damaged zone (EDZ). The specimens used by GRS for the laboratory tests were extracted from boreholes B4 and B5. (Compare to Fig. 2.2).

At this time the salt concrete was exposed to the convergence of the rock salt for about ten years.

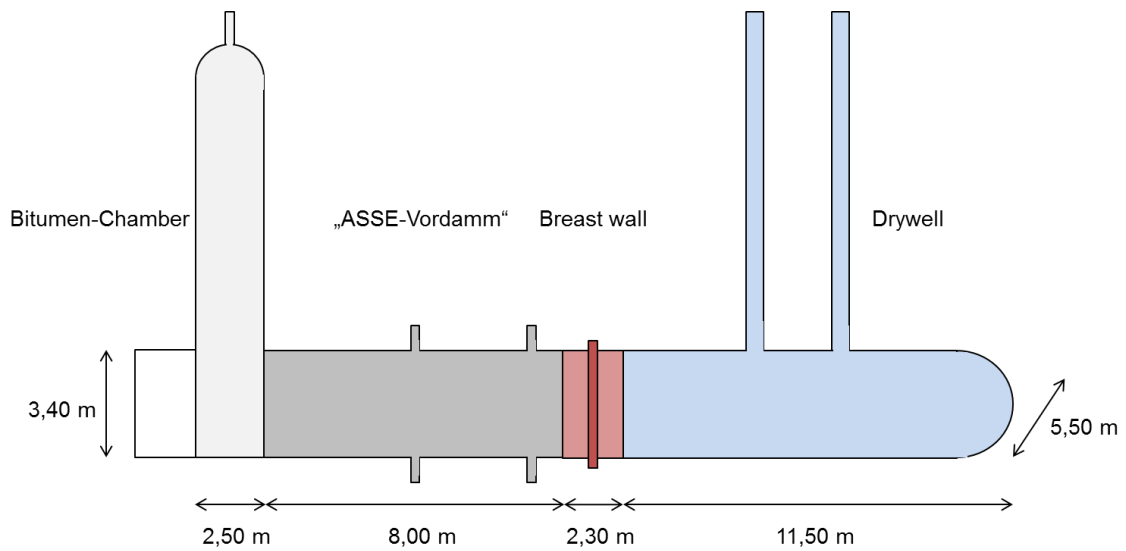


Fig. 2.1 Simplified illustration of the whole dam structure

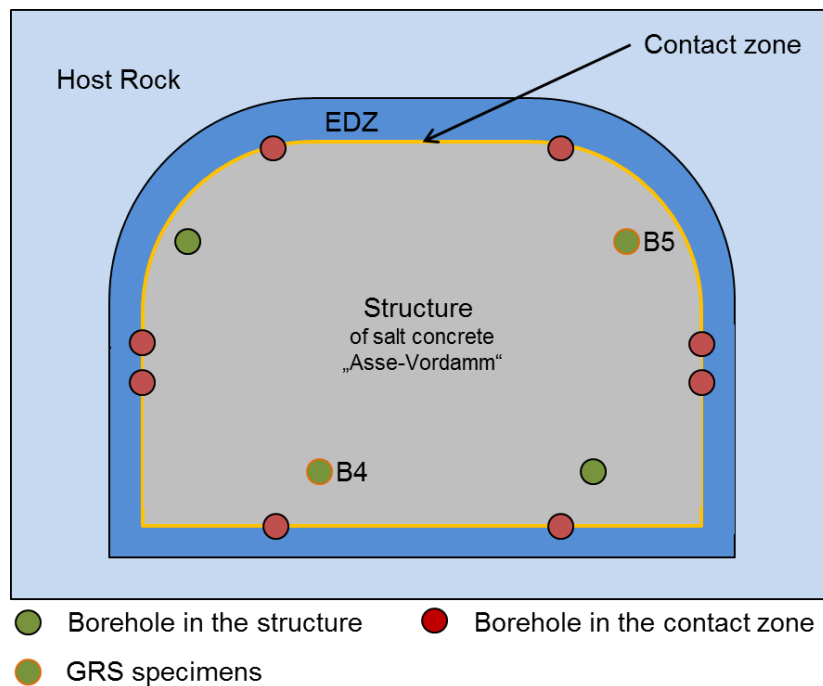


Fig. 2.2 Definition of the three devices of a sealing element and identification of the boreholes

3 Laboratory experiments

3.1 Material stability

3.1.1 Experimental layout

Damage tests were carried out on 3 salt concrete samples in a triaxial apparatus with measurement of deformation and gas permeability under various stress conditions. From the pictures in Fig. 3.1 one can clearly recognize the open voids marked in red and filled with resin during the sample preparation procedure.

The average porosity of the samples is about $\phi = 6\%$ with a grain density $2.17 - 2.2 \text{ g/cm}^3$. The average water content is at a level of $w = 2$ weight-%.

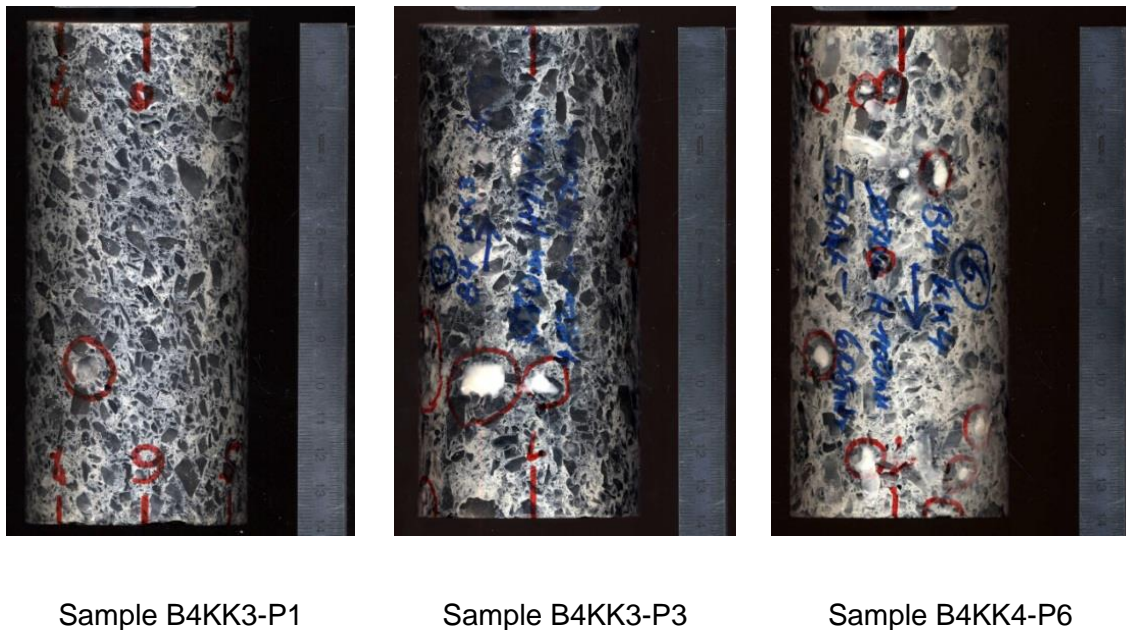


Fig. 3.1 Salt concrete samples before testing

Figure 3.2 illustrates schematically the assembly of a sample in a triaxial cell. The sample was isolated in a jacket and porous discs at top and bottom. The annular gap between sample and jacket was sealed with silicon to avoid leakage. To reduce friction

resistance between the sample and the load pistons, a thin sand layer of ~ 1 mm was put between the porous disc and the end face, or thin silicon strips with 0.2 mm thickness and ~ 5 mm width were laid between the piston and the end face.

The samples were loaded in two phases of isostatic pre-compaction and deviatoric loading. The aim of the isostatic pre-compaction was to approach the intact state of the samples with respect to permeability. But it has to be pointed out that no effective healing has to be expected during the pre-compaction phase. This was performed by simultaneously increasing axial and radial stress to $\sigma_a = \sigma_r = 5$ MPa at a loading rate of 1 MPa/min, then keeping stress constant for hours. Then the axial and radial stresses were increased twice up to a level of 20 MPa and unloading to a low stress of $\sigma_a = \sigma_r = 1 - 3$ MPa. The subsequent deviatoric loading to damage of the samples was carried out by increasing axial deformation ε_a at radial stress of $\sigma_r = 1 - 3$ MPa. A low strain rate of $\dot{\varepsilon}_a = 1 \cdot 10^{-7} \text{ s}^{-1}$ was applied.

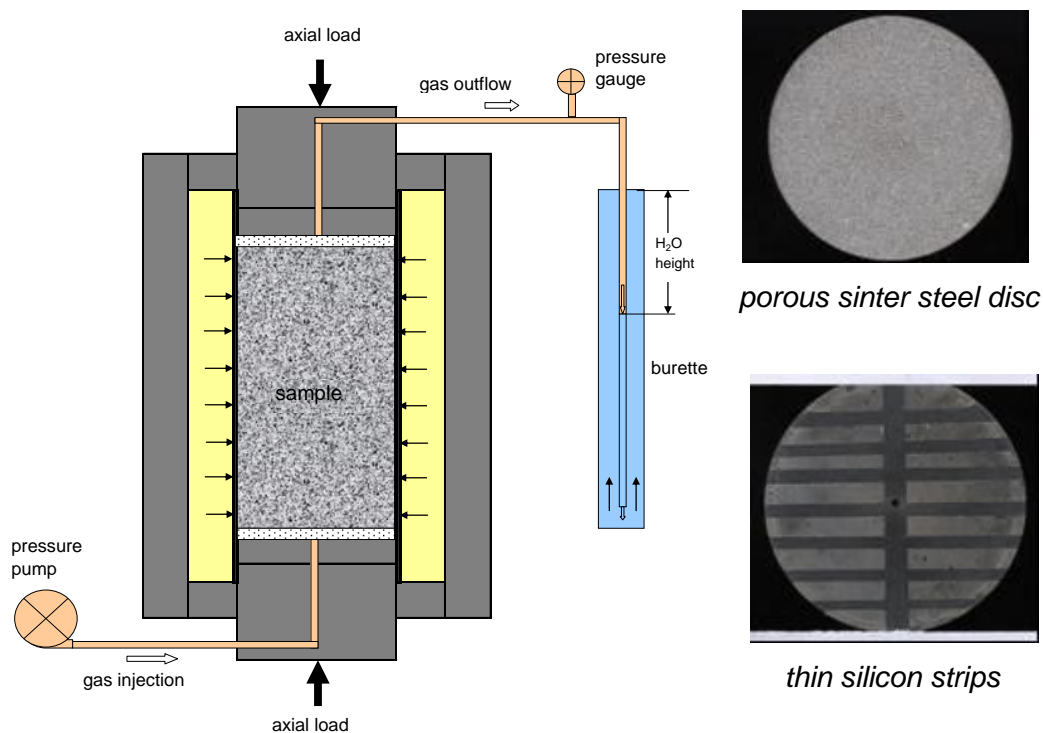


Fig. 3.2 Principle of triaxial compression tests with permeability measurement

During the tests, axial strain was measured by a LVDT-transducer installed outside of the cell, while volumetric strain was determined both directly from the volume change of the confining oil in the cell by using a pressure/volume GDS-controller and indirectly by strain gauges attached on the sample surface at the middle of the length. Permea-

bility changes induced by the mechanical loading were measured along the sample axis by injecting dry nitrogen gas to the bottom at constant pressure and recording the outflow at the opposite side. The gas outflow was continuously recorded by using a burette. During steady state gas flow, the permeability is determined according to Darcy's law for compressive media:

$$k = \frac{2 \cdot Q \cdot \mu \cdot L \cdot p_o}{A \cdot (p_g^2 - p_o^2)} \quad (3.1)$$

where k is the intrinsic permeability (m^2), Q is the flow rate of the gas (m^3/s), μ is the gas dynamic viscosity ($\text{Pa}\cdot\text{s}$), L is the length of the sample (m), A is the section of the sample (m^2), p_o is the atmospheric pressure (Pa), p_g is the gas injection pressure (Pa). This measuring system allows a precise determination of low permeability down to $\sim 10^{-21} \text{ m}^2$.

3.1.2 Testing procedure

PRE-Compaction

Triaxial compressions tests (TC-Test) were performed in order to investigate the mechanical stability of salt concrete. Onset of dilatancy, start of gas flux and failure of the specimens were determined under different radial stresses. The results of the TC-Tests aim at a better understanding of the difference in deformation behaviour of salt concrete with respect to uniaxial creep testing.

The tests were performed on three specimens under stress control in the GRS laboratory. The specimens for the triaxial compaction tests had a diameter of 70 mm and a length of 140 mm before testing and had been obtained by core-drilling from a real plug installed in a salt mine.

In the first step, the specimens were compacted for about 22 hours at an isotropic stress level of 5 MPa. Then, the axial and radial stresses were increased twice up to a level of 20 MPa. After 24 hours, the compaction phase ended. The idea of this compaction phase is to reach the state of compaction that the specimens had before extraction from the drift sealing element, see Fig. 3.3, Fig. 3.4 and Fig. 3.5.

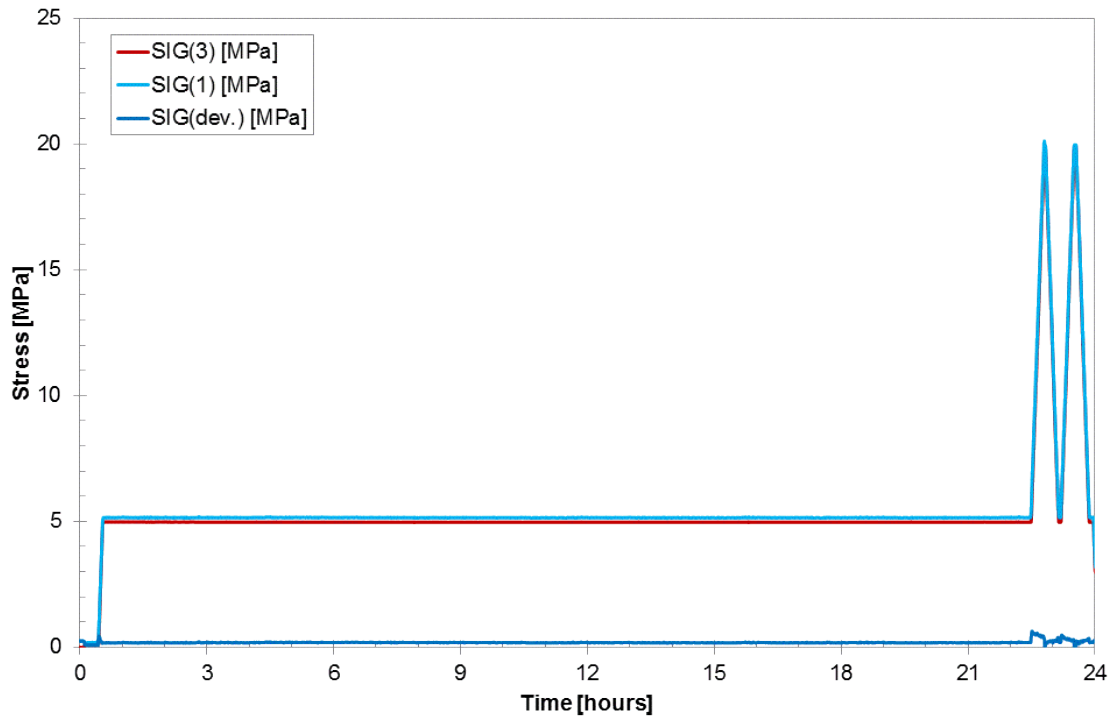


Fig. 3.3 Stress evolution of a salt concrete sample under isostatic compaction

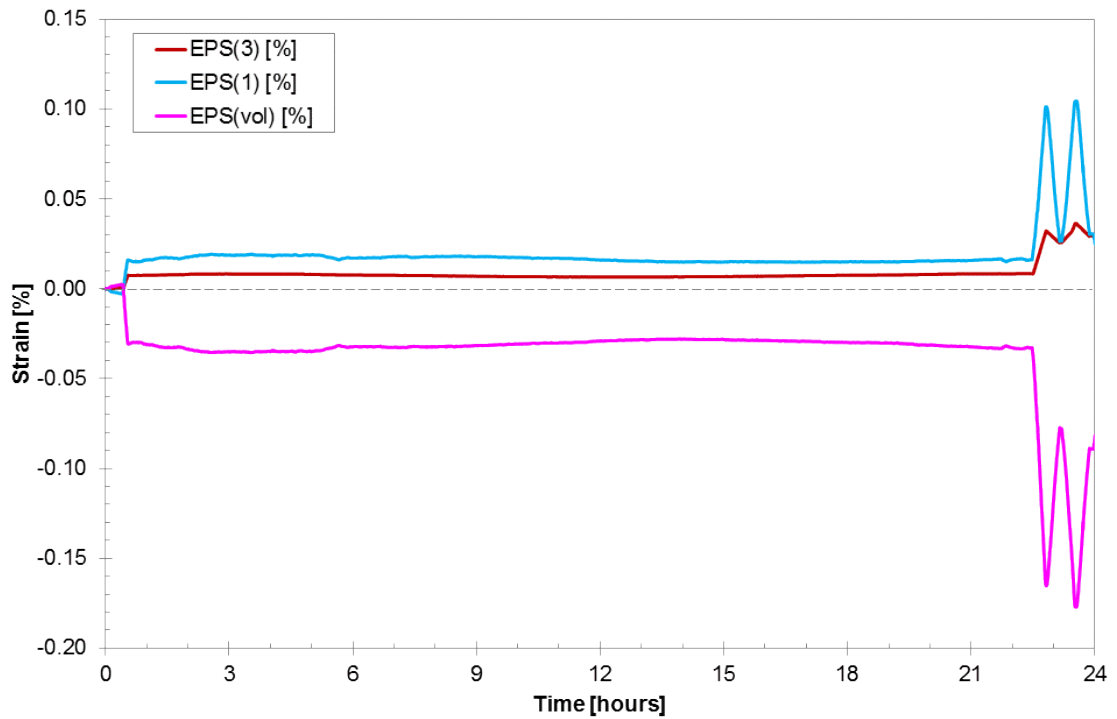


Fig. 3.4 Strain evolution of a salt concrete sample under isostatic compaction

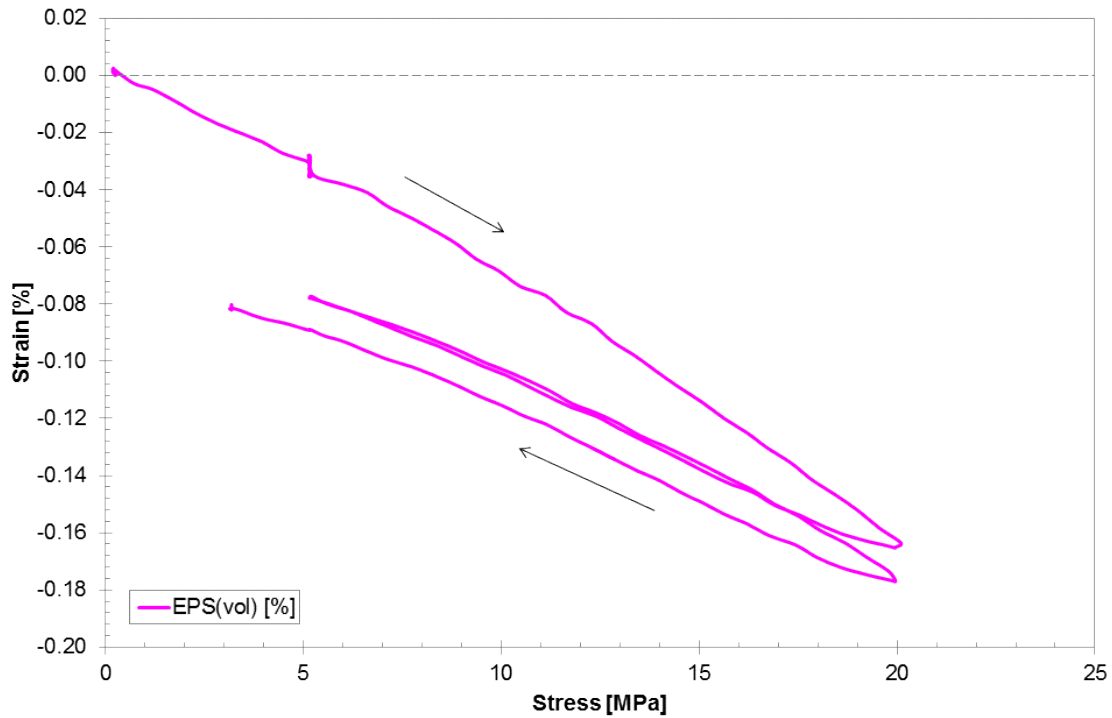


Fig. 3.5 Isostatic pre-compaction behaviour of a salt concrete sample

Deviatoric compression

Second step of the test was to deform the specimens under deviatoric stress. For that purpose, three specimens were subjected to three confining stresses of 1, 2 and 3 MPa. The axial stress was increased until the failure load level of the sample was reached. During the tests gas was injected in axial direction for permeability measurement.

The results of the TC-Tests with a confining stress of 3 MPa are presented in Fig. 3.6. In the figure, the deviatoric stress and the volumetric strain are shown versus the axial strain. The deviatoric stress increases up to a stress level of 40 MPa. The failure stress is reached at an axial strain of 2 %. After failure, gas permeability measurements are performed. Axial deformation is kept constant during the measurement. Hence, stresses show relaxation behaviour during the gas permeability measurements. Afterwards, axial stress is increased further. The volumetric strain decreases in the beginning of the test, due to the compaction of the specimen. Volumetric strain starts to increase when axial strain reaches values of about 0.9 %. This point is defined as the onset of dilatancy, which is marked by formation of microcracks leading to volume increase. At this point, the deviatoric stress is about 36 MPa. By ongoing increase of deviatoric stress

the microcracking and the specimen volume increases further. At a certain point of the test the microcracks are connected and a gas flow could be detected.

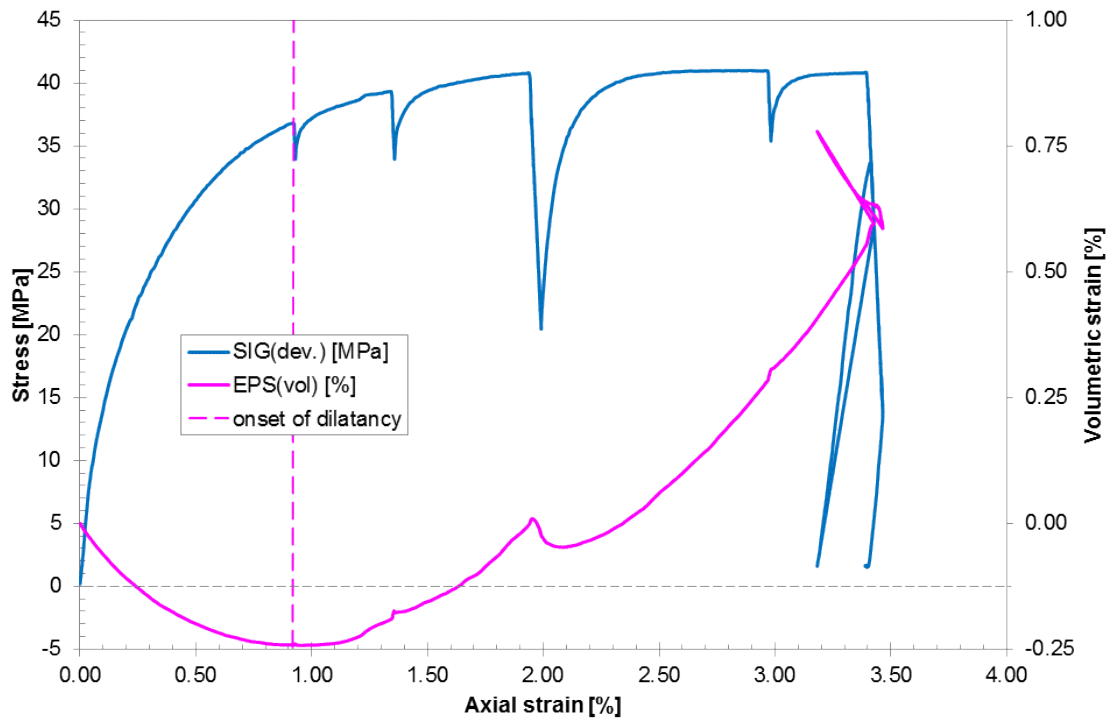


Fig. 3.6 Stress-strain behaviour of a salt concrete sample deformed by deviatoric loading at confining stress of 3 MPa

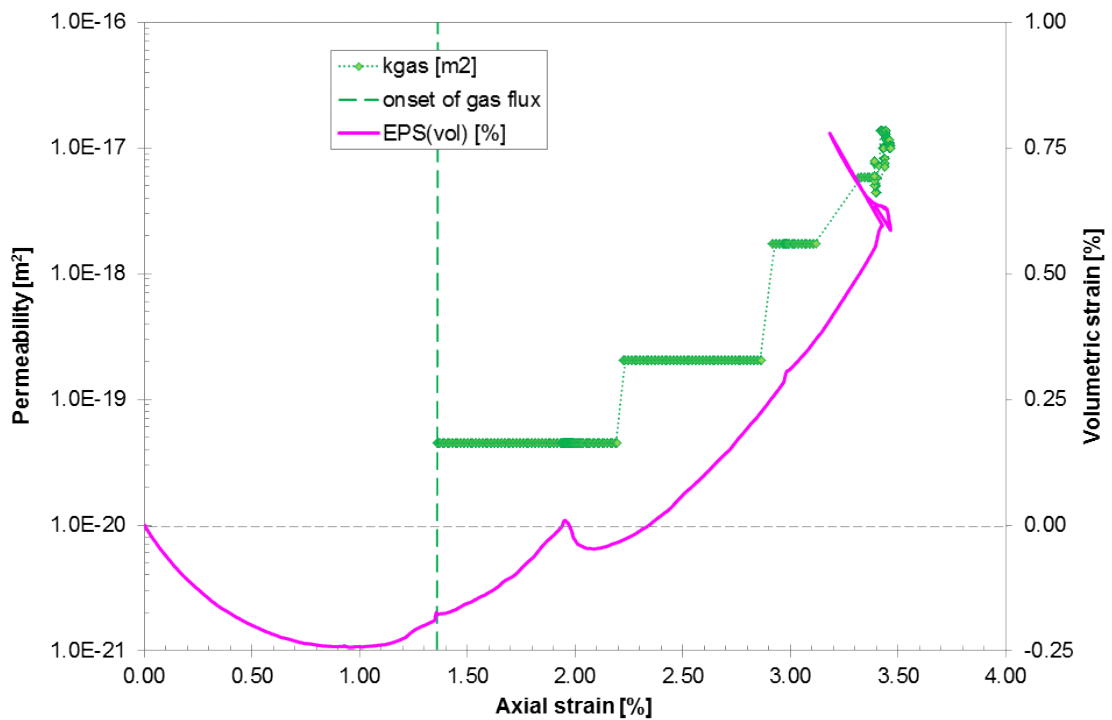


Fig. 3.7 Strain-permeability behaviour of a salt concrete sample deformed by deviatoric loading at confining stress of 3 MPa

3.1.3 Measurement results and interpretation

The results of the triaxial compression tests show that salt concrete exhibits elastic and plastic material behaviour during the compaction phase showing reversible and irreversible deformations. This compaction test phase was identical for all three specimens.

During the deviatoric stress phase (shown for salt concrete in Fig. 3.8), the results of the tests are different due to different confining stresses. It is possible to identify the onset of dilatancy by the evolution of volumetric strains (Fig. 3.9). In all three tests, the onset of gas flux is measured at higher deviatoric stress levels than the onset of dilatancy (Fig. 3.10). The boundary for the failure of the specimen increases with higher confining stress, analogue to the onset of dilatancy. The onset of gas flux and the failure of the specimens occurred nearly at the same deviatoric stress level.

Consequently, the test results show that the investigated salt concrete samples were gas-tight until the load limit was reached. Generally, no damage is expected in the salt concrete specimens below deviatoric stresses of 30 MPa.

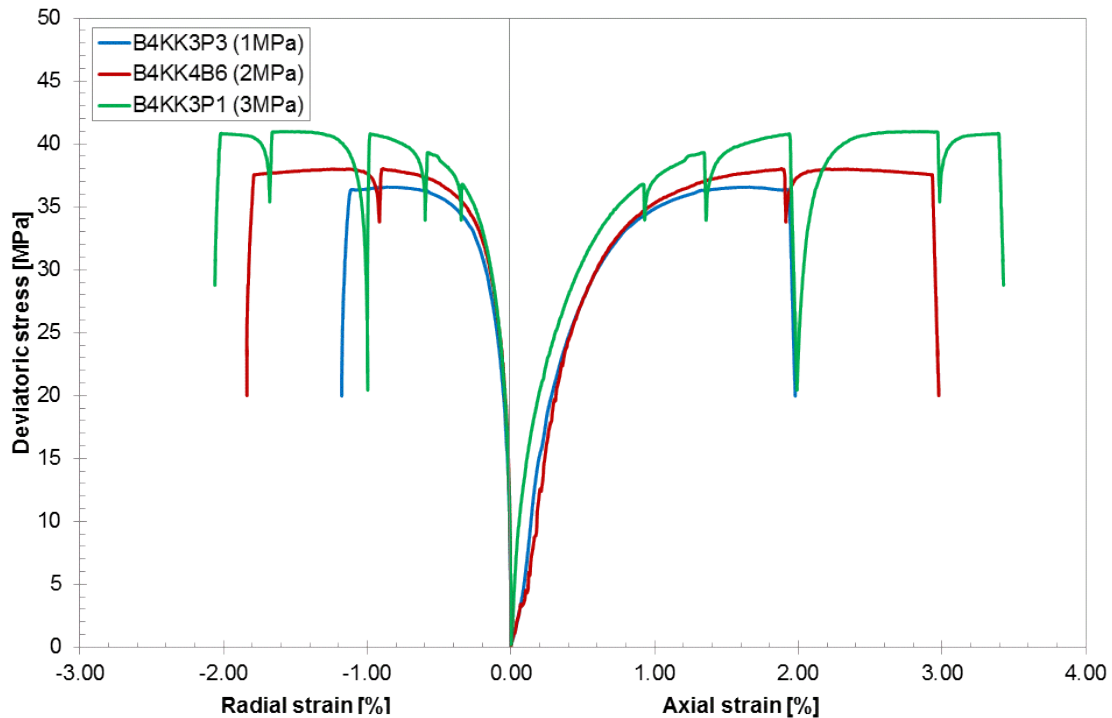


Fig. 3.8 Stress-strain curves obtained on the salt concrete samples at different confining stresses

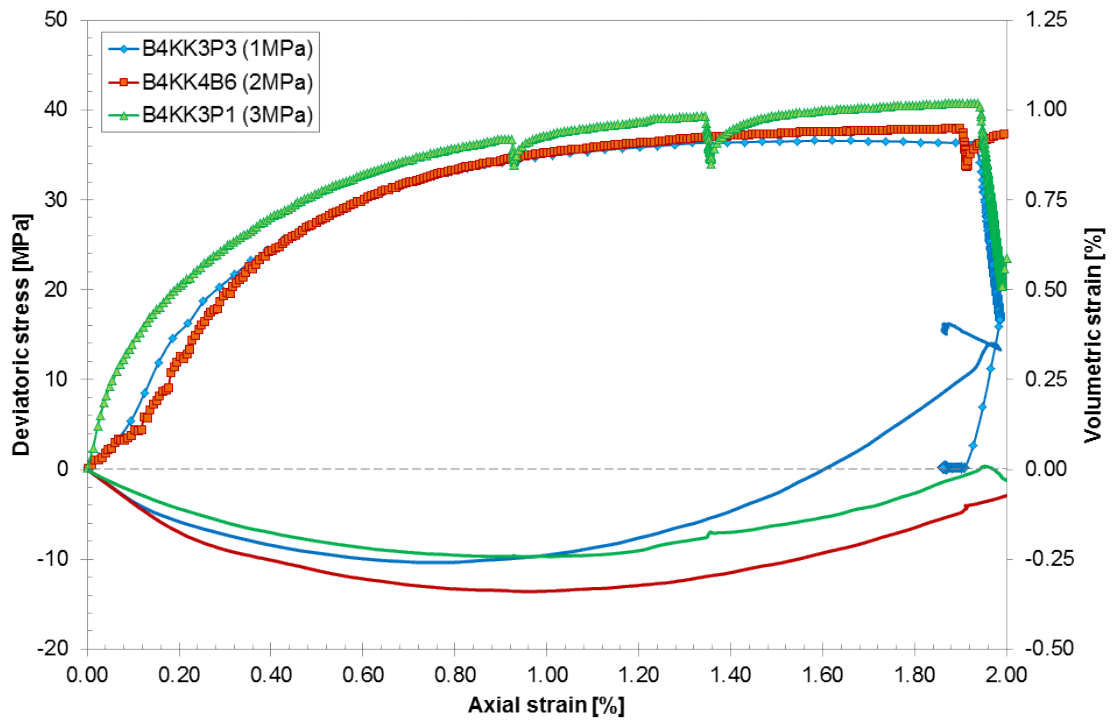


Fig. 3.9 Stress-strain curves obtained on the salt concrete samples at different confining stresses

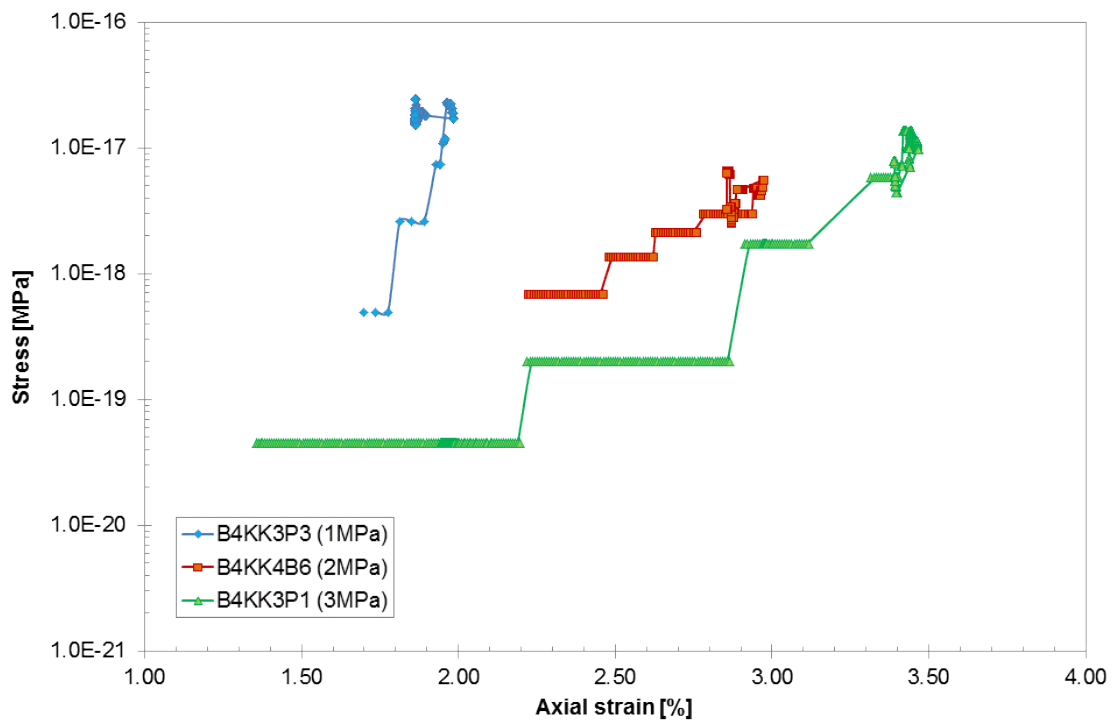


Fig. 3.10 Strain-permeability curves obtained on the salt concrete samples at different confining stresses

3.2 Long-term deformation behaviour

3.2.1 Experimental layout

Uniaxial creep tests were performed in five rigs in air-controlled room. One rig allows five samples being simultaneously tested at the same load up to 500 kN at ambient temperature. Fig. 3.11 shows the rig for uniaxial creep tests on five samples. Axial load was applied equally to the five samples by means of an oil balance with accuracy higher than $\pm 0.5\%$. Axial deformation of each sample was originally measured by displacement transducers (LVDT) with an accuracy of ± 0.1 mm. The strain measurement was then improved by several strain gauges of higher solution of 10^{-6} . They were directly glued on the samples for both axial and radial strain measurements.

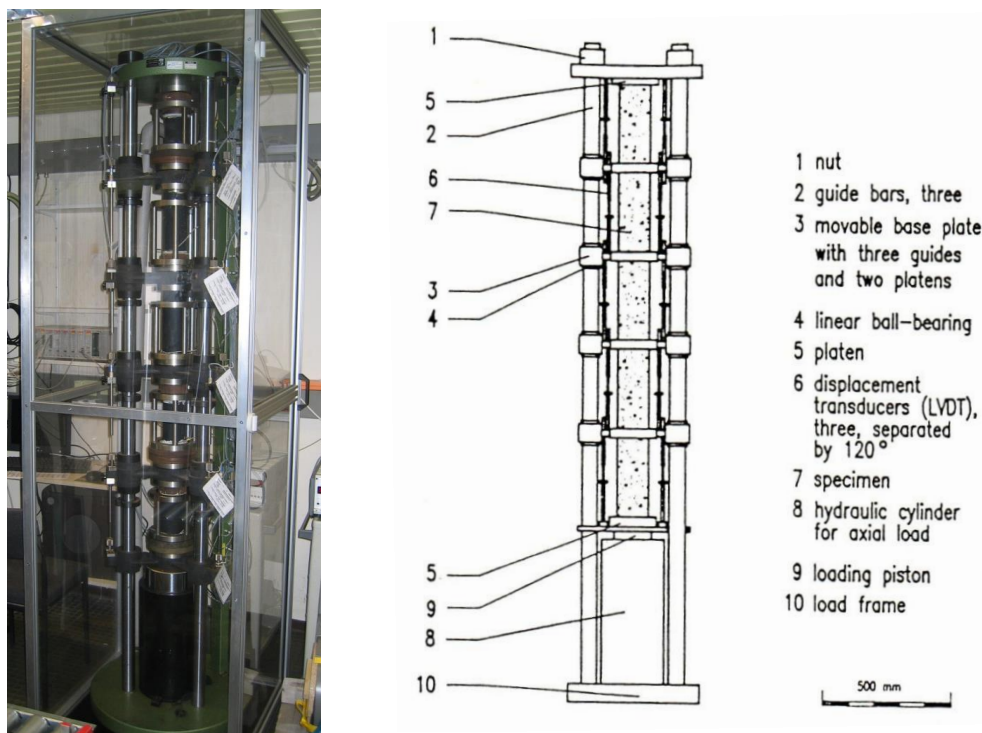


Fig. 3.11 Rig for uniaxial creep tests on five samples one upon another

3.2.2 Testing procedure

Aim of these tests is to determine the deformation of the samples in terms of strains and strain rates in order to describe the time-dependent uniaxial creep behaviour of salt concrete at different stress states.

The uniaxial creep tests (UC-Test) were carried out on five specimens in a uniaxial apparatus at the GRS laboratory. The initial dimension of the specimens was 80 mm in diameter and 160 mm in length. The specimens were tested in one apparatus at the same time, the specimens were arranged above each other. This way all specimens were submitted to nearly identical stress conditions, see Fig. 3.13.

The axial and radial deformations were measured for each specimen. The measurements of the axial deformations were carried out using “Linear Differential Variable Transformers” (LDVT) and strain gauges (DMS), the radial deformations by using strain gauges only.

In the following analysis, only the results for axial deformation measured by LDVT are considered. The reason for this approach is that the LDVT measure the change of the whole length of the specimen while the strain gauges measure only a fraction. Thus, the measurement with the LDVT is more representative for the overall sample behaviour. The denotations SC(1048) up to SC(1052) serve as identification for the individual specimens of the uniaxial tests.

The UCc-Tests were executed at three different stress states. First, the axial stress was set to 5 MPa. The following steps were performed at 10 MPa and 20 MPa, respectively. During the tests the temperature was around 25 °C. The axial stress causes a reduction of the length and an increase in diameter of the specimens.

All tests lasted over nearly 300 days with each step duration of 76 to 106 days. Uniaxial strain-time curves measured on 5 samples are illustrated in Fig. 3.12, whereas the stress and temperature boundary conditions are shown in Fig. 3.13.

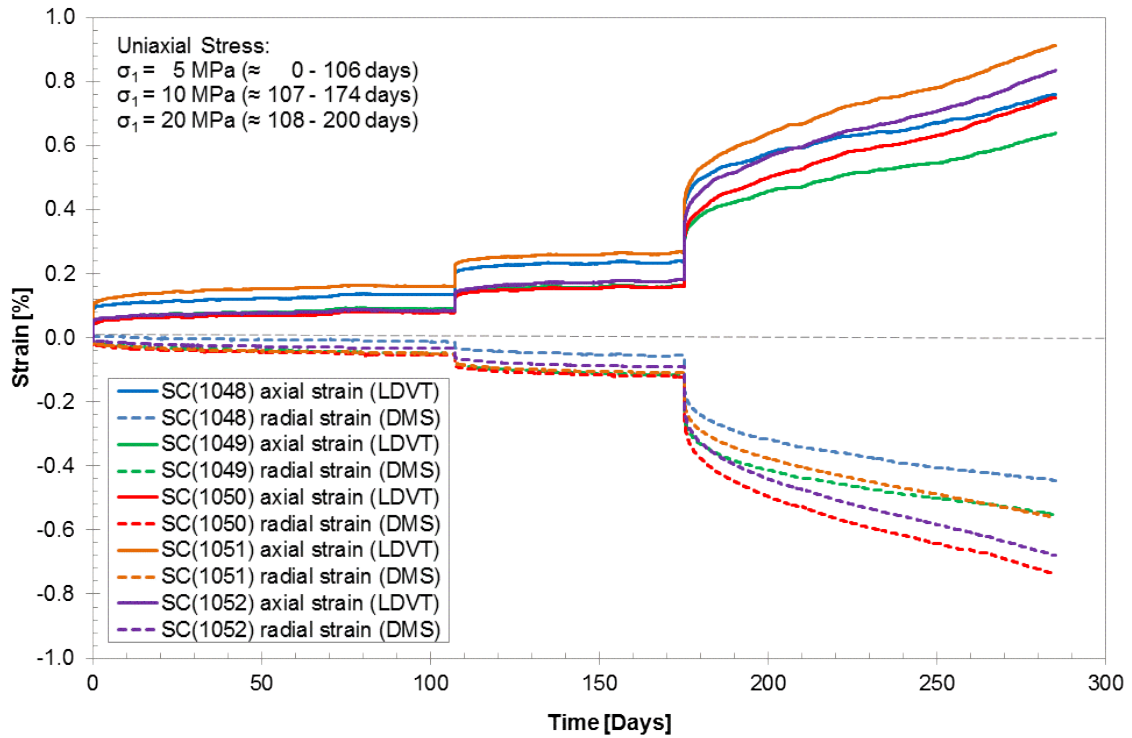


Fig. 3.12 Long-term uniaxial creep behaviour of five salt concrete samples under multi-step loads – axial and radial strains

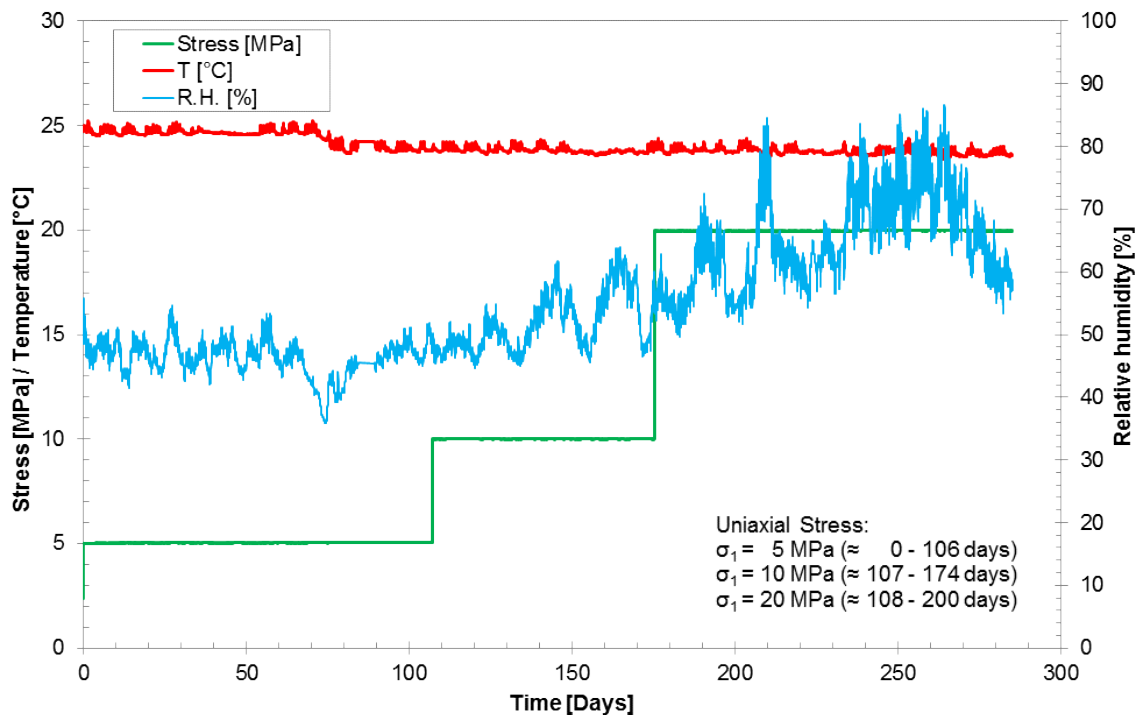


Fig. 3.13 Long-term uniaxial creep behaviour of five salt concrete samples under multi-step loads – stress, temperature and relative humidity evolution

3.2.3 Measurement results and interpretation

The following figures Fig. 3.14 up to Fig. 3.18 show the axial strains and the strain rates as a function of time for the individual specimen. Strain rates are averaged over seven days.

The figures show that at the first two stress levels strains scarcely increase while strain rates quickly decrease. That means that there is no stationary creep. Strains increase at the third stress level, and strain rates seem to stabilize in the range of 10^{-10} s^{-1} , which could imply a steady state creep at this stress level.

The results of the uniaxial creep test show that material behaviour is different at lower stress levels of 5 MPa and 10 MPa and at a stress level of 20 MPa. While strains are small at lower stresses, a distinct creep deformation occurs at a stress level of 20 MPa.

The reason for the different deformation behaviour at various stress levels might be that the cement structure of the salt concrete bears first to uniaxial stresses up to 10 MPa. Cement is expected to have an elastic material behaviour without viscoplastic deformations after the water curing process has finished. Although, there was no significant time dependent deformation at lower stresses, creep rates could be derived.

When the stress level was increased up to 20 MPa, the cement structure of the salt concrete was damaged. Consequently, the salt grit structure of the salt concrete was subjected to the load, and because of the viscoplastic material behaviour of salt grit the specimens exhibited explicit creep behaviour, Fig. 3.19.

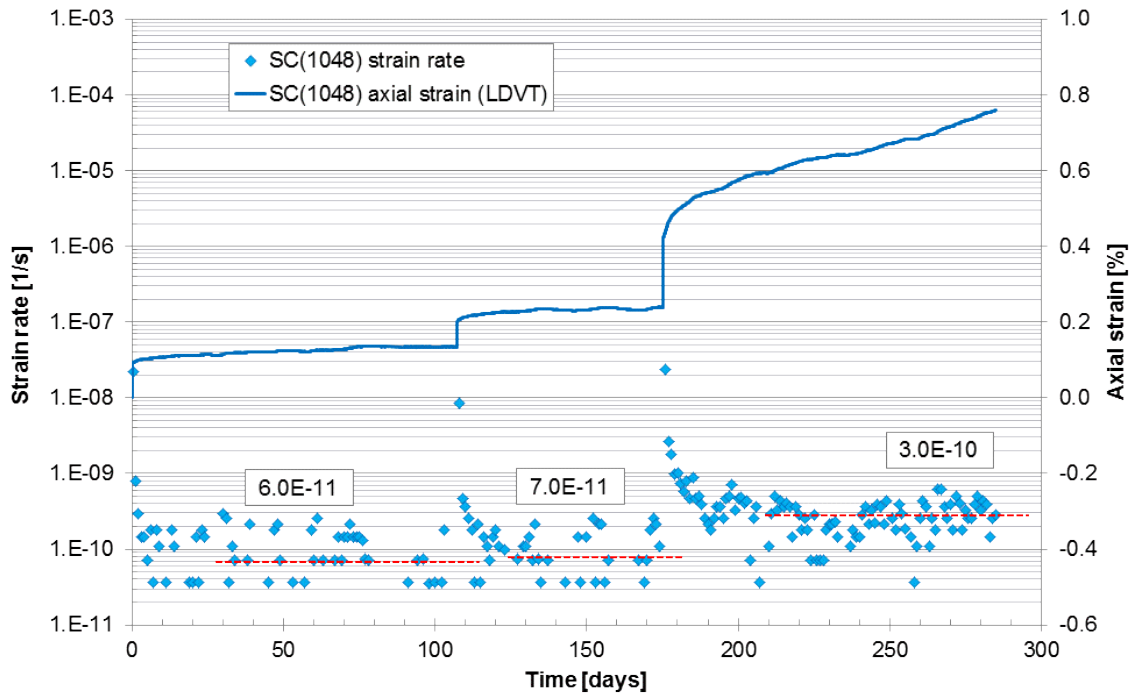


Fig. 3.14 Long-term uniaxial creep behaviour of salt concrete sample no.1048 under multi-step loads – axial strain and derived creep rates

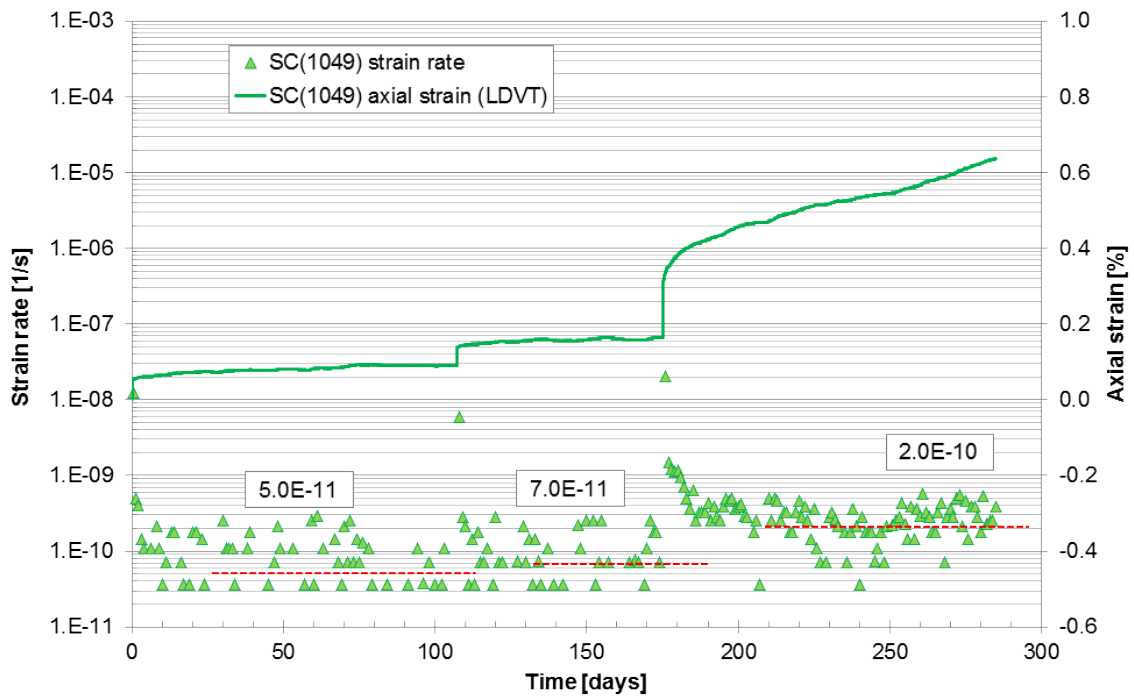


Fig. 3.15 Long-term uniaxial creep behaviour of salt concrete sample no.1049 under multi-step loads – axial strain and derived creep rates

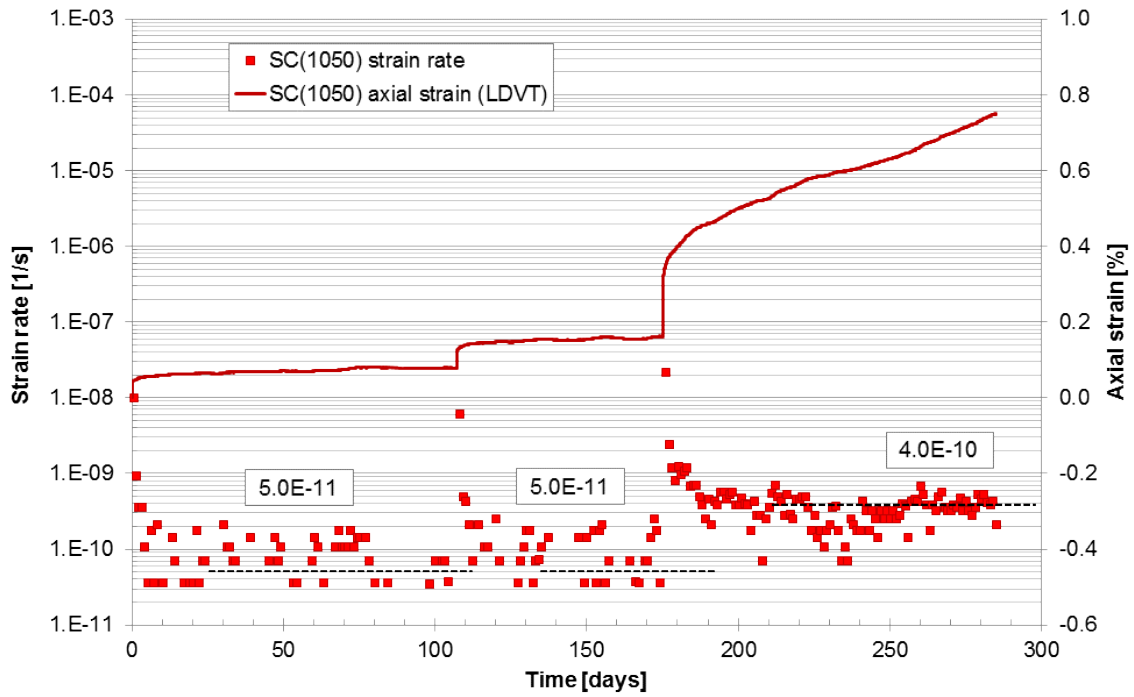


Fig. 3.16 Long-term uniaxial creep behaviour of salt concrete sample no.1050 under multi-step loads – axial strain and derived creep rates

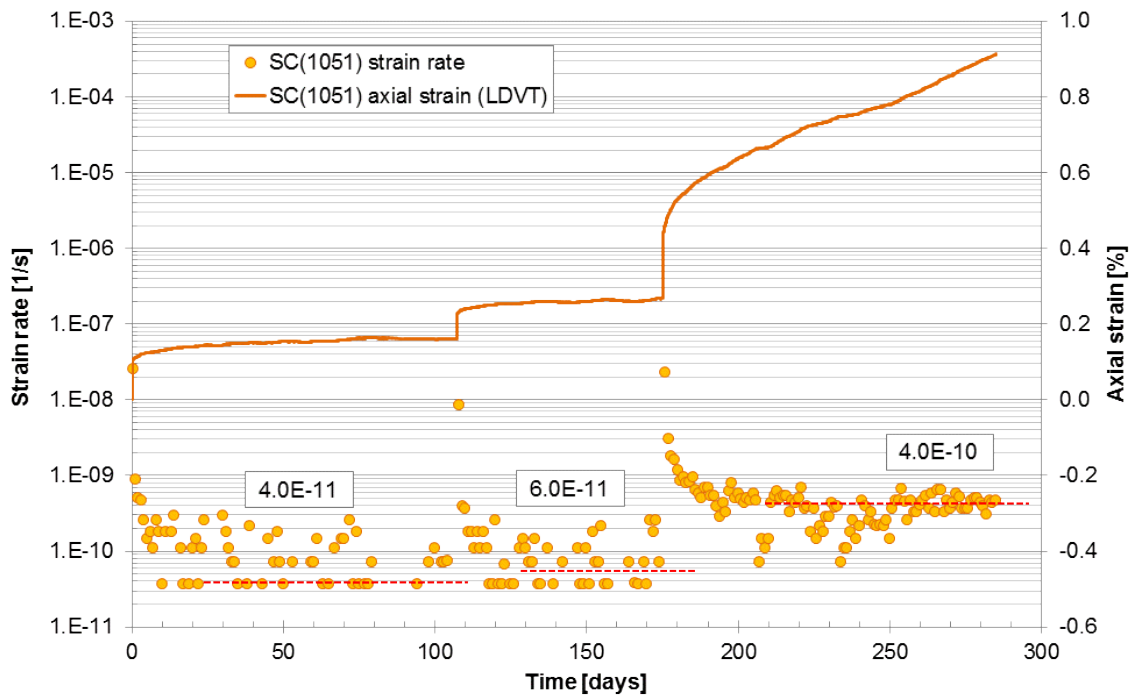


Fig. 3.17 Long-term uniaxial creep behaviour of salt concrete sample no.1051 under multi-step loads – axial strain and derived creep rates

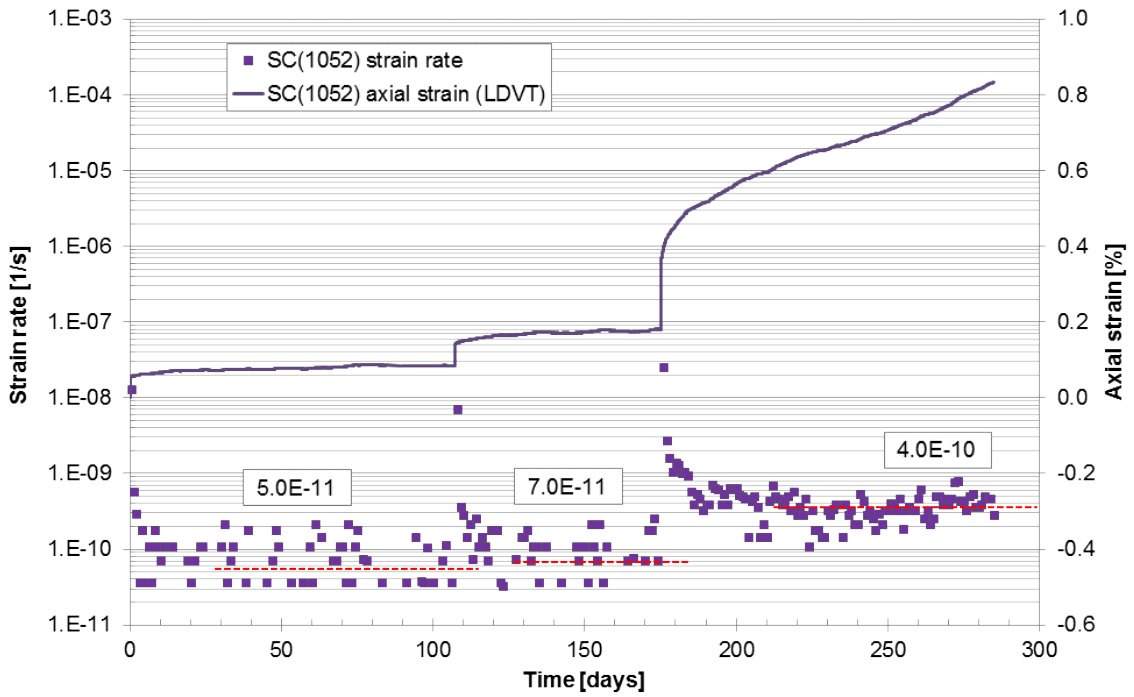


Fig. 3.18 Long-term uniaxial creep behaviour of salt concrete sample no.1052 under multi-step loads – axial strain and derived creep rates

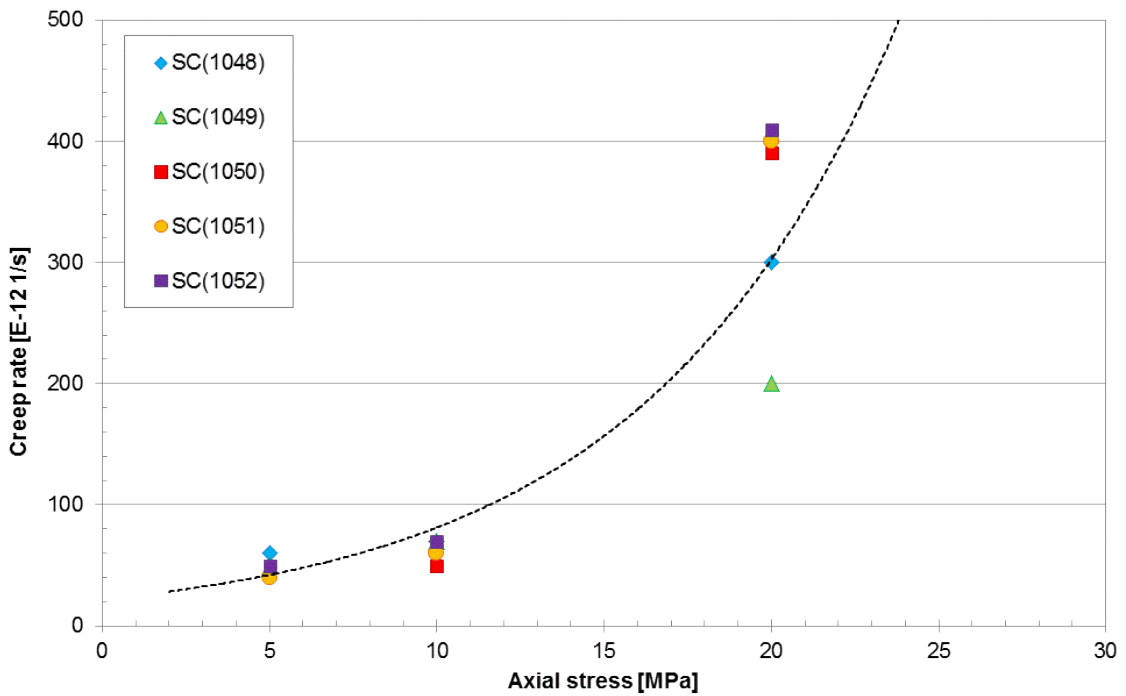


Fig. 3.19 Steady-state creep rates obtained on five salt concrete samples as a function of applied uniaxial loads

4 Modelling work

4.1 Physical Modelling

LINEAR ELASTICITY LAW (HOOKE)

The LINEAR ELASTICITY law (HOOKE) describes linear elastic material behavior. There is a linear relation between stress and strain, see eq. (4.1).

$$E = E_0 + (\phi - \phi_0) \frac{dE}{d\phi} \geq E_{min} \quad (4.1)$$

HOOKE is described by the Youngs Modulus E , the reference porosity ϕ and the Poisson Ratio ν . The parameters were not changed during the exercises.

DISLOCATION CREEP

The DISLOCATION CREEP law (DC) describes the creep behavior of porous materials that include salt grains. Deformations are generated by intracrystalline deformation mechanism. The deformation depends on the deviatoric stresses.

Eq. (4.2) describes the viscoplasticity. It is active for any stress level, because there is no yield condition. The parameter η describes the material viscosity, Φ is a scalar function, F is a stress function and G is a flow rule:

$$E \frac{d\varepsilon^{DC}}{dt} = \frac{1}{\eta_{DC}^a} \Phi(F) \frac{\delta G}{\delta \sigma'} \quad (4.2)$$

Parameters F and G are functions of the stress invariants (eq. (4.3)). The parameter n is the power of the rock power law and α_p describes a material parameter, defined in eq. (4.4)

$$= G = \sqrt{q^2 + \left(\frac{-p}{\alpha_p}\right)^2} \quad \Phi(F) = F^n \quad (4.3)$$

$$\alpha_p = \left(\frac{\eta_{DC}^v}{\eta_{DC}^d} \right)^{\frac{1}{n+1}} \quad (4.4)$$

The following equations describe the relationship of viscosity, void ratio and the dependence of deformation on temperature:

$$\frac{1}{\eta_{DC}^v} = A(T)g_{DC}^v(e) \quad (4.5)$$

$$\frac{1}{\eta_{DC}^d} = A(T)g_{DC}^d(e) \quad (4.6)$$

$$g_{DC}^v(e) = 3(g - 1)^n f \quad (4.7)$$

$$g_{DC}^d(e) = \left(\sqrt{\frac{1+g+g^2}{3}} \right)^{n-1} \left(\frac{2g+1}{3} \right) f + \frac{1}{\sqrt{g}} \quad (4.8)$$

$$A(T) = A_A \exp\left(\frac{-Q_A}{RT}\right) \quad (4.9)$$

Several parameters are needed for simulation activities using CODE_BRIGHT: A pre-exponential parameter A_A , which describes the ability to creep, the activation energy Q_A , which is equal to 54.000 J/mol and the stress power n , which is 5. The pre-exponential parameter is the varied parameter of this constitutive law during the simulation.

VISCOPLASTICITY

The basic equation for the VISCOPLASTICITY model (VP) is:

$$\frac{d\varepsilon}{dt} = A\langle\Phi(F)\rangle \frac{\delta G}{\delta \sigma} \quad (4.10)$$

Following relationships of the yield function F and the viscoplastic flow rule G are used for describing dilatancy:

$$\begin{aligned} F &= a_1 q - bp \\ G &= a_1 q - abp \\ \Phi(F) &= F^m \text{ for } F \geq 0; \Phi(F) = 0 \text{ for } F < 0 \end{aligned} \quad (4.11)$$

$$\begin{aligned}
 b &= a_3 + a_2(W_d)^{0.25} - a_4(W_d - W_{d0})^{0.25} \\
 a &= a_5 + a_6W_d + a_7(W_d - W_{d0})^2 \\
 dW_d &= qd\varepsilon_d
 \end{aligned}
 \tag{4.12}$$

Parameters a_1 to a_7 were needed for calculation as well as the stress power m , the viscosity A and the activation energy Q . All parameters are listed in tab. 4.1. Additionally, it is marked, which parameters were kept constant and which parameters were varied during the exercises. The influence of each parameter to the calculation process is explained shortly.

Table 4.1: Parameters for VP. Constant and varied parameters are marked and its influence to the process of calculation is described so far as known. Values, marked with *, were only varied by calculation of the triaxial compression test: here the values were set to zero

Parameter	Value		Influence
	constant	varied	
Stress power m	8	-	Elastic step
Viscosity A	-	yes	Transient creep deformation
Activation energy Q	54.000 J/mol	-	
W_d	3.5	-	Work by plastic deformations
a_1	-	yes	Limit the volume increase and influence the breaking point
a_2	-	yes	Limit the volume increase
a_3	2.5	-	
a_4	0.7 (0)	*	Stable calculation process by $a_2 > 0$
a_5	0.02	-	
a_6	0.02 (0)	*	Stable calculation process by $a_2 > 0$
a_7	$a_7 = a_6$	-	

4.2 Numerical simulation

4.2.1 Simulation of the triaxial compression test

MODEL GEOMETRY

To simulate the triaxial compression test, a model was designed similar to the laboratory TC-Test. This model consists of the salt concrete specimen with a length of 140 mm and the steel piston of the uniaxial apparatus with a length of 280 mm as shown in Fig. 4.1.

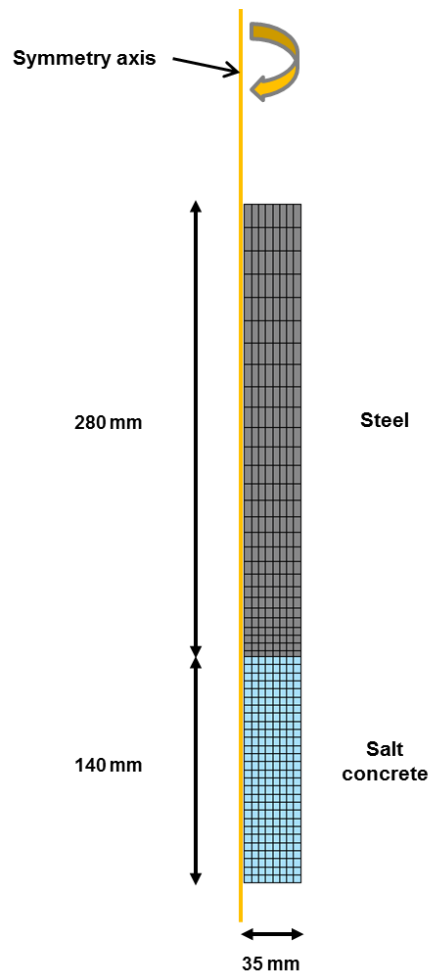


Fig. 4.1 Model of the salt concrete specimens for TC-Test for the numerical calculation using CODE_BRIGHT.

The model was generated in GiD as an axial symmetric 2D-model because of the symmetry of the salt concrete specimen. Consequently the width of the model is 35 mm.

BOUNDARY CONDITIONS

For constraining displacements in horizontal and vertical direction at the bottom of the salt concrete and in horizontal direction at the steel piston, nodal forces were generated at these parts of the model. The fixed boundary condition at the bottom does not accord to the real situation of the test specimen. But these boundary conditions were necessary for numerical calculation of the model. Axial and radial stresses were modeled as boundary stresses, fig. 4.2. In calculations, only the deviatoric stress phase of TC-Test were modelled, because this phase is interesting for understanding the deformation behavior of salt concrete and the dilatancy evolution. Following calculations were only done for a radial stress of 3 MPa.

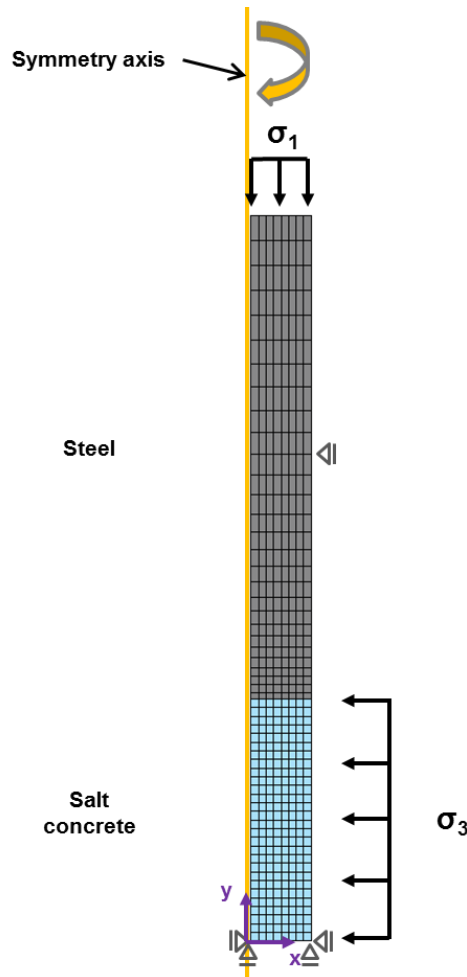


Fig. 4.2 Specimen for the TC-Test: Boundary conditions for numerical calculation using CODE_BRIGHT.

Initial temperature, stress and porosity were generated on the surfaces of salt concrete and steel piston. The initial temperature corresponded to real temperature of 25 °C dur-

ing the laboratory test and the initial stress correlated to atmospheric pressure of 0.1 MPa. Initial porosity of salt concrete was in accordance with average porosity of the specimens. The used initial values are shown in Tab. 4.2.

Table 4.2: Values of initial conditions for TC-Test

	Salt concrete	Steel
Initial temperature [°C]	25	25
Initial stress [MPa]	-0.1	-0.1
Initial porosity [-]	0.06	0.001

MESH GENERATION

The mesh for simulation of the triaxial compression test was carried out with rectangular elements. The salt concrete was meshed with 224 elements. These elements are nearly quadratic and have the same dimension over the whole length of salt concrete specimen. The steel piston consists of the same number of elements as the salt concrete. These elements are nearly of the same dimension near the boundary layer than the elements of salt concrete and they have an increasing ratio in y direction. In this way, the discretization near to the boundary layer became finer, because it was expected, that the deformation and stresses are sensitive in this zone. The number of nodes for the used mesh is 513. The mesh is shown in Fig. 4.2.

MATERIAL PROPERTIES

Different constitutive laws were used in order to describe the mechanical behavior of the specimens. For the steel piston linear elastic material behavior is expected: so HOOKE was used. The following calculation parameters are assigned, see Tab. 4.3:

Table 4.3: Material properties for LINEAR ELASTICITY law

	E-Modulus E [MPa]	Poisson ratio ν [-]	Reference po- rosity Φ₀ [-]
Salt concrete	10.000	0.18	0.06
Steel	250.000	0.27	0.001

According to the results of the laboratory tests salt concrete is supposed to have a linear elastic part and a viscoplastic part of deformation behavior. Therefore HOOKE and VP were used for first calculations. Second, the influence of stationary creep to TC-Test was investigated by DC.

Parameters for DC for salt concrete were taken from rock salt. This constitutive law for DC is able to simulate stationary creep. The used parameters are shown in Tab. 4.4

Table 4.4: Material properties for DISLOCATION CREEP law

	Creep class	Pre-exponential parameter $A_A [1/1 * MPa^n]$	Activation energy $Q_A [J/m]$	Stress power $n [-]$
Salt concrete	2	$0.26e^{-6}$	54.000	5

To describe transient creep and dilatancy of salt concrete, the constitutive model for VP was used. The parameters, which were used in the first calculation, derive from rock salt.

Table 4.5: Parameter for VISCOPLASTICITY model for description of transient creep and dilatancy of rock salt

Stress power $m [-]$	Viscosity $A [MPa^{-1} * s]$	Activation energy $Q [J/mol]$	$a_6 [-]$	$W_{d0} [-]$
8	$5 * 10^{-9}$	54.000	0.02	3.5
$a_1 [-]$	$a_2 [-]$	$a_3 [-]$	$a_4 [-]$	$a_5 [-]$
2.5	1.8	2.5	0.7	0.02

Additional to the parameters used for HOOKE, DC and VP parameters were needed for the description of solid phase properties. These selected parameters of salt concrete are similar to the parameters for rock salt, Tab. 4.6. The density is the measured average density of the specimens from UCc-Tests.

Table 4.6: Solid phase properties for calculation using CODE_BRIGHT

	Specific heat $C_s [J/(kg * K)]$	Density $\rho_s [kg/m^3]$	Expansion coefficient $\alpha_s [1/^\circ C]$	Reference temperature $T_0 [^\circ C]$
Salt concrete	855	2.070	$4.2e^{-5}$	35
Steel	500	7.850	$1,0e^{-5}$	35

During the ongoing calculation activities selected parameters for viscoplasticity behavior were varied. In this way calculation results were able to fit to the laboratory results.

PARAMETER CALIBRATION

This modelling exercise was used for a better understanding of damage behavior of salt concrete. Hence only the compression phase of the laboratory tests was considered for simulation.

Exercise TC 1: HOOKE was used for describing material behavior of the steel piston and HOOKE and VP were used for describing the salt concrete in the first modelling exercise. Because it was not possible to simulate the failure process of the sample, parameter a_1 was varied. In this way the level of breaking point could be influenced.

Exercise TC 2: In the next step failure parameters for the VP were varied, because it was not possible to describe the deformations behavior analogue to laboratory test by only varying a_1 . VP was chosen, because only this constitutive model is able to describe the nonlinear deformation behavior of salt concrete as seen in the results of the laboratory tests. Parameter a_2 limits the extension of volume strain, if it is bigger than zero, a_4 and a_6 influence the stability of calculation process for $a_2 > 0$. For describing the triaxial tests, it is necessary, that the specimens deform volumetric. So all this parameters were set to zero in order to allow volumetric deformations. The parameter a_1 was used again for varying the failure point at once.

Exercise TC 3: In the third exercise, best fitting parameters from previous calculations were used, but with using DC additionally. It was tested, whether stationary creep is triggered in this kind of calculations, or not. In the laboratory tests stationary creep was not expected due to the fact that the execution of the tests was very short. It is important to know for further calculations, if the DC considers this circumstance.

Verification: The calculation exercises, described before, were executed for the conditions of the triaxial test by a radial stress of 3 MPa. Then, the laboratory test by radial stress of 1 MPa and 2 MPa were simulated using the parameters of Exercise TC 3 from the triaxial test with a radial stress of 3 MPa. In this way it was shown, whether the parameters are applicable to all TC-Tests.

The following Tab. 4.7 shows the calculation time steps for different radial stresses:

Table 4.7: Calculation time steps of calculation for the compaction phase of TC-Test with different radial stresses

Interval	Time [Hours]	Simulation
Radial pressure of 1 MPa		
1	0.0 – 0.1	Axial and radial stress of 1 MPa
2	0.1 – 6.3	Axial stress increases to 38 MPa by a loading of 0.1 MPa per minute. Radial stress constant of 1 MPa.
Radial pressure of 2 MPa		
1	0.0 – 0.1	Axial and radial stress of 2 MPa
2	0.1 – 6.4	Axial stress increases to 40 MPa by a loading of 0.1 MPa per minute. Radial stress constant of 2 MPa.
Radial pressure of 3 MPa		
1	0.0 – 0.1	Axial and radial stress of 3 MPa
2	0.1 – 7.4	Axial stress increases to 44 MPa by a loading of 0.1 MPa per minute. Radial stress constant of 3 MPa.

MODELLING RESULTS VERSUS EXPERIMENTAL DATA

In Exercise TC 1 HOOKE was used for describing the material behavior of the steel piston and HOOKE and VP were used for describing the material behavior of salt concrete. VP should describe shear thickening material behavior of salt concrete analogue to the TC-Test. The used constitutive laws, their parameters and the varied ones are summarized in Tab. 4.8.

Table 4.8: Used constitutive laws for modelling salt concrete TC behaviour (varied parameters are marked in red)

LINEAR ELASTICITY	E [MPa]	ν [-]	ϕ_0 [-]		
	10.000	0.18	0.06		
DISLOCATION CREEP	A_A [1/1*MPaⁿ]	Q_A [J/mol]	n [-]		
	-	-	-		
VISCOPLASTICITY	m [-]	A [MPa⁻¹*s]	Q [J/mol]	a_6 [-]	W_d [-]
	8	$5 \cdot 10^{-9}$	54.000	0.02	3.5
	a_1 [-]	a_2 [-]	a_3 [-]	a_4 [-]	a_5 [-]
	varied	1.8	2.5	0.7	0.02

The first calculation was executed using all parameters correspondent to Tab. 4.5. Parameter a_1 was equal to 2.5. The nodes, at which stresses and displacements were detected for further evaluation of the results, are shown in Fig. 4.3.

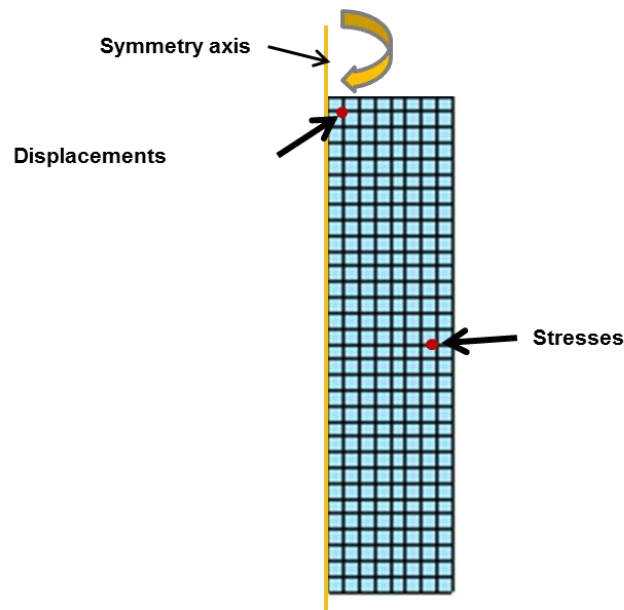


Fig. 4.3 Nodes on the specimen, at which stresses and displacements were detected.

The purple curve in Fig. 4.4 shows the results received with parameter a_1 is 2.5. Here the deviatoric stress respectively the volumetric strain is shown versus the axial strain. The laboratory results are shown in grey. The calculation process stopped before the final axial stress of 44 MPa was reached according to the lab test results, because the calculation failed at a deviatoric stress of 23 MPa. There was no dilatancy foreseen so that the specimen failed directly. This is used to see the development of volumetric strain. In lab tests dilatancy occurs, if the curve deviates from the linear slope. In the mode, calculations stopped directly, if the curve started to deviate from the linear slope. So no increase of porosity and consequently no dilatancy was modelled.

Now the stability of salt concrete was improved in order to load the specimen with the whole axial stress correspondent to the laboratory test. Therefore the parameter a_1 was decreased. In this way the stability of salt concrete increased. This proceeding aims to find the value of a_1 , at which the specimen carries the whole deviatoric stress of 44 MPa. The results are shown in Fig. 4.4. If a_1 decreased, the specimen was able to carry higher deviatoric stresses. Calculation process stopped later by using a decreased a_1 and consequently increased the material stability. A full calculation was executed successfully by a_1 equal to 1.93. The aim, that an execution of the whole calculation process is possible, was finally reached. The specimen could carry the whole deviatoric stress. But the simulation curve shows a linear gradient and an adaptation to the curve of laboratory test does not occur.

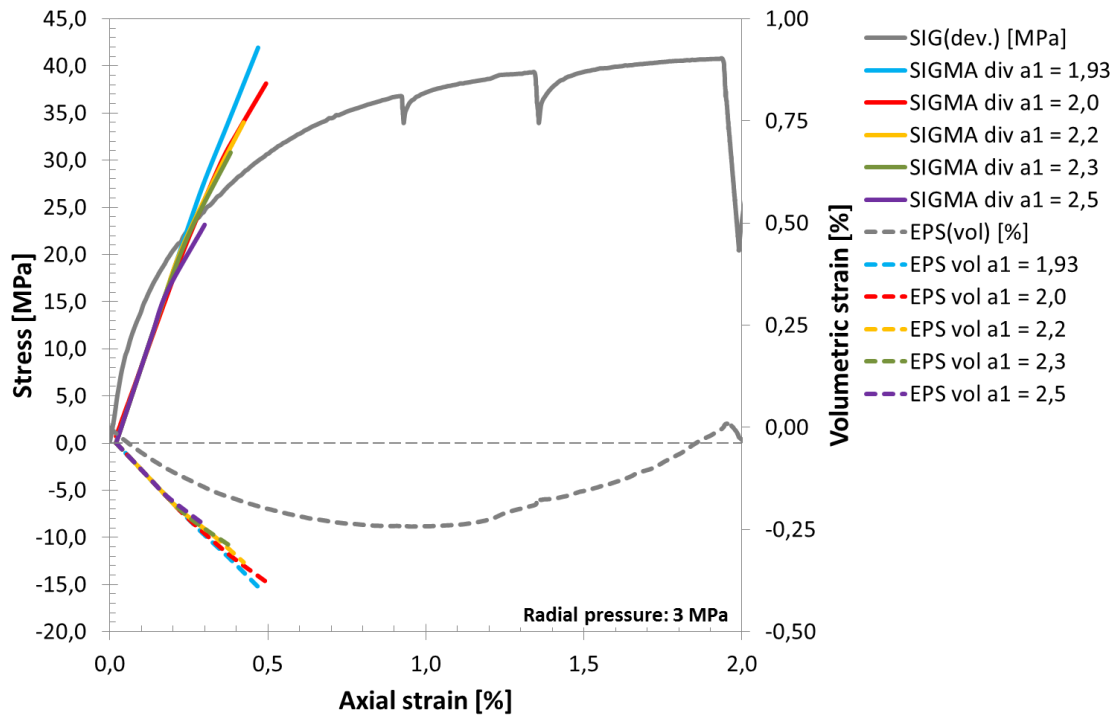


Fig. 4.4 Results of Exercise TC 1. Here LINEAR ELASTICITY law and VISCOPLASTICITY model are used. Axial load is 44 MPa

In Exercise TC 2 also HOOKE and VP was used. All parameters are summarized in Tab. 4.9. This exercise aimed to find a combination of parameters, which allows an increase of porosity and consequently a volume increase and onset of dilatancy for a better adaptation of calculation to laboratory results.

Table 4.9: Used constitutive laws for modelling salt concrete TC behaviour (varied parameters are marked in red)

LINEAR ELASTICITY	E [MPa]	ν [-]	ϕ_0 [-]		
		10.000	0.18	0.06	
DISLOCATION CREEP	A_A [1/1*MPa ⁿ]	Q_A [J/mol]	n [-]		
	-	-	-		
VISCOPLASTICITY	m [-]	A [MPa ⁻¹ *s]	Q [J/mol]	a_6 [-]	W_d [-]
	8	$5 \cdot 10^{-9}$	54.000	0	3.5
	a_1 [-]	a_2 [-]	a_3 [-]	a_4 [-]	a_5 [-]
	varied	0	2.5	0	0.02

Initial point of Exercise TC 2 should be a calculation, which is comparable to the result of Exercise TC 1: A linear slope, which describes the stress load without failure of the specimen and without onset of dilatancy. This is necessary for a better interpretation of further calculation results. But the material stability correspondent to Exercise TC 1

was not sufficient anymore, because a_2 , a_4 and a_6 were set to zero now and allow maximal extension of volume (If a_2 , a_4 and a_6 are zero, W_d drops out). Consequently the material stability decreased. Hence a_1 was decreased to 1.33 for reaching a higher failure point and reaching the requirements correspondent to the exercise before (Compare Fig. 4.5).

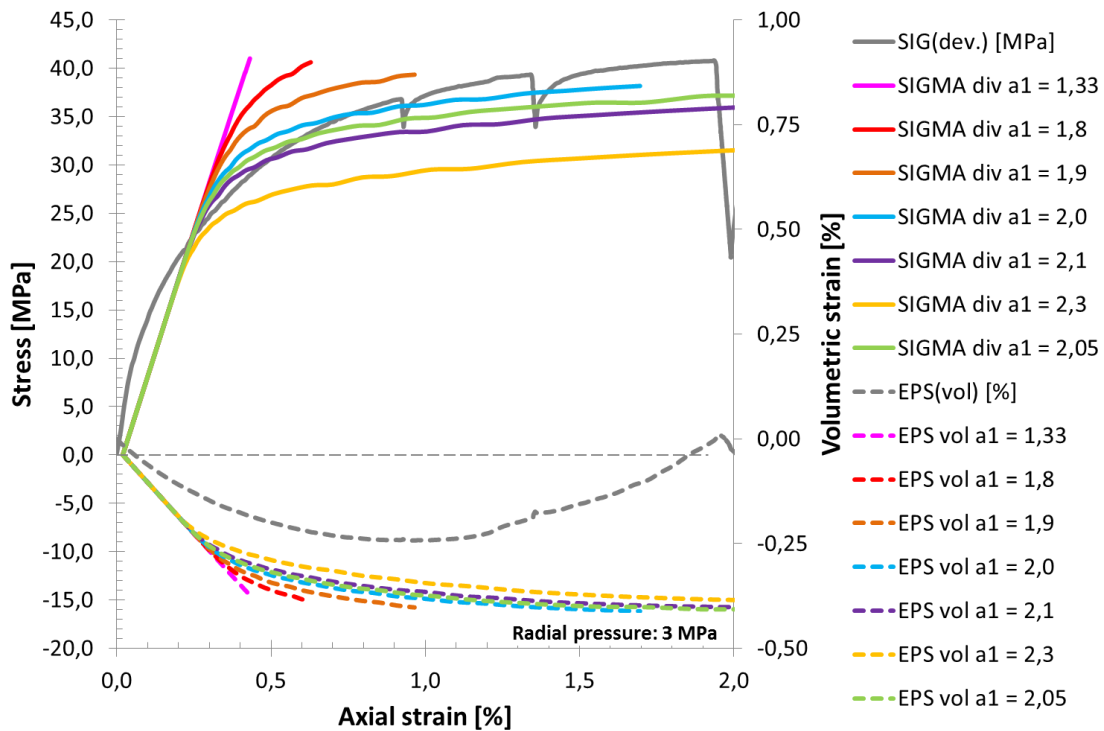


Fig. 4.5 Results of Exercise TC 2. Here LINEAR ELASTICITY law and VISCOPLASTICITY model are used. Parameters a_2 , a_4 and a_6 are set to zero. a_1 is varied. For further calculations $a_1 = 2.05$ is chosen (green curve).

Below a_1 was increased step by step. Fig. 4.5 shows a representative assortment of the results of executed calculations. All curves show a linear gradient at first, the gradient of all curves decreases dependent to the value of a_1 . The calculations of Exercise TC 2 were executed completely. Maximal reached axial strains were determined by the stiffness of the material. The stiffness respectively stability of the material depends on the value of a_1 . If a_1 was small, the material had a higher stiffness and less deformation. If a_1 was increased, the material stiffness became smaller and axial strains were higher. Additionally the maximal acceptable deviatoric stress is smaller by a salt concrete with smaller stiffness. So the gradient of the curves approximate to the hori-

zontal line after the stress limit was reached (as to see at the curves by a_1 equal to 2.05 / 2.1 and 2.3): Axial strains further increase but deviatoric stress stay nearly constant.

In consideration of the development of volumetric strain is to see, that the curves differ clearly to the linear slope. So an increase of porosity and consequently an onset of dilatancy were simulated by using parameters after Tab. 4.9.

For further calculations a value of a_1 equal to 2.05 was chosen, because this curve describes the laboratory test in the best manner in maximal deviatoric stresses and in reached axial strain.

In exercise TC 3 the influence of DC to the TC-Test by numerical calculations was checked. Normally stationary creep, which was simulated by DC, should have no influence to the deformations, if the test period is only a few hours as in this TC-Test. For further calculation it is important to know, if CODE_BRIGHT considers this circumstance. Below the calculations results from Exercise TC 2 are opposed to the results from Exercise TC 3, which considers HOOKE, DC and VP.

Table 4.10: Used constitutive laws for modelling salt concrete TC behaviour (varied parameters are marked in red)

LINEAR ELASTICITY	E [MPa]	ν [-]	ϕ_0 [-]		
	10.000	0.18	0.06		
DISLOCATION CREEP	A_A [1/1*MPaⁿ]	Q_A [J/mol]	n [-]		
	0.26e ⁻⁶	54.000	5		
VISCOPLASTICITY	m [-]	A [MPa⁻¹*s]	Q [J/mol]	a_6 [-]	W_d [-]
	8	5*10 ⁻⁹	54.000	0.0	3.5
	a_1 [-]	a_2 [-]	a_3 [-]	a_4 [-]	a_5 [-]
	2.05	0.0	2.5	0.0	0.02

The results in Fig. 4.6 show, that DC has no influence of the deviatoric stress and the volumetric strain. The curves of both parts of calculation are nearly identically. The small deviations also could be from the individual steps of iteration during calculation.

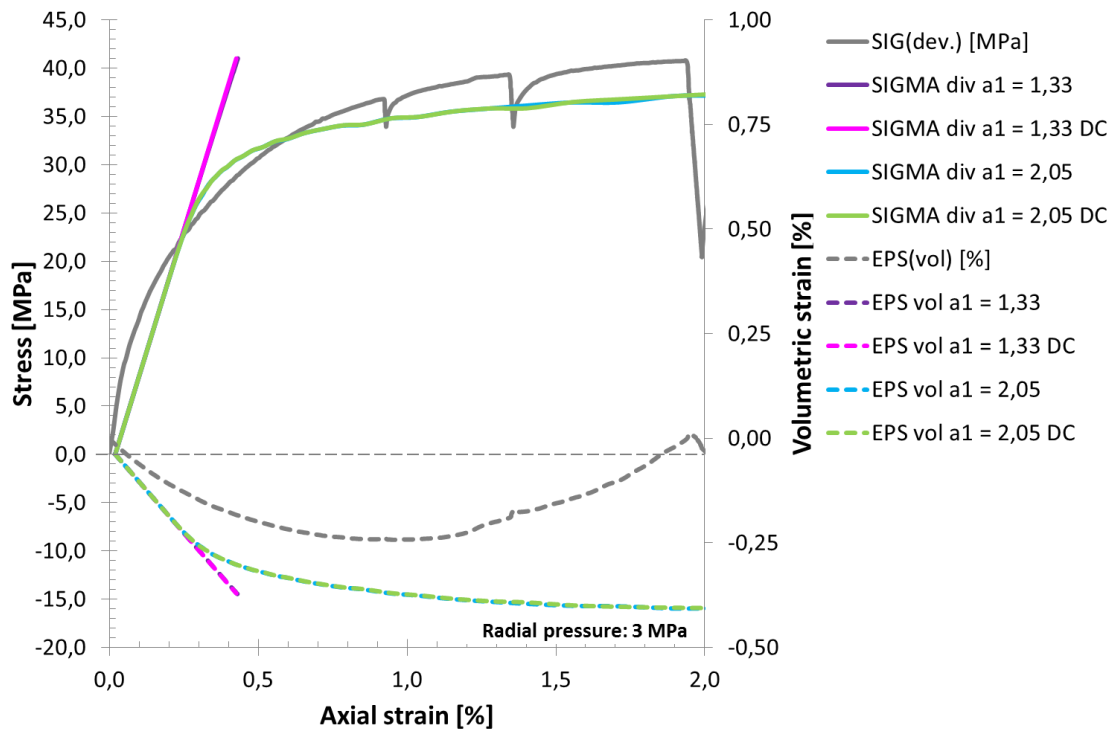


Fig. 4.6 Comparison of calculation results of Exercise TC 2 and TC 3 with and without DISLOCATION CREEP law. The results confirm that DISLOCATION CREEP law is only considered by longer time periods. Calculations, which were executed with DISLOCATION CREEP law are marked with “DC”

Consideration of onset of dilatancy

Consecutively the onset of dilatancy was considered on the basis of calculation results. For this the results from Exercise TC 2 were used with values of a_1 equal to 1.33 and 2.05. The results are shown in Fig. 4.7. The onset of dilatancy is described by the deviation of the curve of volumetric strain from the linear slope by a_1 equal to 1.33. The criterion for the onset of dilatancy was chosen different to the criterion used for the laboratory test analysis. In the calculation results no increase of volumetric strain was reached, which was the used criterion in the laboratory tests. So the criterion of the laboratory tests was not applicable here. If dilatancy insert in Exercise TC 2, the axial strain was around 0.22 % and the deviatoric stress was 21 MPa. Generally the reached deviatoric stress is circa 3 MPa smaller than in the laboratory test. It was around 37 MPa. The volumetric strains are circa 50 % higher than the maximum volumetric strain of laboratory tests by an axial strain of 0.9 %. But basically, the calculations results characterize the general trend of the laboratory test.

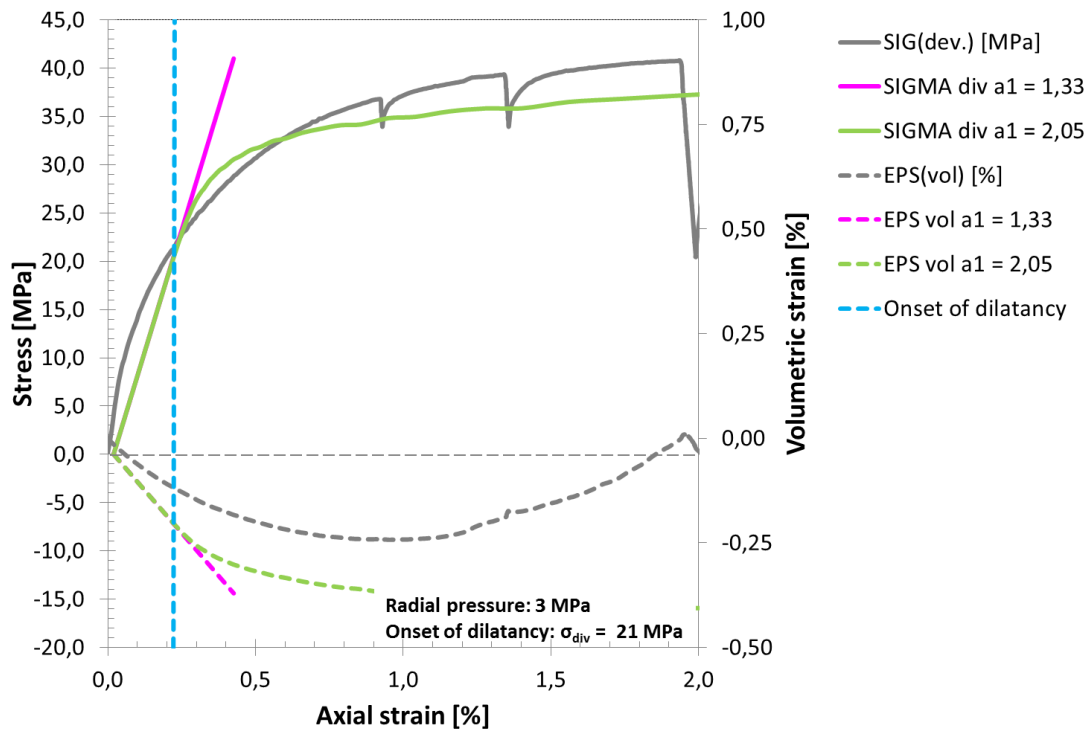


Fig. 4.7 Calculation results of Exercise TC 2 and a radial stress of 3 MPa. The pink curve shows the results without dilatancy, the green one with dilatancy. The onset of dilatancy is defined as the start of deviation of the curve with dilatancy to the linear curve without dilatancy

Verification

All calculations in this chapter correspond to the conditions of the TC-Test by a radial stress of 3 MPa until now. Currently, the chosen parameters were verified by calculations of the TC-Test with radial stresses of 1 and 2 MPa. HOOKE and VP was used correspondent to Exercise TC 2.

Fig. 4.8 shows the calculations results with a radial stress of 2 MPa. The onset of dilatancy was nearly at the same point by a radial stress of 2 MPa as by a radial stress of 3 MPa. If the dilatancy insert, a deviatoric stress of 21 MPa and an axial strain of 0.23 % was reached. The deviatoric stress during calculation was 3 MPa smaller than in the laboratory tests. These values correspond to the results of Exercise TC 2 with a radial stress of 3 MPa. The development of the calculated volumetric strains accords here very good with the volumetric strains of laboratory test. The curve progression is nearly the same until the volume of the laboratory specimen increases. This increase of volume could not described by the VP and the used parameters of Exercise TC 2.

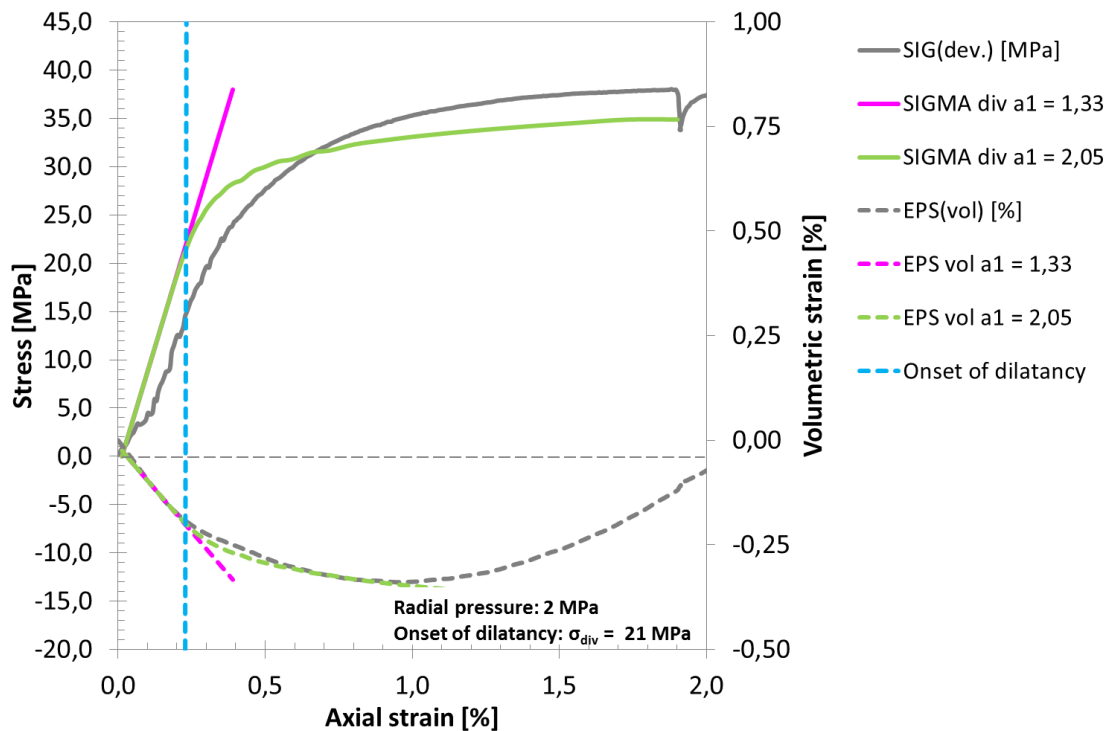


Fig. 4.8 Calculation results of Exercise TC 2 and a radial stress of 2 MPa. The pink curve shows the results without dilatancy, the green one with dilatancy. The onset of dilatancy is defined as the start of deviation of the curve with dilatancy to the linear curve without dilatancy

The conditions for the onset of dilatancy by a radial stress of 1 MPa are different to the calculations before, Fig. 4.9. Here the onset of dilatancy was reached at axial strain of 0.18 % and deviatoric stress of 17 MPa. The stability of the specimen decreases, because of the lower radial stress. This corresponds to the results of the laboratory test. The maximal deviatoric stress in the laboratory test was 36 MPa, in the calculation 33 MPa. The difference between these values of deviatoric stress of laboratory and calculations results is the same as in the calculations results before. Certainly there is again a difference of volumetric strains between laboratory and calculations results. Both volumetric strains are smaller than in tests before. Reason for the decrease of both volumetric strains could be the smaller radial stress and the resulting loss of stability. So the specimen cannot compact in the same range than before, because it was damaged earlier. The smaller deviatoric stress level by the onset of dilatancy supports this thesis.

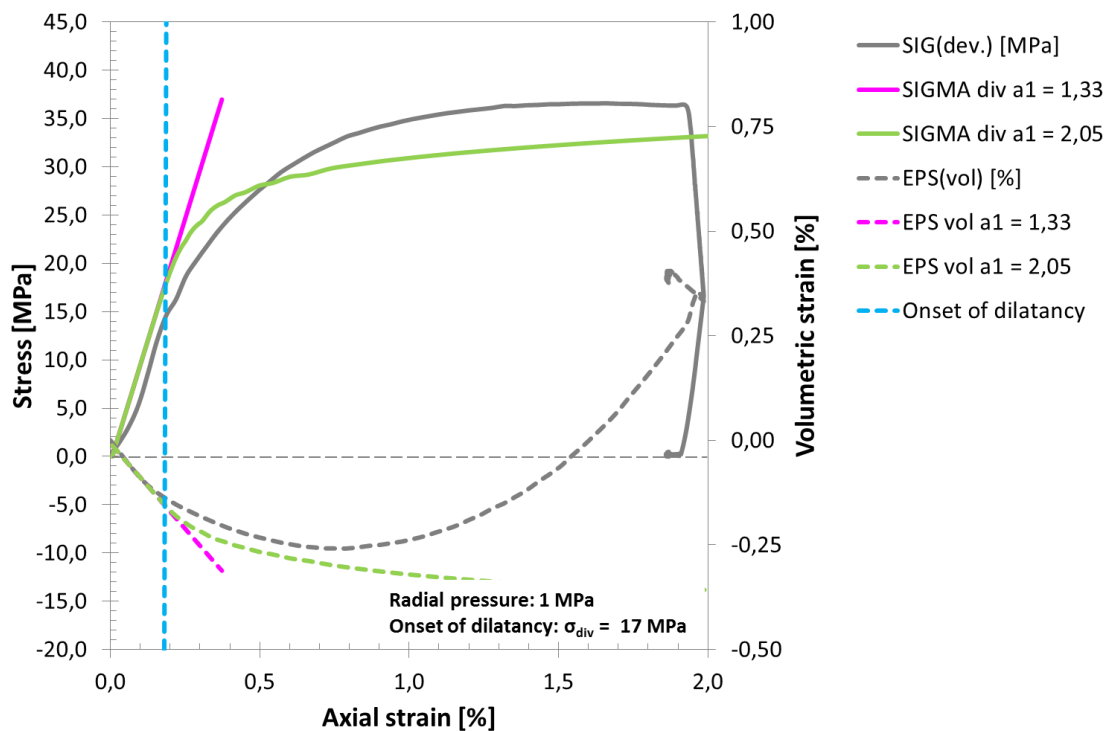


Fig. 4.9 Calculation results of Exercise TC 2 and a radial stress of 1 MPa. The pink curve shows the results without dilatancy, the green one with dilatancy. The onset of dilatancy is defined as the start of deviation of the curve with dilatancy to the linear curve without dilatancy

Interim results

The comparison between laboratory and calculation results shows, that simulation of the TC-Test on salt concrete is possible by using HOOKE and VP. Therefore, VP has been varied with respect to rock salt. The final parameters used for TC-Test are summarized in Tab. 4.11.

Table 4.11: Final parameters used for the Linear Elasticity law and VISCOPLASTICITY model in TC-Test

LINEAR ELASTICITY	E [MPa]	ν [-]	ϕ_0 [-]		
	10.000	0.18	0.06		
VISCOPLASTICITY	m [-]	A [MPa ⁻¹ *s]	Q [J/mol]	a ₆ [-]	W _d [-]
	8	5*10 ⁻⁹	54.000	0	3.5
	a ₁ [-]	a ₂ [-]	a ₃ [-]	a ₄ [-]	a ₅ [-]
	2.05	0	2.5	0	0.02

Deficits of the TC-Test simulation are that volume increase as reaction to the damage of the specimen cannot be considered as well as the respective reduction of stresses, if

the failure level was reached. Equivalent to the calculation results of TC-Test it can be expected that the onset of dilatancy in the UCc-Test starts during the increase of axial stresses from 10 MPa to 20 MPa. The results of this chapter are considered by the simulation of the UCc-Test using the VP parameter set in Tab. 4.11.

4.2.2 Simulation of the uniaxial creep test

MODEL GEOMETRY

For simulation of the uniaxial creep test, a model was designed similar to the model of the TC-Test in GiD. The length of the salt concrete specimen is 160 mm and the length of steel piston is 320 mm as shown in Fig. 4.10. The width of this model is 40 mm. Due to the symmetry of salt concrete specimen this model was generated in terms of an axial symmetric 2-D model.

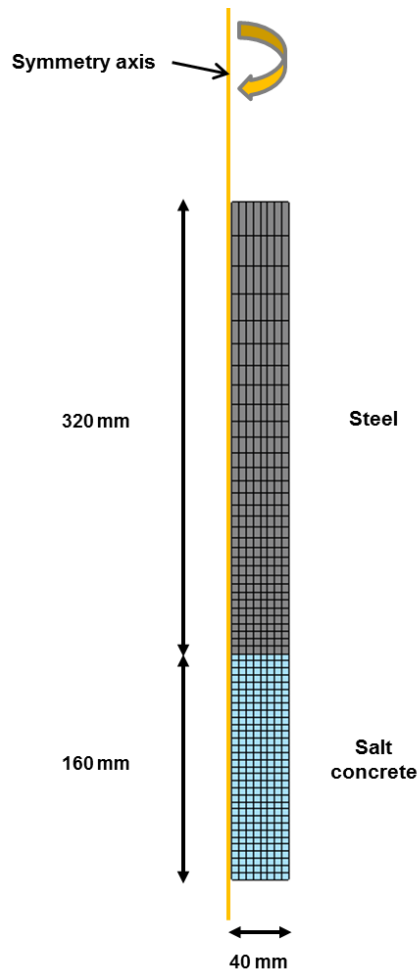


Fig. 4.10 Model of the salt concrete specimens for UCc-Test for the numerical calculation using CODE_BRIGHT, showing geometry and meshing details

BOUNDARY CONDITIONS

Boundary conditions were generated as nodal forces at the bottom of the salt concrete specimen and as collateral ones at the steel piston. They constrain displacements in

horizontal and vertical direction at the bottom of the salt concrete and horizontal displacements at the steel piston. The fixed boundary condition at the bottom does not represent the situation in the laboratory, but was necessary for numerical calculations. Axial stress was modelled as boundary stress at the top of steel piston. The axial stresses (σ_1) reached from 5 MPa to 20 MPa. An atmospheric pressure (p_{atm}) of 0.1 MPa was applied radial to the salt concrete specimen (Compare Fig. 4.11).

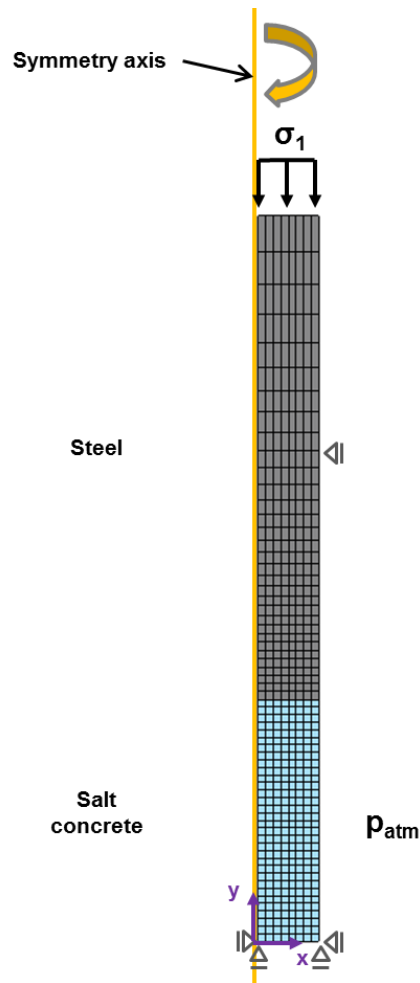


Fig. 4.11 Specimen for the UCc-Test: Depiction of conditions for numerical calculation using CODE_BRIGHT

Initial temperature, stress and porosity were generated on the surfaces of salt concrete and steel piston similar to the TC-Test. The parameters were the same as before as in the calculation exercise before (Compare Tab. 4.1).

MESH GENERATION

The mesh of this model was carried out with rectangular elements. The salt concrete was meshed with 256 quadratic elements using the same dimension. The feed size averages 0.5 mm in each case. The steel piston consists of 256 elements. These elements are nearly quadratic at the boundary layer to the salt concrete and become rectangular in y direction. The reason was the same as by TC-Test calculation exercises: in order to get a finer discretization near the boundary layer. The number of nodes for the whole model was 585. The mesh is shown in Fig. 4.10. Due to the layout of the mesh, displacements at the contact zone between salt concrete specimen and steel piston were not possible.

MATERIAL PROPERTIES

Different constitutive laws were used in order to describe the mechanical behavior of the specimens. For the steel piston HOOKE was used as in TC-Test. According to the results of the UCc-Test, salt concrete is supposed to have a linear elastic part and a viscoplastic part of deformation behavior. Therefore HOOKE, DC and VP were used for calculation. Parameters for HOOKE are shown in Tab. 4.12.

Table 4.12: Final used parameters for the Linear Elasticity law

	E-Modulus E [MPa]	Poisson ratio ν [-]	Reference porosity Φ_0 [-]
Salt concrete	10.000	0.18	0.06
Steel	250.000	0.27	0.001

Parameters for the calculation of DC for salt concrete were taken from rock salt in the first calculation because salt concrete includes around 70 % crushed salt and there are no creep parameters for salt concrete until now. This constitutive law for DC is only able to describe stationary creep. The parameters are shown in Tab. 4.13.

Table 4.13: Material properties for DISLOCATION CREEP law of saline materials

	Creep class	Pre-exponential parameter A_A [1/1*MPaⁿ]	Activation energy Q_A [J/mol]	Stress power n [-]
Salt concrete	5	$2.08e^{-6}$	54.000	5

To describe transient creep and dilatancy of salt concrete, the VP was used. The parameters are shown in Tab. 4.14.

Table 4.14: Parameter for VISCOPLASTICITY model for description of transient creep and dilatancy of salt concrete

Stress power m [-]	Viscosity A [$\text{MPa}^{-1} \cdot \text{s}$]	Activation energy Q [J/mol]	a_6 [-]	W_{d0} [-]
8	$5 \cdot 10^{-9}$	54.000	0.02	3.5
a_1 [-]	a_2 [-]	a_3 [-]	a_4 [-]	a_5 [-]
2.5	1.8	2.5	0.7	0.02

Additional to the parameters used for HOOKE, DC and VP, some parameters were needed for description of solid phase properties (Tab. 4.6).

PARAMETER CALIBRATION

Different types of exercises were executed for finding the best approximation of calculation results to the laboratory test findings.

Exercise UCc 1: HOOKE and DC were used. First a calculation was executed using parameters correspondent to rock salt, because salt concrete consists of about 70 % crushed salt. So potentially a time dependent deformation behavior similar to rock salt by stationary creep is expected. Further calculations were executed using varied pre-exponential parameters. In this way a creep class should be found, which describes real strains and strain rates of salt concrete related to stationary creep. Calculated creep classes and appropriate pre-exponential parameter are shown in Tab. 4.15.

Table 4.15: Variation of creep classes and appropriate pre-exponential parameters for first calculations [BGR03]

Creep class	0	1	2	3	4	5	6
Pre-exponential parameter	$0.065e^{-6}$	$0.13e^{-6}$	$0.26e^{-6}$	$0.52e^{-6}$	$1.04e^{-6}$	$2.08e^{-6}$	$4.16e^{-6}$

Exercise UCc 2: Now the pre-exponential parameter for each stress level was varied. For each stress level the pre-exponential parameter was considered individually. The pre-exponential parameter was used independently to the creep classes, because it

was expected, that a better adaptation to the laboratory results could be reached. Here HOOKE and DC were used.

Exercise UCc 3: This exercise considered only the third stress level of 20 MPa (marked as phase 2), because laboratory tests and calculations before showed, that there is a difference between the deformation behavior in first and second stress level and the third stress level. Exercise UCc 3 aimed to describe the combination of linear elastic, transient and stationary creep and shear thickening deformations. Exercise UCc 3 was subdivided in parts a) to d). In part a) calculation was executed on the basis of the results from TC-Test using HOOKE and VP with parameters from Exercise TC 2. Part b) described the deformation behavior including HOOKE and VP, but here volumetric extensions were limited again and the material stability was increased. In part c) calculations was executed using HOOKE, VP and additional DC. The pre-exponential parameter was adapted. Finally the shear thickening deformations were adapted again in part d), because the interaction of HOOKE, VP and DC had to be considered.

Exercise UCc 4: Now the VP was adapted to stress levels of 5 MPa and 10 MPa (marked as phase 1). HOOKE, DC and VP should simulate linear elastic and transient creep deformations. DC was used because, it was expected, that the influence of stationary creep is very small in phase correspondent to laboratory results. This assumption was checked. Furthermore the influence of stationary creep in phase 2 will be considered in the end of Exercise UCc 4 again.

Exercise UCc 4 was subdivided in three parts. Part a) investigated the influence of viscosity to transient creep. In part b) the stiffness of the salt concrete was adapted by parameter a_1 . Finally the volumetric extension was adapted by parameter a_2 in part c).

In **Exercise UCc 5** the results of phase 1 (Exercise UCc 4) and phase 2 (Exercise UCc 3) were brought together.

The level of axial stress is the changing condition between the different intervals in each calculation exercise. The increase of axial stress was simulated in smaller intermediate steps analogue to the progression of pressure in UCc-Test. The calculation was executed in six intervals as constituted in Tab. 4.16. These time steps apply for all calculations.

Table 4.16: Time steps of calculation at UCc-Test

Interval	Time [Days]	Simulation
1	0.00 – 0.01	Axial stress increases from 0.1 MPa to 5 MPa
2	0.01 – 106.00	Axial stress of 5 MPa
3	106.00 – 106.01	Axial stress increases from 5 MPa to 10 MPa
4	106.01 – 174.00	Axial stress of 10 MPa
5	174.00 – 174.01	Axial stress increases from 10 MPa to 20 MPa
6	174.01 – 341.00	Axial stress of 20 MPa

MODELLING RESULTS VERSUS EXPERIMENTAL DATA

In Exercise UCc 1 HOOKE was used for description of the material behavior of the steel piston by simulation of the UCc-Test as in TC-Test before. In Exercise UCc 1 HOOKE and DC were used for description of the material behavior of the salt concrete. The used constitutive laws and its parameters are shown in Tab. 4.17. This exercise aimed to check, if DC could describe the time dependent deformation behavior of salt concrete and which pre-exponential parameters suits best. So the pre-exponential parameter was the varied value in this exercise.

Table 4.17: Exercise UCc 1 - Active constitutive laws for salt concrete are colored. Changed respectively varied parameters are marked red

LINEAR ELASTICITY	E [MPa]	ν [-]	ϕ_0 [-]		
	10.000	0.18	0.06		
DISLOCATION CREEP	A_A [1/1*MPaⁿ]	Q_A [J/mol]	n [-]		
	varied	54.000	5		
VISCOPLASTICITY	m [-]	A [MPa⁻¹*s]	Q [J/mol]	a_6 [-]	W_d [-]
	-	-	-	-	-
	a_1 [-]	a_2 [-]	a_3 [-]	a_4 [-]	a_5 [-]
	-	-	-	-	-

A first calculation was executed with a pre-exponential parameter of $2.08 \cdot 10^{-6}$. This value corresponds to the creep behavior of rock salt. Displacements were determined correspondent to Fig. 4.3 and displacements in [m] were converted in strains in [%]. In Fig. 4.12 the results of the laboratory UCc-Test are compared to the calculation results (showed in grey). The calculation results clearly show the different axial stress levels. Elastic deformations could be identified by sudden increase of the curve, that increased by each step. Stationary creep could be identified by the linear gradient of the curve. Certainly elastic deformations were very small in all stress levels and the deformations

of stationary creep were very small in first stress level and very high for second and third stress level.

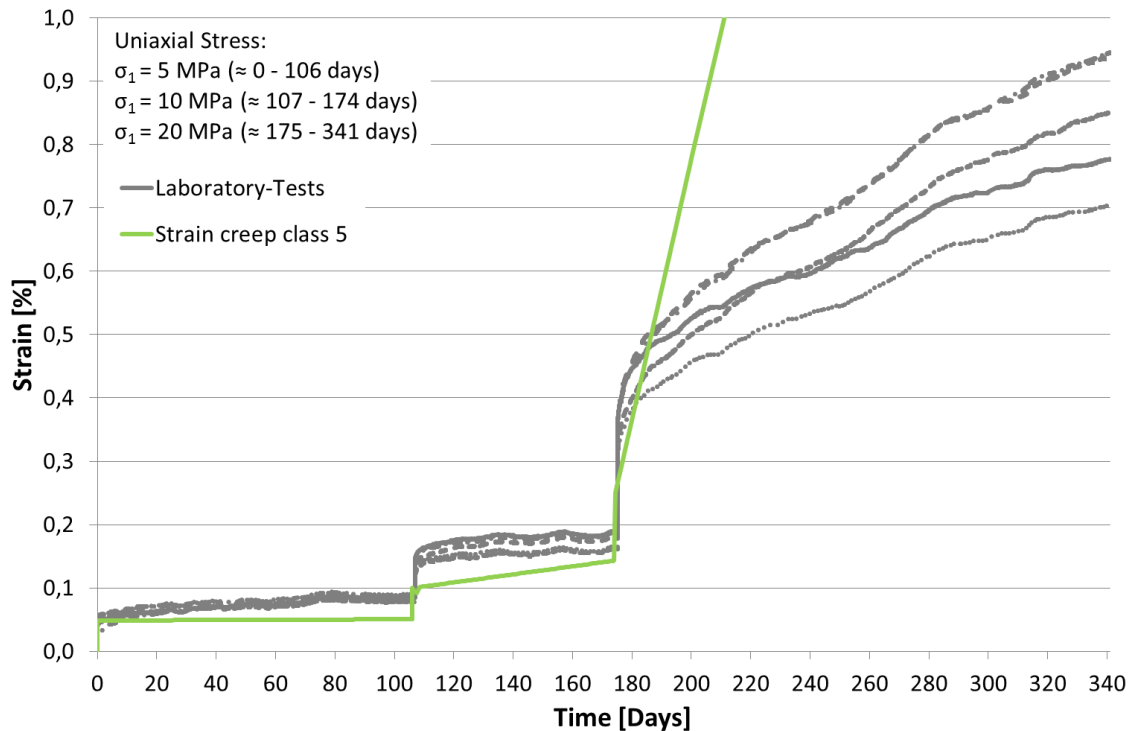


Fig. 4.12 Comparison between the results of the laboratory UCC-Test and the result of calculation of UCC-Test using LINEAR ELASTICITY law and DISLOCATION CREEP law by a pre-exponential parameter of $2.08e-6$ (creep class 5)

In the following, the pre-exponential parameters were varied. So the time dependent deformation behavior correspondent to creep classes 0 to 6 was considered. The results are shown in Fig. 4.13. At the first stress level of 5 MPa all curves show nearly the same deformation behavior. Elastic deformations could be simulated, but there were no creep deformations. Development of strains became different at the stress level of 10 MPa. Strains modeld with creep class 6 were clearly too high. Strains modelled with other creep classes could be in the right range. In order to evaluate this, a different presentation of the results is necessary (Follows in Fig. 4.14 and in Fig. 4.15). When the stress level increased to 20 MPa strains of each creep class became clearly different. Generally high creep classes have higher strains than lower ones. The curve of creep class 2 with a pre-exponential parameter of $0.26 \cdot 10^{-6}$ shows the best suiting gradient compared to the gradients of the UCC-Test at first sight. Consequently the curve of creep class 2 (brown curve) was considered more exactly.

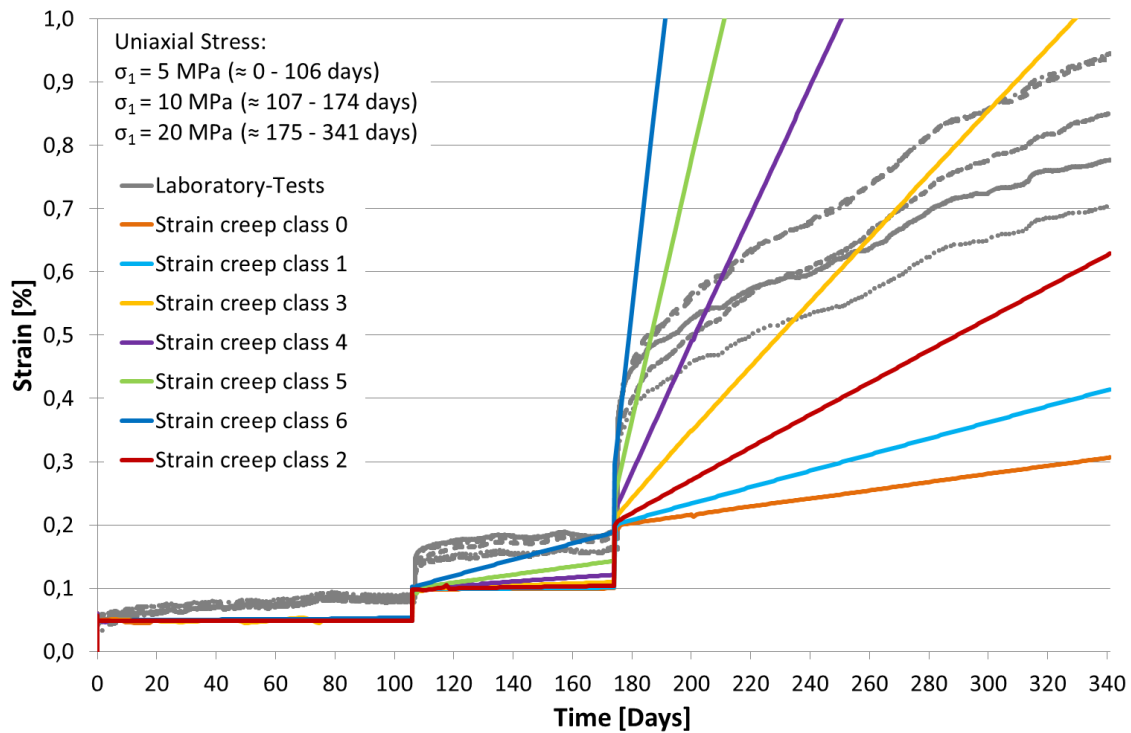


Fig. 4.13 Comparison between the results of the laboratory UCc-Test and the modelling using LINEAR ELASTICITY law and DISLOCATION CREEP with various pre-exponential parameters correspondent to creep classes 0 to 6

In the following, strain rates derived from laboratory tests and from calculation will be compared. Therefore, an average value of all stationary creep levels of each specimen was constituted as shown in Fig. 4.14 (only for sample SC1048). The same was done for the calculation results. In this manner one specific strain rate could be determined for each stress level and each specimen. The summarized results are shown in Fig. 4.15.

This simplified depiction of strain rates shows that all strain rates of the laboratory tests are in the same range for the individual stress level. The strain rates of first and second stress level are very similar while strain rates increase at third stress level. This notice supports the perception that deformation behavior changes. if the axial stress is increased up to 20 MPa. Fig. 4.15, which shows the average values of strain rates from each specimen versus the axial stress. allows a better interpretation of the results. Calculated strain rates are explicitly too small by a stress level of 5 MPa. They are around two orders of magnitude smaller than in the laboratory test. The difference is smaller at a stress level of 10 MPa, but still around one order of magnitude. Strain rates of laboratory tests accord well with the calculated strain rates in the third stress level of 20 MPa.

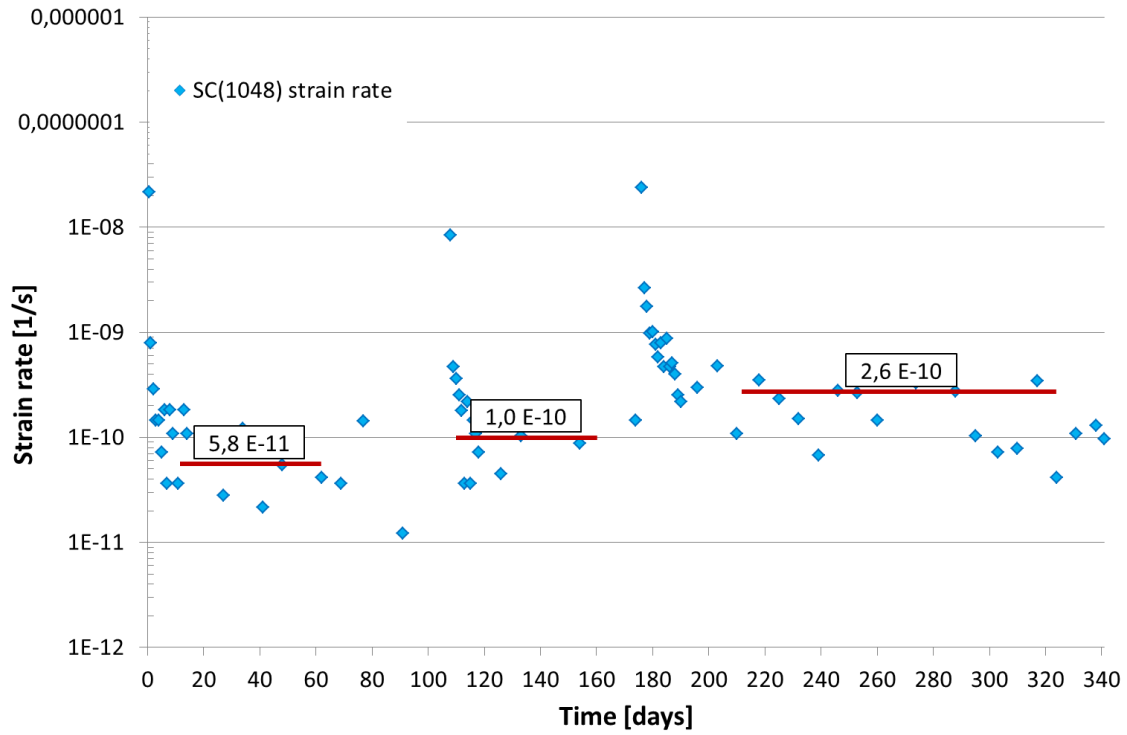


Fig. 4.14 Average determination of strain rates for specimen SC(1048)

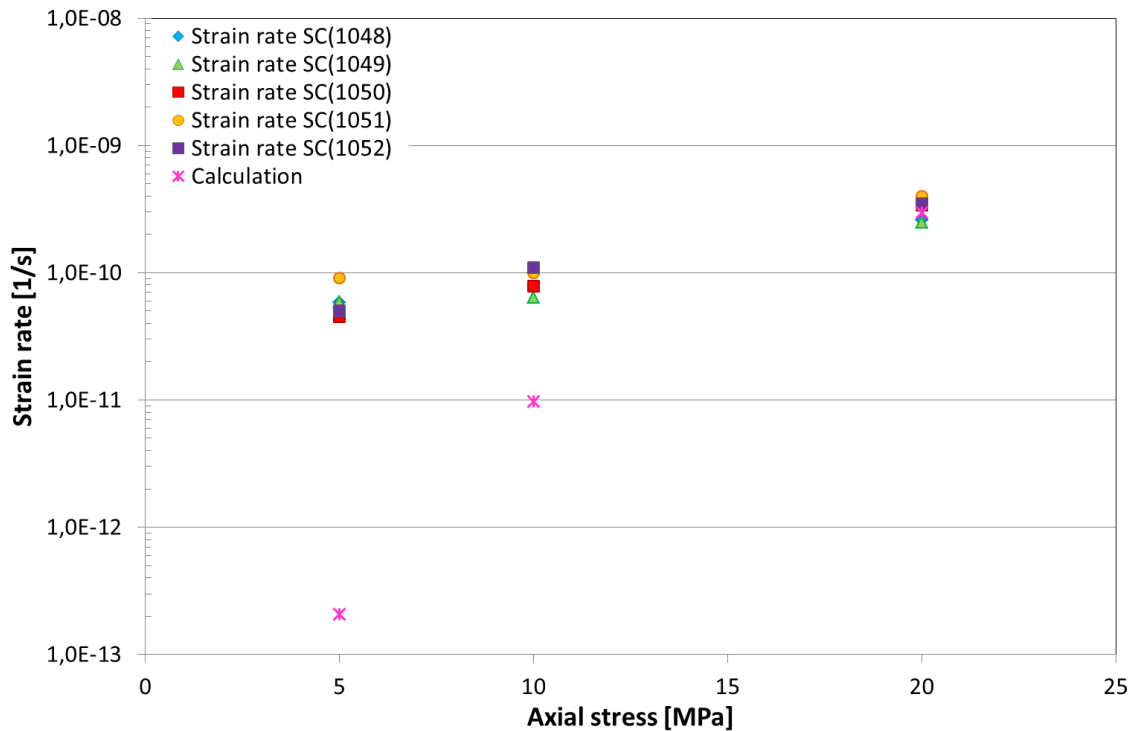


Fig. 4.15 Average strain rates of the various specimen of the laboratory UCc-Test and calculated strain rate using LINEAR ELASTICITY law and DISLOCATION CREEP with a pre-exponential parameter of $0.26e-6$ (creep class 2).

So Exercise UCc 1 shows that a calculation of the deformation behavior of salt concrete analogue to the laboratory tests using HOOKE and DC with one pre-exponential parameter is not possible. The salt concrete shows differences in its deformation behavior dependent to the axial stress. especially if the axial stress increases up to 20 MPa. Additional elastic deformations were not in the right range and deformations from transient creep were not able to reproduce using HOOKE and DC.

In Exercise UCc 2 the same constitutive laws were used similar to the exercise before. But now each stress level was considered for itself so that for each stress level an individual pre-exponential parameter was occupied. In this way a better agreement of strain rates in the first and second stress level should be found.

Table 4.18: Exercise UCc 2 - Active constitutive laws for salt concrete are colored. Changed respectively varied parameters are marked red

LINEAR ELASTICITY	E [MPa]	ν [-]	ϕ_0 [-]		
	10.000	0.18	0.06		
DISLOCATION CREEP	A_A [1/1*MPaⁿ]	Q_A [J/mol]	n [-]		
	varied	54.000	5		
VISCOPLASTICITY	m [-]	A [MPa⁻¹*s]	Q [J/mol]	a_6 [-]	W_d [-]
	-	-	-	-	-
	a_1 [-]	a_2 [-]	a_3 [-]	a_4 [-]	a_5 [-]
	-	-	-	-	-

Fig. 4.16 shows the calculation results of several pre-exponential parameters from $2.08 \cdot 10^{-6}$ (corresponds to creep class 2) up to $66.56 \cdot 10^{-6}$ for the stress level of 5 MPa, only. The selection of the pre-exponential parameter was geared to the end value of strain, which was reached after 106 days, if development of strains from laboratory results and calculations are compared. The pink and green curve shows a good agreement to laboratory results. Because of the discontinuities in the green curve, the pink curve with a pre-exponential parameter of $40.0 \cdot 10^{-6}$ was chosen. The discontinuities in the beginning of the curves results probably from the process of iteration. If the iteration process starts, a balance has to be found.

In the second stress level of 10 MPa the deformations of the specimens of laboratory tests were higher, so lower pre-exponential parameters for calculation were needed in contrast to the stress level of 5 MPa (Fig. 4.17). The gradient is too small for pre-exponential parameters of $0.26 \cdot 10^{-6}$ and $0.52 \cdot 10^{-6}$ and the gradient is too big, if pre-

exponential parameters greater than $1.6 \cdot 10^{-6}$ were used. So a pre-exponential parameter of $1.04 \cdot 10^{-6}$ was chosen for stress level two.

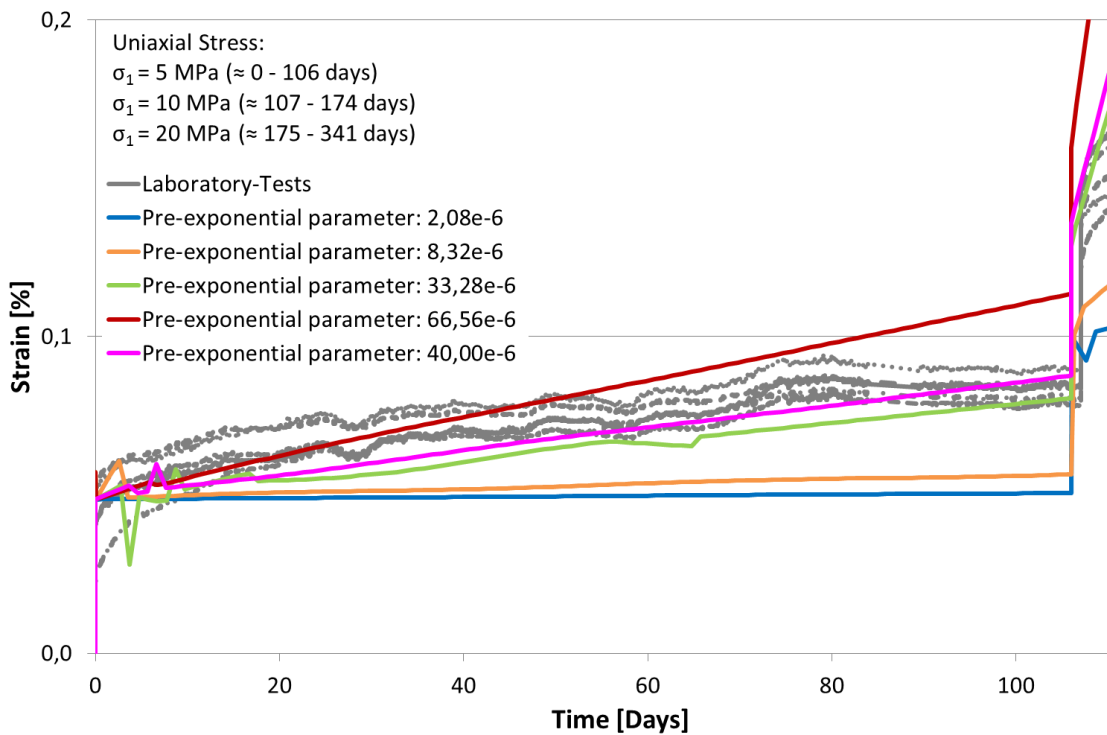


Fig. 4.16 Variation of pre-exponential parameter in first stress level of 5 MPa

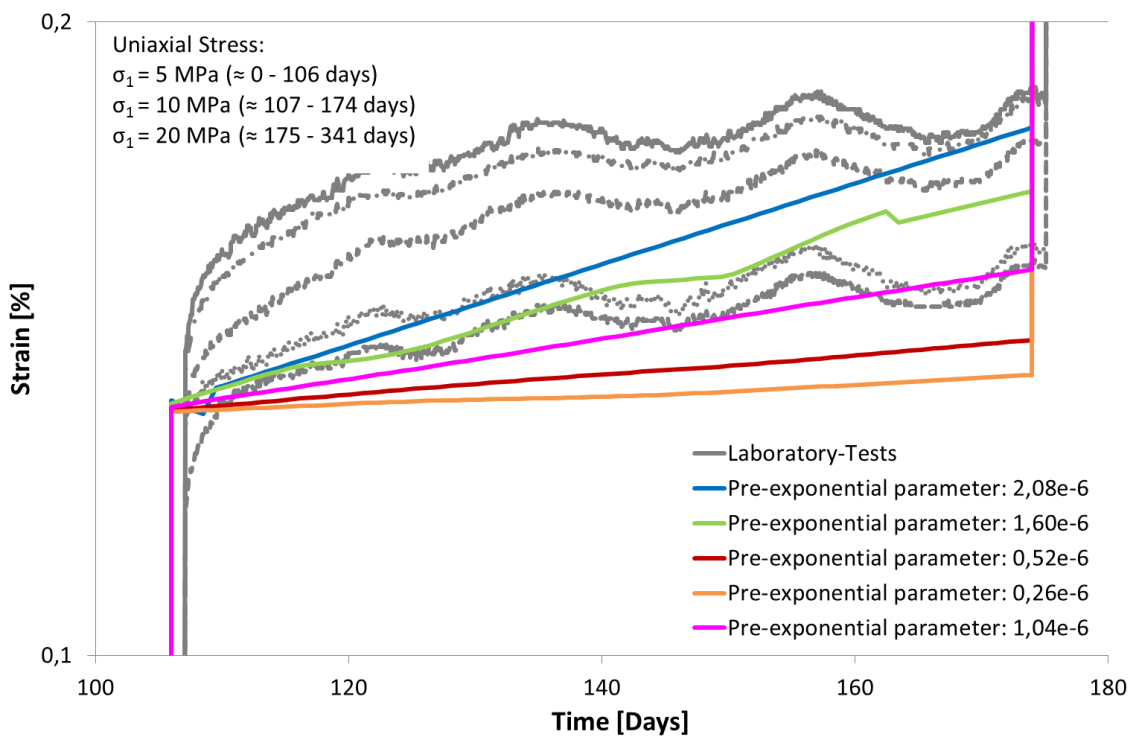


Fig. 4.17 Variation of pre-exponential parameter in second stress level of 10 MPa

The deformations increased significantly, if the axial stress reached a value of 20 MPa. Consequently the pre-exponential parameter had to decrease. For this stress level a pre-exponential parameter of $0.2 \cdot 10^{-6}$ was chosen (Fig. 4.17), because the associated curve approximate well to the gradient of laboratory results.

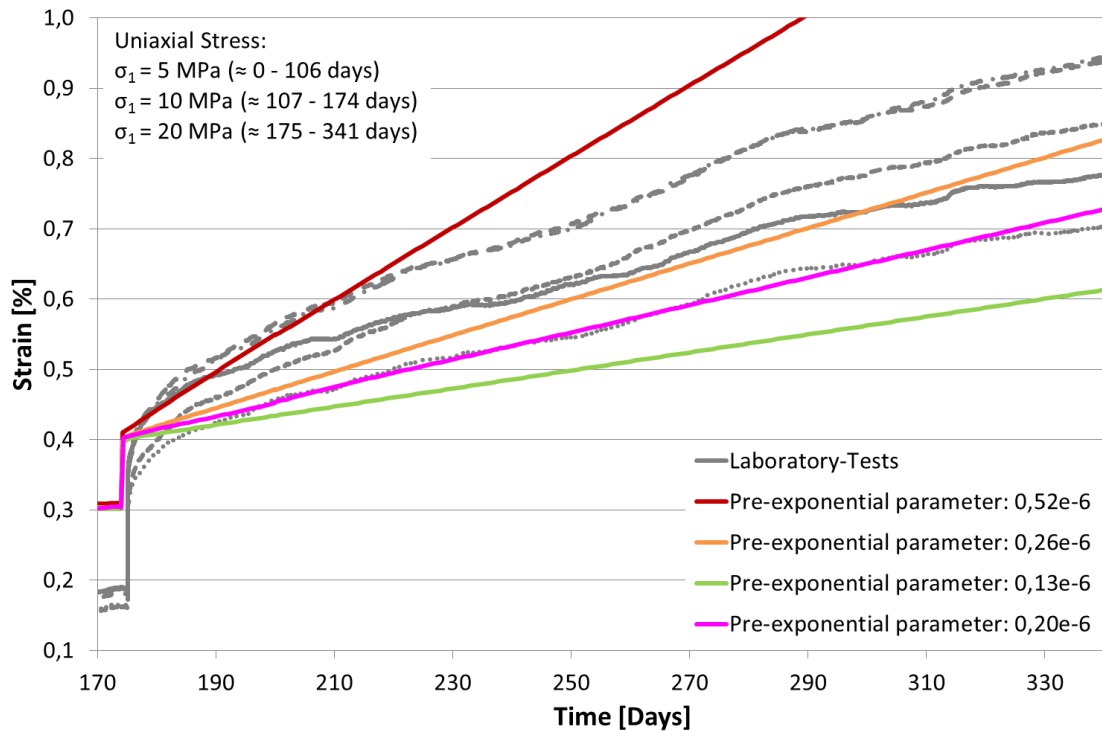


Fig. 4.18 Variation of pre-exponential parameter in third stress level of 20 MPa

After an individual pre-exponential parameter for each stress level was found, all pre-exponential parameters were summarized in one calculation. The development of strains is shown in Fig. 4.19. Here the gradients of the curves of laboratory tests and from calculation are similar. Elastic deformations from calculation accord to laboratory test results in first and second stress level, but are too small in third stress level.

Strain rates are compared in Fig. 4.20. They are in the same range in each stress level for laboratory and calculation results. But in first and second stress level, no constant strain rate were reached.

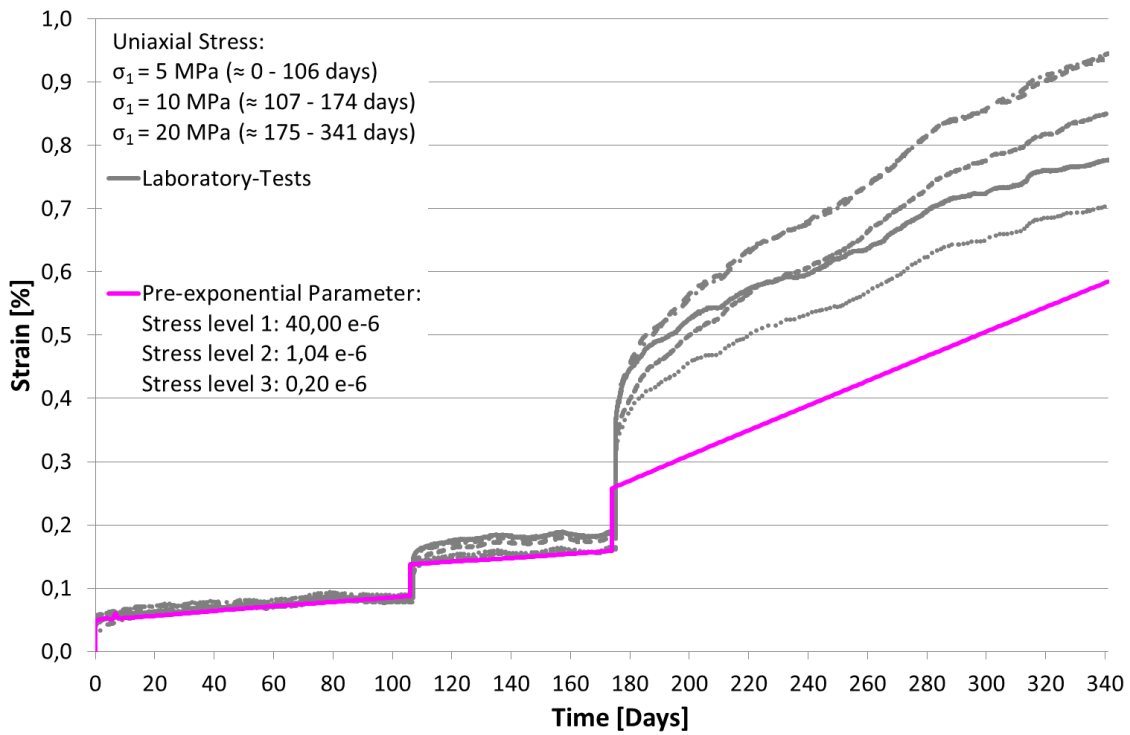


Fig. 4.19 Calculation using an individual pre-exponential parameter for each stress level

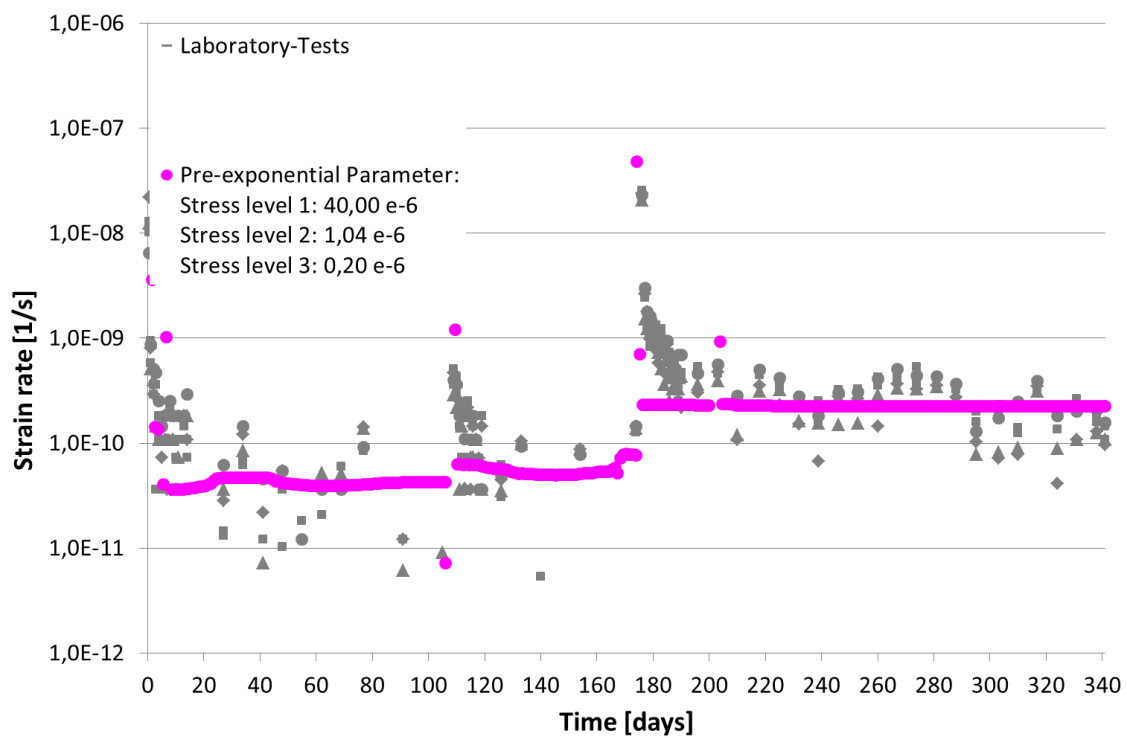


Fig. 4.20 Strain rates for calculation using different pre-exponential parameters in each stress level

Additional calculation results show, that the process of iteration was not stable for all pre-exponential parameters, when the value was between two creep classes. The green curve in Fig. 4.17 clearly shows the respective behavior and the development of strain rates in Fig. 4.20.

Further deficit of Exercise UCc 1 and 2 is that the used constitutive laws were not able to describe transient creep and dilatancy. Therefore, no further application for approach using only HOOKE and DC by different pre-exponential parameters follows.

Finally the comparison between laboratory and calculation results, using HOOKE and DC supports the thesis from simulation of the TC-Test, that a different deformation behavior of the salt concrete is expected, if the stress increases from 10 to 20 MPa. This perception was used for next calculations. Hence further calculations were graduated in two phases:

- Phase 1 describes the deformation behavior for stress levels of 5 MPa and 10 MPa and
- Phase 2 describes deformation behavior at a stress level of 20 MPa.

The description starts with phase 2, due to the connection to the TC-Test calculation results.

Adaptation in phase 2

Until now only HOOKE and DC were used for describing the UCc-Test. But it was not possible to describe transient creep or shear thickening deformations by using only these constitutive laws. Hence the VP will be adapted to phase 2 in the following steps.

The VP, which was used for calculation of the TC-Test, was used in Exercise UCc 3a. The parameters were used for the first calculation, which were defined for the calculation of TC-Test. Additionally only HOOKE was used correspondent to the Exercise TC 2. Used constitutive laws and its parameters are summarized in Tab. 4.19.

Table 4.19: Exercise UCc 3a - Active constitutive laws for salt concrete are colored. Changed respectively varied parameters are marked red

LINEAR ELASTICITY	E [MPa]	ν [-]	ϕ_0 [-]		
	10.000	0.18	0.06		
DISLOCATION	A_A	Q_A [J/mol]	n [-]		

CREEP	[1/1*MPa ⁿ]				
	-	-	-		
VISCOPLASTICITY	m [-]	A [MPa ⁻¹ *s]	Q [J/mol]	a ₆ [-]	W _d [-]
	8	5*10 ⁻⁹	54.000	0.0	3.5
	a ₁ [-]	a ₂ [-]	a ₃ [-]	a ₄ [-]	a ₅ [-]
	2.05	0.0	2.5	0.0	0.02

The elastic deformation at the first stress level is in the right range, but there are no viscoplastic deformations. In second stress level elastic deformations are too small and viscoplastic deformations too high (Fig. 4.23). In the third stress level strains are clearly too high and reach values higher than 25 % (Fig. 4.21). The development of porosity is able to differ between transient creep deformations and the dilatancy induced deformations. Fig. 4.22 shows, that porosity slightly decrease in second stress level and clearly increase in third stress level. Transient creep generated deformations in the second stress level because the decreasing porosity indicates, that the specimen was compacted. Deformations in third stress level were generated by dilatancy, because the volume of the specimen increased. This supports the assumption of a different deformation behavior in phase 1 and phase 2. So in further calculations only the third stress level (correspond to phase 2) was considered. Phase 1 will then be considered in the next section.

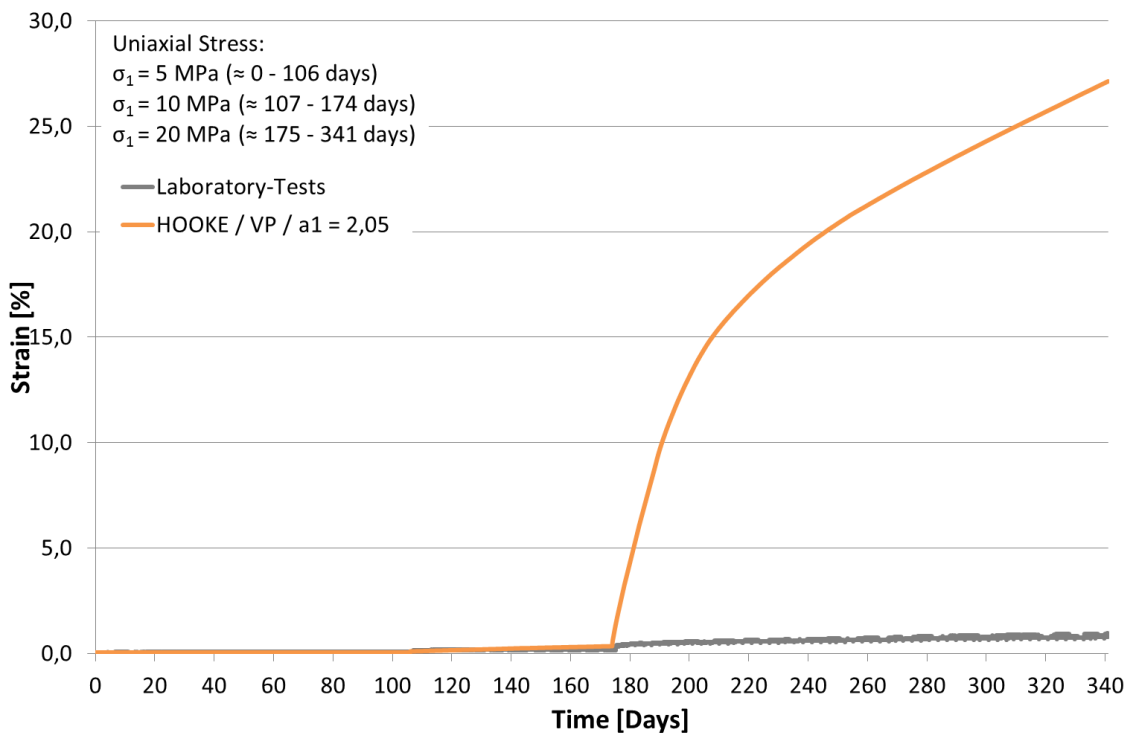


Fig. 4.21 Calculation of the UCc-Test using the LINEAR ELASTICITY law and VISCOPLASTICITY model with parameters of Exercise TC 2

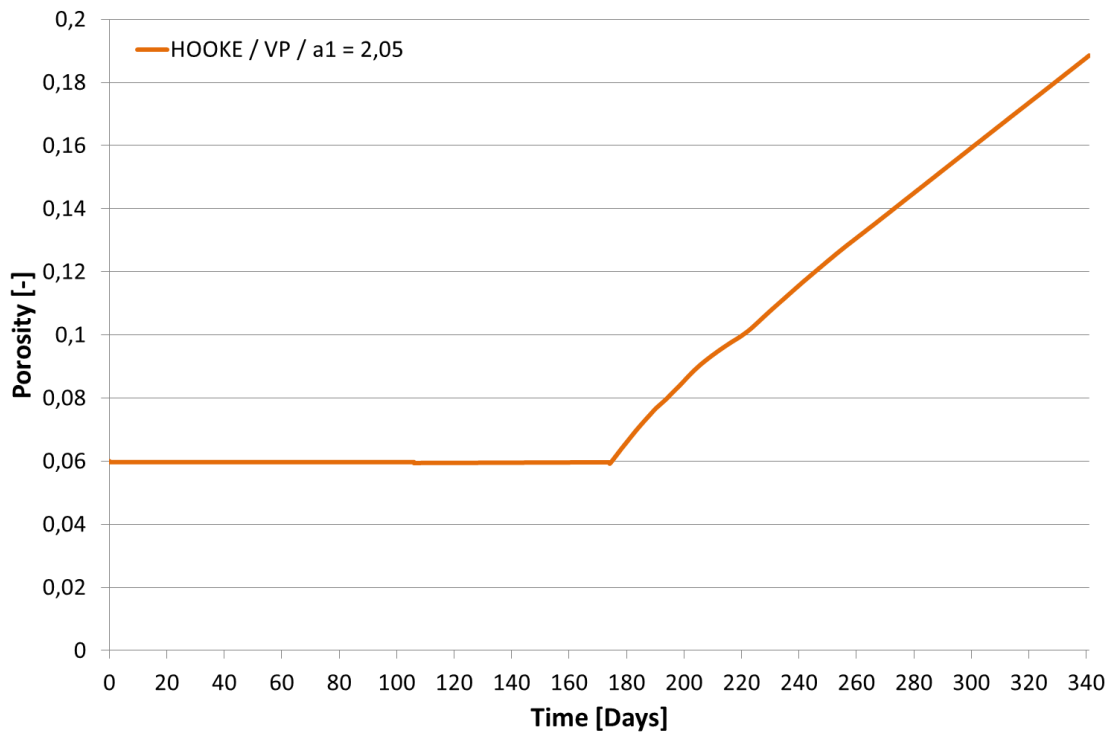


Fig. 4.22 Development of porosity using the LINEAR ELASTICITY law and VISCOPLASTICITY model with parameters of Exercise TC 2

Because the parameters analogue to TC-Test were not suitable for simulating the UCc-Test, the parameter a_1 for the stability of the material and a_2 , a_4 and a_6 for limiting of volumetric strain were varied in Exercise UCc 3b.

Table 4.20: Exercise UCc 3b - Active constitutive laws for salt concrete are colored. Changed respectively varied parameters are marked red

LINEAR ELASTICITY	E [MPa]	ν [-]	ϕ_0 [-]		
	10.000	0.18	0.06		
DISLOCATION CREEP	A_A [1/1*MPaⁿ]	Q_A [J/mol]	n [-]		
	-	-	-		
VISCOPLASTICITY	m [-]	A [MPa⁻¹*s]	Q [J/mol]	a_6 [-]	W_d [-]
	8	$5 \cdot 10^{-9}$	54.000	0.02	3.5
	a_1 [-]	a_2 [-]	a_3 [-]	a_4 [-]	a_5 [-]
	varied	1.8	2.5	0.7	0.02

At first volumetric deformations were limited again. Values of parameter a_2 , a_4 and a_6 were used correspondent to Tab. 4.13. Deformations became smaller in this way, but especially in third stress level they were still too big (Fig. 4.23, purple curve). The porosity increased around 1 % in the third stress level (Fig. 4.24).

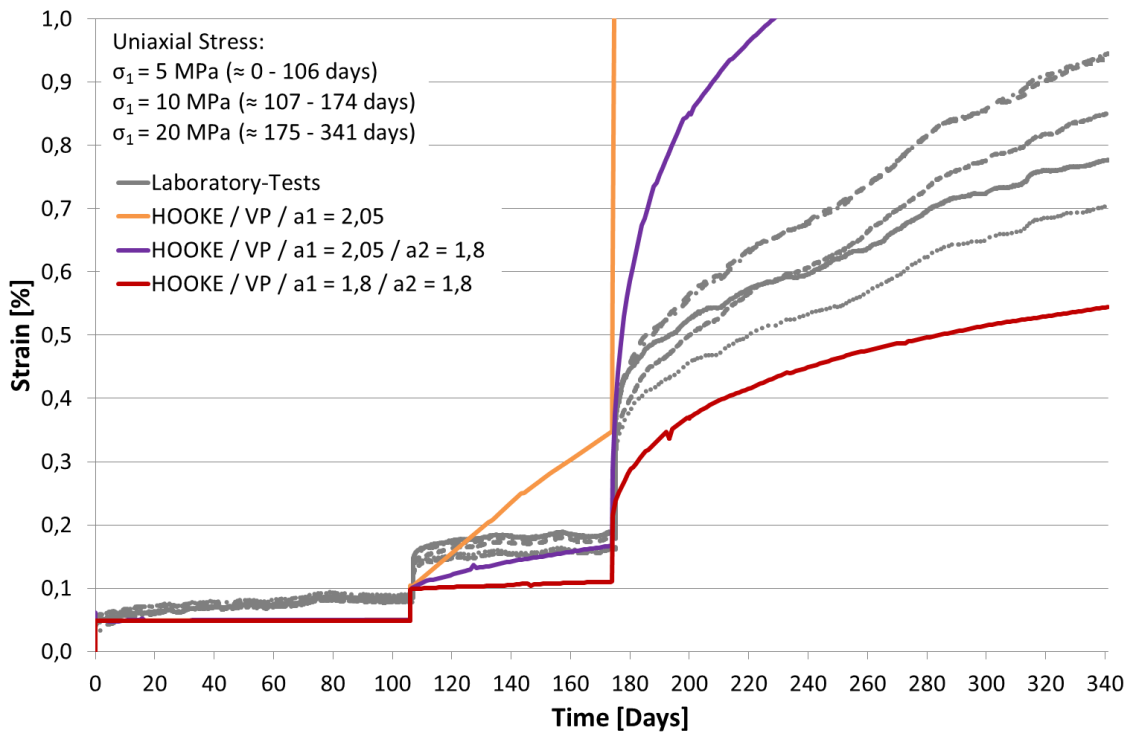


Fig. 4.23 Exercise UCc 3a-b - Variation of parameter a_1 and a_2 plus variation of the pre-exponential parameter (PP)

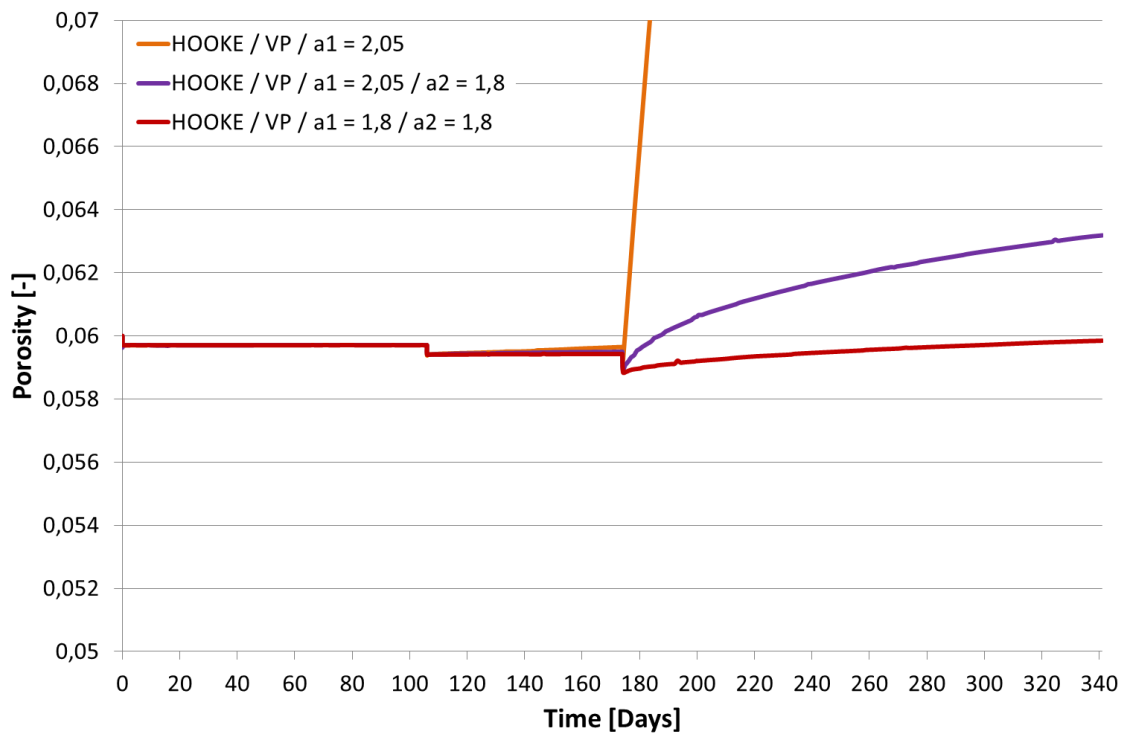


Fig. 4.24 Exercises UCc 3a-b - Development of porosity for calculations in phase2

It was expected, that during calculation dilatancy was still too high by an axial stress of 20 MPa with respect to the laboratory results. Hence dilatancy was limited using a_1

equal to 1.8. Now deformations in third stress level became smaller (red curve in Fig. 4.25) and were located below the deformations of the laboratory test. The increase of porosity was clearly smaller now, Fig. 4.26.

Correspondent to laboratory results a combination of viscoplastic deformations and stationary creep is expected by an axial stress level of 20 MPa. Hence, in Exercise UCc 3c stationary creep was considered by DC using the pre-exponential parameter of $0.2 \cdot 10^{-6}$ analogue to the individual adaptation in third stress level in Exercise UCc 2.

Table 4.21: Exercise UCc 3c - Active constitutive laws for salt concrete are colored. Changed respectively varied parameters are marked red

LINEAR ELASTICITY	E [MPa]	ν [-]	ϕ_0 [-]		
	10.000	0.18	0.06		
DISLOCATION CREEP	A_A [1/1*MPaⁿ]	Q_A [J/mol]	n [-]		
	varied	54.000	5		
VISCOPLASTICITY	m [-]	A [MPa⁻¹*s]	Q [J/mol]	a_6 [-]	W_d [-]
	8	$5 \cdot 10^{-9}$	54.000	0.02	3.5
	a_1 [-]	a_2 [-]	a_3 [-]	a_4 [-]	a_5 [-]
	1.8	1.8	2.5	0.7	0.02

Now the gradient of the curve was too steep (Fig. 4.25, blue curve). The difference of the gradient between this calculation and Exercise UCc 2 could result from the additionally viscoplastic deformations here. This means, that by using DC and VP for calculation a smaller pre-exponential parameter has to be used. Below a pre-exponential parameter equal to $0.065 \cdot 10^{-6}$ was used. The green curve shows a good agreement to laboratory test in curvature and gradient in the lower sector of laboratory tests (Fig. 4.25). Additionally the porosity increased in third stress level (Fig. 4.26), which supports, that the onset of dilatancy occurred first by an axial stress of 20 MPa.

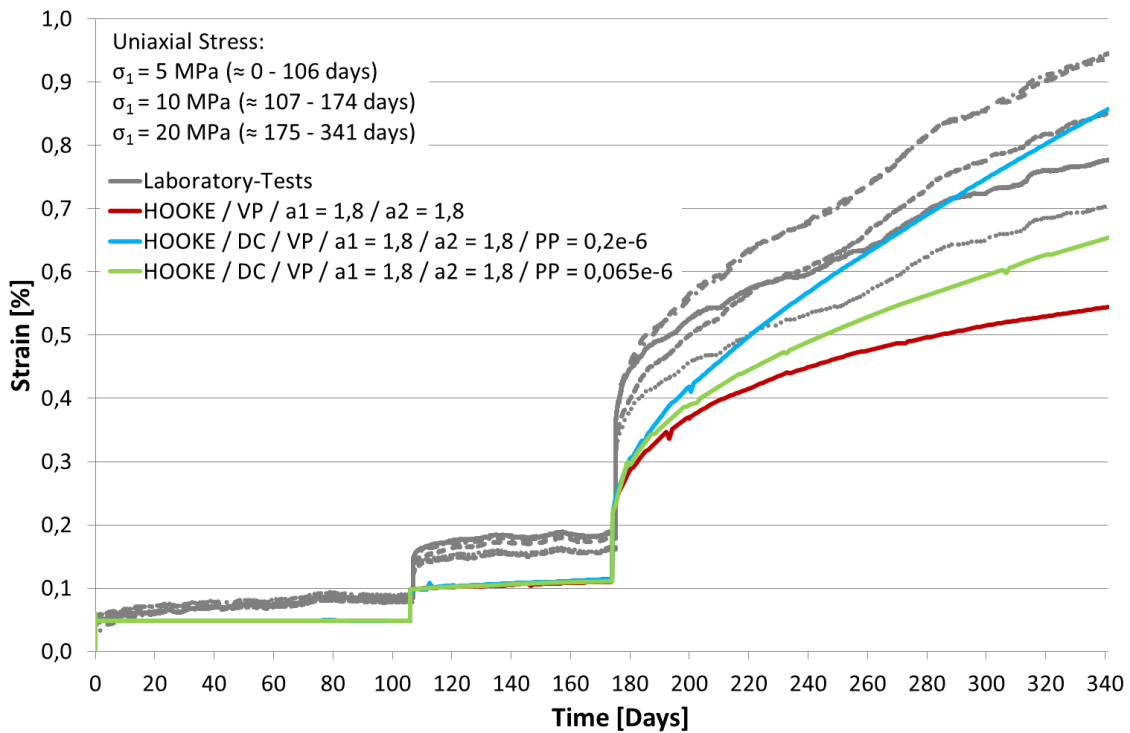


Fig. 4.25 Exercise UCc 3c - Variation of parameter a_1 and a_2 plus variation of the pre-exponential parameter (PP) by using LINEAR ELASTIC LAW, DISLOCATION CREEP law and VISCOPLASTICITY model

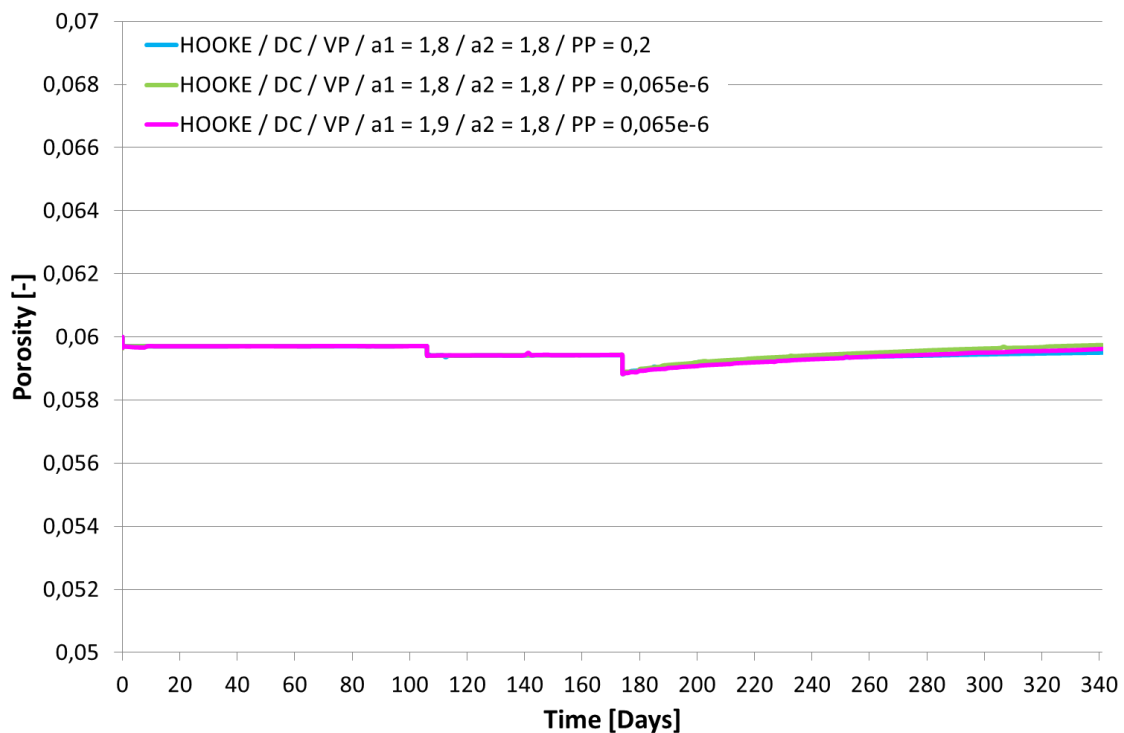


Fig. 4.26 Exercises UCc 3c-d - Development of porosity for calculations in phase2

Probably volumetric deformation could be higher against the result of the parameter combination from Exercise UCc 3c (green curve). Hence parameter a_1 was increased to 1.85 and 1.9 in the following Exercise UCc 3d.

Table 4.22: Exercise UCc 3d - Active constitutive laws for salt concrete are colored. Changed respectively varied parameters are marked red

LINEAR ELASTICITY	E [MPa]	ν [-]	ϕ_0 [-]		
	10.000	0.18	0.06		
DISLOCATION CREEP	A_A [1/1*MPaⁿ]	Q_A [J/mol]	n [-]		
	0.065e ⁻⁶	54.000	5		
VISCOPLASTICITY	m [-]	A [MPa⁻¹*s]	Q [J/mol]	a_6 [-]	W_d [-]
	8	5*10 ⁻⁹	54.000	0.02	3.5
	a_1 [-]	a_2 [-]	a_3 [-]	a_4 [-]	a_5 [-]
	varied	1.8	2.5	0.7	0.02

Calculations results show that deformations increase using higher values of a_1 . The sector of laboratory results is well covered by using a_1 from 1.8 up to 1.9. The curve for a_1 equal to 1.8 is located in the lower sector and for a_1 equal to 1.9 in the upper sector. The results are showed in Fig. 4.27.

Additionally strain rates reached a similar range than in the laboratory tests (Fig. 4.28). The nomenclature of the strain rates results from the discontinuities, which are shown in the development of strains in Fig. 4.27. For an exponential smoothing of the curves an adaptation of the iteration steps is necessary. This adaptation will follow in the end of UCc-Test simulation, because here the development of strain and strains rates was only considered quantitatively here (not shown in the figures).

The development of porosity shows for all calculations that the porosity increases in third stress level. So there is an interaction of elastic deformations, transient and stationary creep and dilatancy. This correlates to assumptions from laboratory tests.

The finally used parameters for calculation of UCc-Test in the third stress level are summarized in Tab. 4.26 in the end of the chapter.

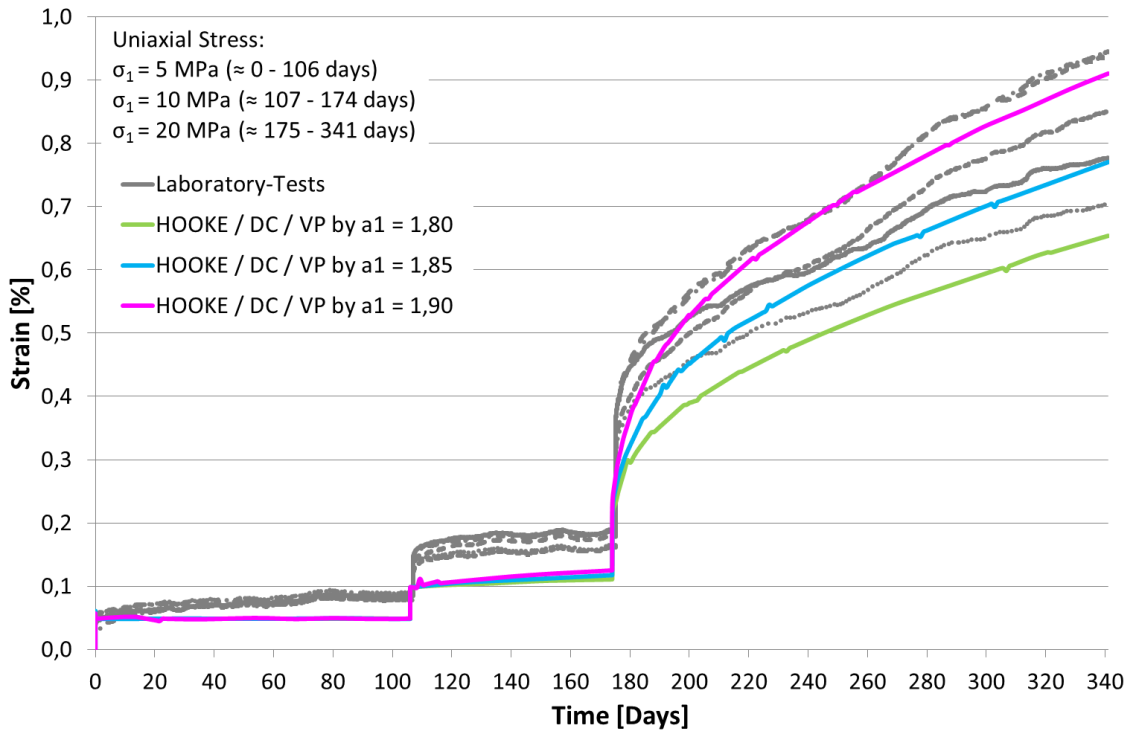


Fig. 4.27 Depiction of the deformation behavior by considering LINEAR ELASTICITY LAW, DISLOCATION CREEP law and VISCOPLASTICITY model after Exercise UCc 3d

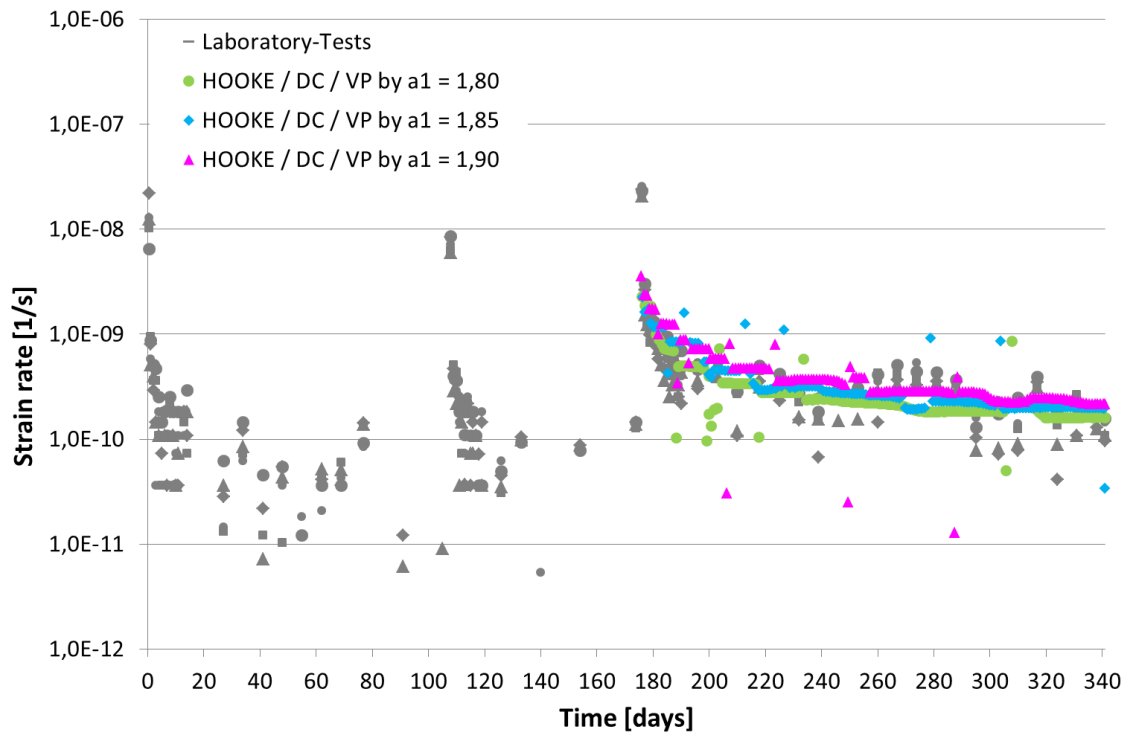


Fig. 4.28 Strains rates in third stress level using parameters of Exercise UCc 3d

Adaptation in phase 1

Now the parameters of VP were adapted to the first and second stress level. Laboratory tests showed that in this phase transient creep is expected. But with using parameters correspondent to Exercise UCc 3, a transient creep behavior could not be reproduced in phase 1. Therefore, the influence of three parameters – viscosity, material stability and volumetric extension – to transient creep behavior was investigated.

In Exercise UCc 4a the influence of viscosity A to transient creep was investigated. The pre-exponential parameter was equal to $0.2 \cdot 10^{-6}$, correspondent to the results of Exercise UCc 2. It was chosen from the third stress level, because investigations before have showed, that only in phase 2 stationary creep can be expected. Deformations in phase 1 occurred probably by elastic deformations and transient creep, so that the pre-exponential parameter has no influence to the evolution of deformations in phase 1. Additional a_1 was set to 1.33 as in Exercise TC 2 because onset of dilatancy should be excluded.

Table 4.23: Exercise UCc 4a - Active constitutive laws for salt concrete are colored. Changed respectively varied parameters are marked red.

LINEAR ELASTICITY	E [MPa]	ν [-]	ϕ_0 [-]		
	10.000	0.18	0.06		
DISLOCATION CREEP	A_A [1/1*MPaⁿ]	Q_A [J/mol]	n [-]		
	0.2e ⁻⁶	54.000	5		
VISCOPLASTICITY	m [-]	A [MPa⁻¹*s]	Q [J/mol]	a_6 [-]	W_d [-]
	8	varied	54.000	0.02	3.5
	a_1 [-]	a_2 [-]	a_3 [-]	a_4 [-]	a_5 [-]
	1.33	1.8	2.5	0.7	0.02

Viscosity was set to $5.0 \cdot 10^{-9}$ 1/s in first calculations correspondent to [Wie10]. The results in Fig. 4.29 show, that only elastic deformations and stationary creep in the third stress level occur (orange curve). This means, that the chosen viscosity is too high for simulating transient creep deformations. Fig. 4.30 shows the development of porosity. Porosity decreases at each increase of stress for this calculation, so that no onset of dilatancy occurred.

Viscosity was increased for next calculation to $5.0 \cdot 10^{-1}$ 1/s and thus deformations increased clearly. The blue curve shows deformations similar to transient creep in all stress levels, but deformations were clearly too high. The porosity increases at second

stress level. Hence, transient creep and dilatancy deformation occur, when viscosity is increased.

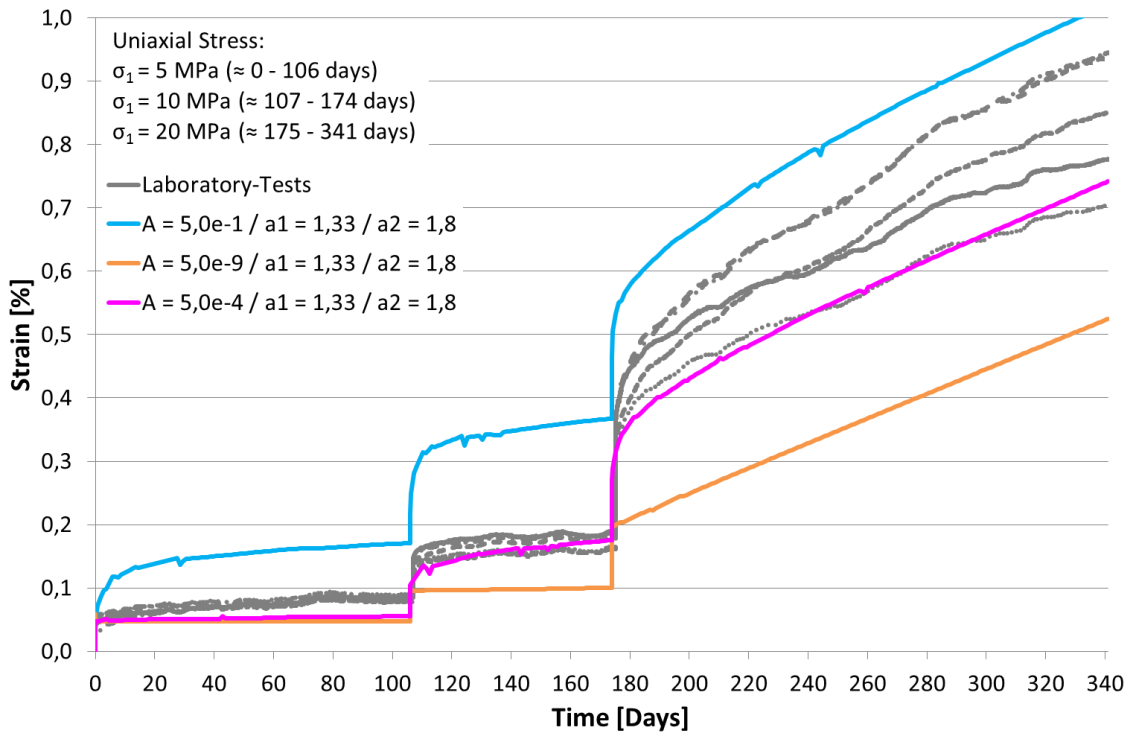


Fig. 4.29 Exercise UCc 4a - Variation of viscosity (A)

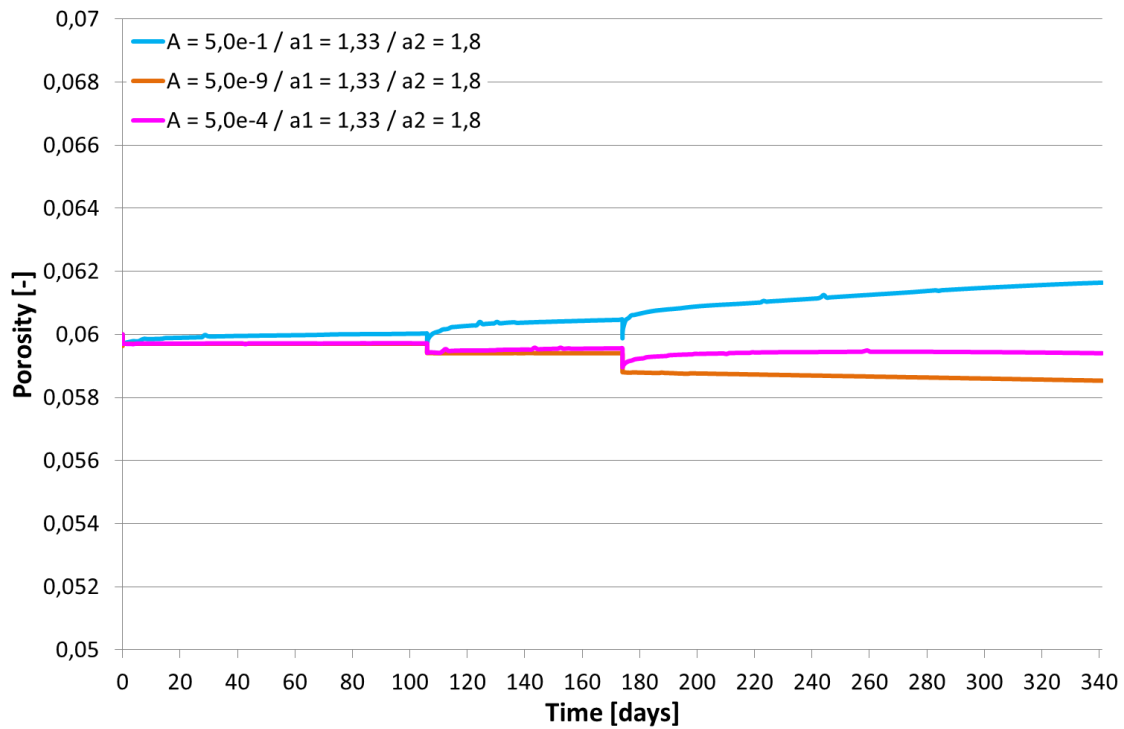


Fig. 4.30 Exercise UCc 4a - Development of porosity by varying viscosity (A)

Hence viscosity was decreased again to $5.0 \cdot 10^{-4}$ 1/s. The results show, that transient creep occurred in second stress level, but not in the first one. Porosity increased rarely in second stress level. Elastic deformations are similar to the elastic deformations of laboratory test. So a viscosity of $5.0e^{-4}$ 1/s was chosen for the next calculations. A better adaptation should be found by variation of parameters for stability of the material and volumetric strains in following exercises.

The peaks in blue and pink curve could occur because the process of iteration was not stable at that point. An adaptation of the steps of iteration would be necessary. But the considerations were only quantitative here and the results are not final. So an adaptation of iteration's steps follows later only for the final results.

In Exercise UCc 4b parameters were used correspondent to Exercise UCc 4a. But a_1 was increased for a better adaptation of the deformations from transient creep. By increasing a_1 the material stiffness decreased and allowed creep deformations at smaller stress levels.

Table 4.24: Exercise UCc 4b - Active constitutive laws for salt concrete are colored. Changed respectively varied parameters are marked red.

LINEAR ELASTICITY	E [MPa]	ν [-]	ϕ_0 [-]		
	10.000	0.18	0.06		
DISLOCATION CREEP	A_A [1/1*MPaⁿ]	Q_A [J/mol]	n [-]		
	$0.2e^{-6}$	54.000	5		
VISCOPLASTICITY	m [-]	A [MPa^{1*s}]	Q [J/mol]	a_6 [-]	W_d [-]
	8	$5.0e^{-4}$	54.000	0.02	3.5
	a_1 [-]	a_2 [-]	a_3 [-]	a_4 [-]	a_5 [-]
	varied	1.8	2.5	0.7	0.02

Results are shown in Fig. 4.31 and the development of porosity in Fig. 4.32. The pink curve shows the calculation result from Exercise UCc 4a using a_1 equal to 1.33. Next calculation was executed using a_1 equal to 1.6 (brown curve). If the material becomes less stiff, deformations increase. But now strains were clearly too high in all stress levels. Consideration of development of porosity shows, that additionally to transient creep shear thickening deformations developed.

Hence an a_1 equal to 1.5 was used (blue curve). The development of strains in first stress level, especially the curvature in the curve, which describes the transient creep,

could be described. Strains in second stress level were too high, additional the porosity increased. So there are shear thickening deformations, too.

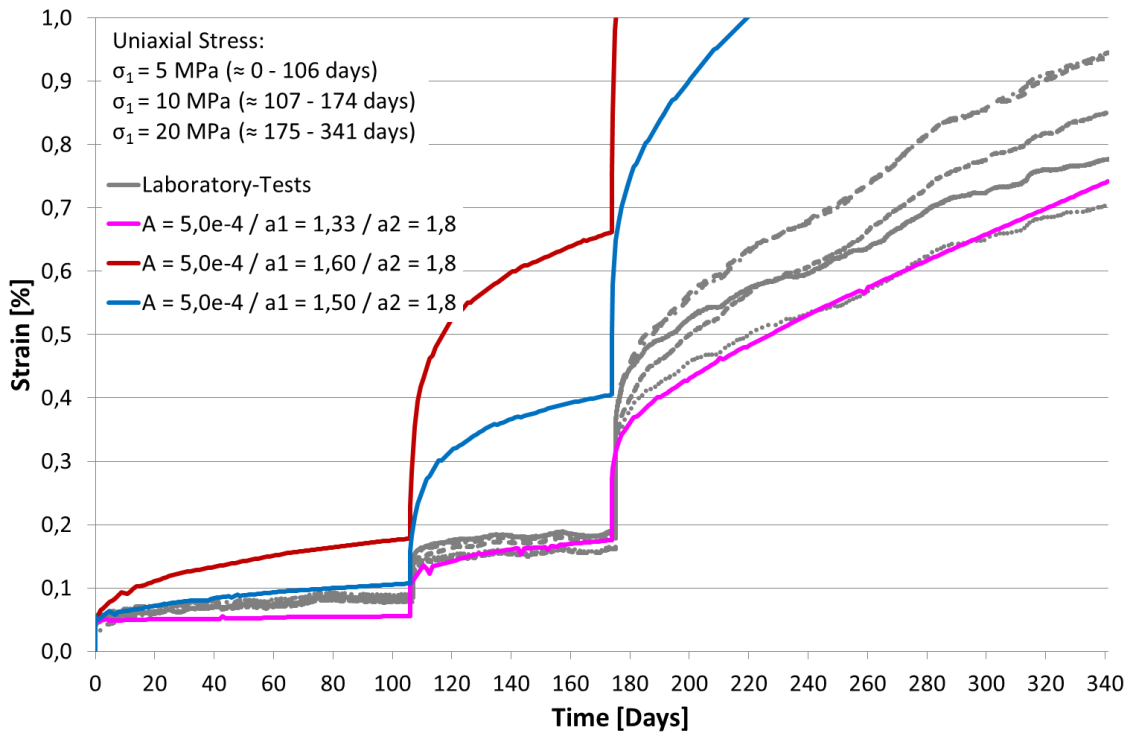


Fig. 4.31 Exercise UCc 4b - Variation of parameter a1

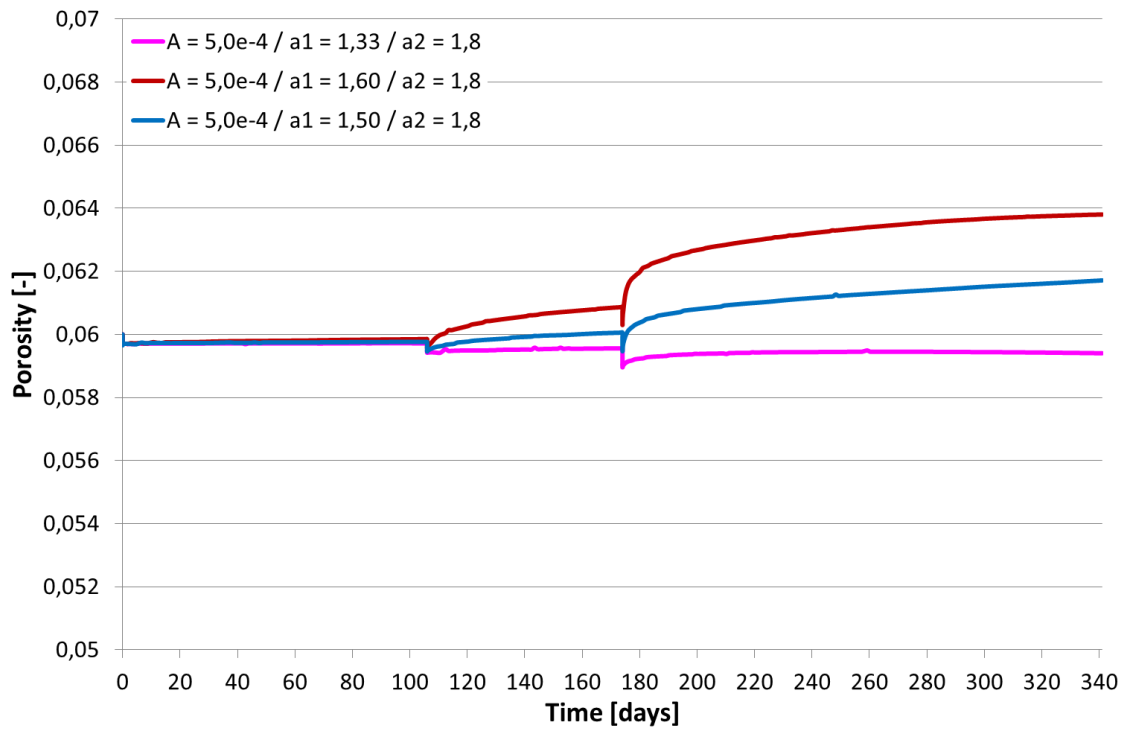


Fig. 4.32 Exercise UCc 4b - Development of porosity

In Exercise UCc 4c volumetric strains have to be limited because strains were still too high and porosity increased in second stress level. Hence, a_2 was varied for limiting the volumetric extension.

Table 4.25: Exercise UCc 4c - Active constitutive laws for salt concrete are colored. Changed respectively varied parameters are marked red

LINEAR ELASTICITY	E [MPa]	ν [-]	ϕ_0 [-]		
	10.000	0.18	0.06		
DISLOCATION CREEP	A_A [1/1*MPa ⁿ]	Q_A [J/mol]	n [-]		
	$0.2e^{-6}$	54.000	5		
VISCOPLASTICITY	m [-]	A [MPa ⁻¹ *s]	Q [J/mol]	a_6 [-]	W_d [-]
	8	$5.0e^{-4}$	54.000	0.02	3.5
	a_1 [-]	a_2 [-]	a_3 [-]	a_4 [-]	a_5 [-]
	1.5	varied	2.5	0.7	0.02

As before, the blue curve in Fig. 4.33 shows calculation result equivalent to Exercise UCc 4b. Below the volumetric strains were limited by increasing a_2 . If a_2 equal to 2.5 was used, strains are similar to laboratory results in first stress level (violet curve). But strains are still too high in second stress level. So a_2 was increased to 3.0 (green curve). Now the development of strains in first and second stress level is similar to laboratory results.

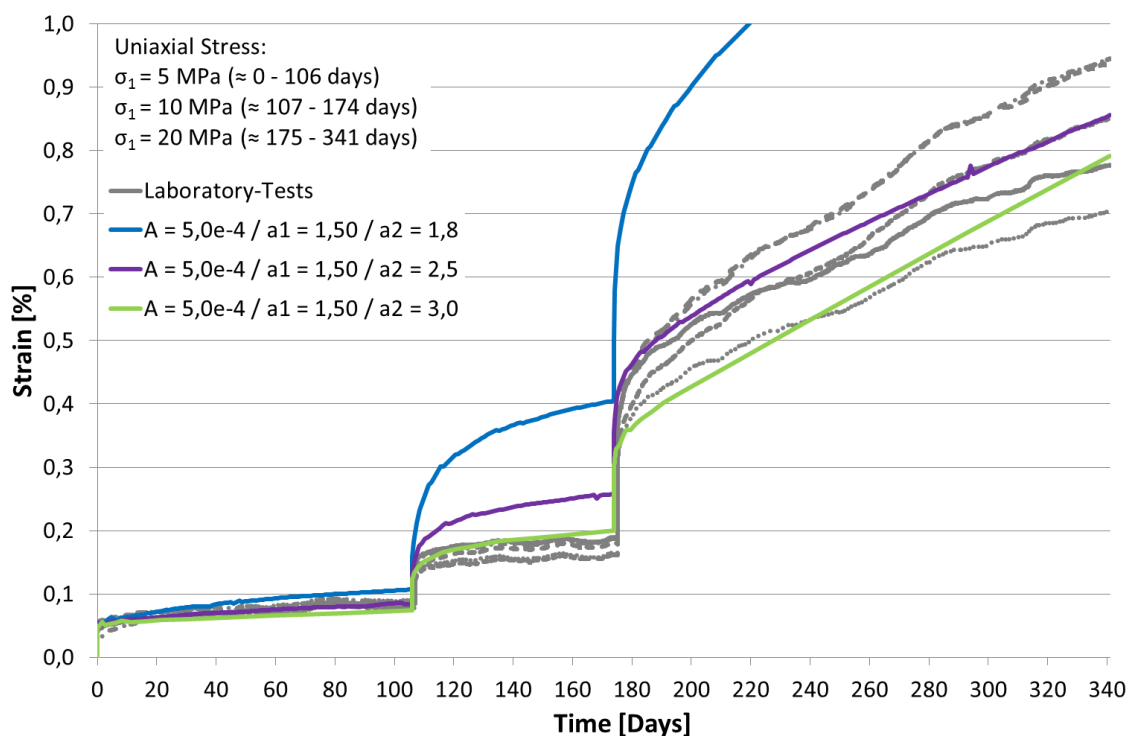


Fig. 4.33 Exercise UCc 4c - Variation of parameter a_2

Additionally porosity did not increase in first and marginal in second stress level (Fig. 4.34). So the part of shear thickening deformations is very small in phase 1 and is in an acceptable range for numerical calculations. In consideration of phase 2 can be seen, that elastic deformations as soon as, transient and stationary creep are in a similar range as in laboratory results. Porosity increased in the beginning of the third stress level, but decreased from 200 days again. So shear thickening deformations are also very small in this phase.

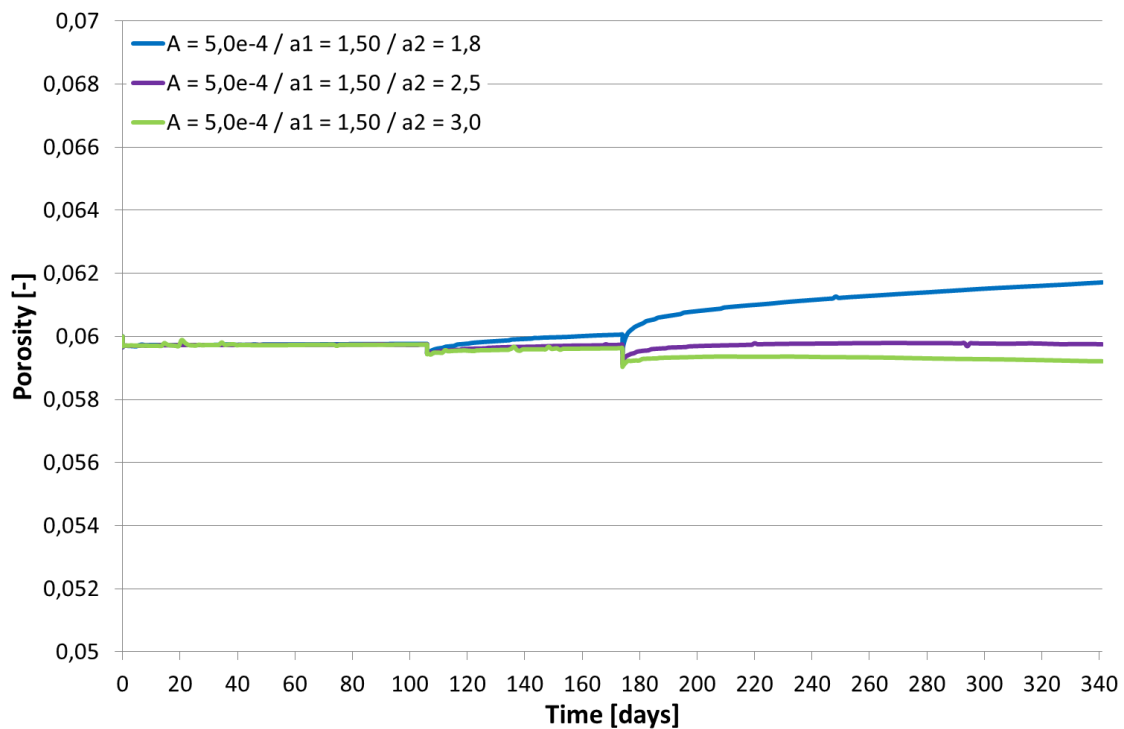


Fig. 4.34 Exercise UCc 4c - Development of porosity

In the sections before parameters for an adaptation in phase 1 and phase 2 were found. But the investigations showed that there was no combination of parameters, which were able to describe the behavior at all stress levels.

Hence the parameters of phase 1 and phase 2 were combined in this Exercise UCc 5. In first and second stress level, parameters of phase 1 were used, in third stress level parameters of phase 2. Tab. 4.26 summarizes all constitutive laws and used parameters of phase 1 and phase 2.

Table 4.26: Exercise UCc 5 - Active constitutive laws for salt concrete are colored. Changed respectively varied parameters are marked red

LINEAR ELASTICITY (Phase 1 / 2)	E [MPa]	ν [-]	ϕ_0 [-]		
	10.000	0.18	0.06		
DISLOCATION CREEP (Phase 1)	A_A [1/1*MPaⁿ]	Q_A [J/mol]	n [-]		
	0.2e ⁻⁶	54.000	5		
DISLOCATION CREEP (Phase 2)	A_A [1/1*MPaⁿ]	Q_A [J/mol]	n [-]		
	0.065e ⁻⁶	54.000	5		
VISCOPLASTICITY (Phase 1)	m [-]	A [MPa⁻¹*s]	Q [J/mol]	a₆ [-]	W_d [-]
	8	5.0e ⁻⁴	54.000	0.02	3.5
	a₁ [-]	a₂ [-]	a₃ [-]	a₄ [-]	a₅ [-]
	1.5	3.0	2.5	0.7	0.02
VISCOPLASTICITY (Phase 2)	m [-]	A [MPa⁻¹*s]	Q [J/mol]	a₆ [-]	W_d [-]
	8	5.0e ⁻⁹	54.000	0.02	3.5
	a₁ [-]	a₂ [-]	a₃ [-]	a₄ [-]	a₅ [-]
	1.9	1.8	2.5	0.7	0.02

The result of the combined constitutive laws is shown by the pink curve in Fig. 4.35. Its development corresponds well to the development of stains of the laboratory test. Probably strain rates could be a little bit too small in first stress level and a little bit too high in second stress level.

Additional the individual deformation components are shown in Fig. 4.35. If the calculation was executed only by HOOKE, there are only elastic deformations at the moment of increasing axial stress and no further deformations until the next increase of axial stress followed. Below HOOKE was combined with transient creep by using the VP with parameters analogue to phase 1. Now there are transient creep deformations in all stress levels. Strains increase fast in the beginning after increasing axial stress. Strain rates decrease gradually and consequently strains increase less with further interval to load increase. This phenomenon is clearly to see in phase 2.

In the next step DC was used additionally to HOOKE and VP. The development in phase 1 is nearly identical to the calculation before. Stationary creep is of less importance in stress levels up to 10 MPa. In third stress level stationary creep becomes relevant. The curve increases and strains increase constant. This corresponds to the assumptions from laboratory results.

All components of deformation are pictured by the pink curve, which was described in the beginning of this section. The components – elastic deformations, transient and stationary creep as soon as dilatancy – are considered by using the combined parameters of phase 1 and phase 2.

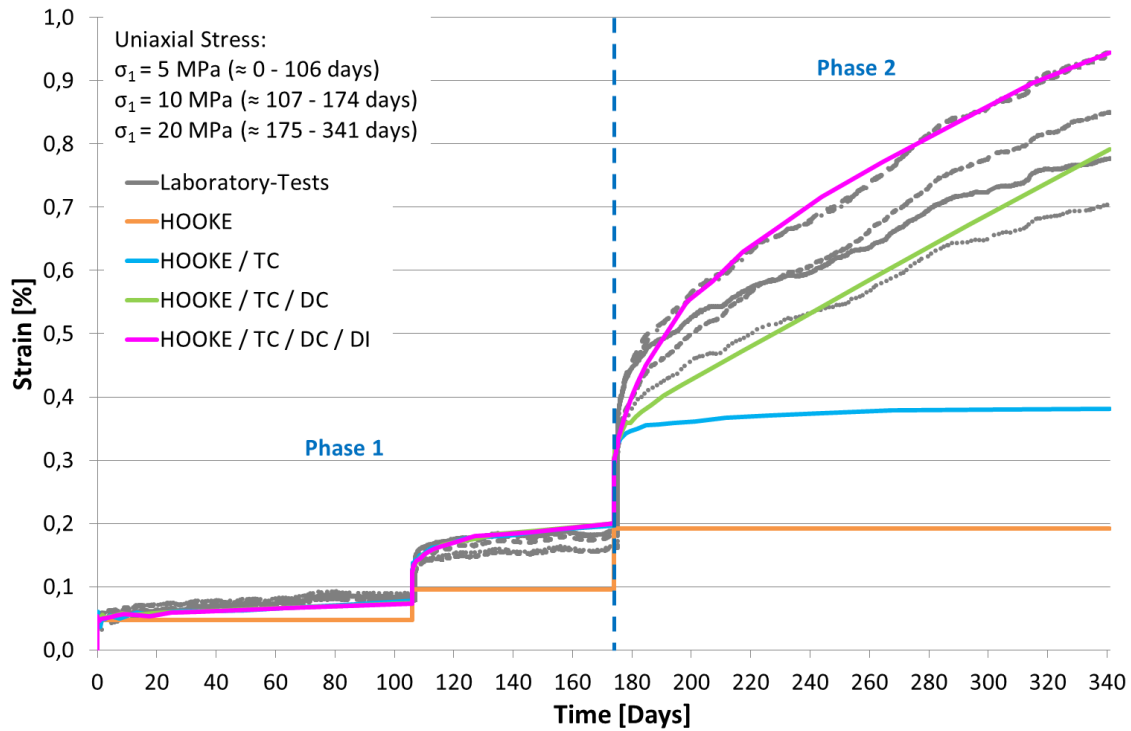


Fig. 4.35 Depiction of the deformation components, which results of the parameter variations before and the combination of adaptation in phase 1 and phase 2. Deformations consist of elastic deformations (HOOKE), transient creep (TC), dislocation creep (DC) and dilatancy (DI)

The development of strain rates is shown in Fig. 4.36 versus time and in Fig. 4.37 versus axial strain. Both figures show the development of strain rates resulting from the individual deformations components correspondent to Fig. 4.35.

If linear elastic and transient creep deformations were combined (using HOOKE and VP with parameters from phase 1), strain rates are high in the beginning after increasing axial stress and become smaller gradually (Fig. 4.36). Two values of strain rate are clearly too small in the first stress level. Probably this might be a problem of iteration, because the curve in Fig. 4.35 has a small break at this moment. This deviation dissolves in further calculations by using more constitutive models. Generally strain rates are in the right range for phase 1. In phase 2 strain rates are too small, because stationary creep and dilatancy were not considered yet. Fig. 4.37 shows the same circum-

stances: Strain rates are in the right range for phase 1, but are clearly too small in phase 2. Consequently strains are too small.

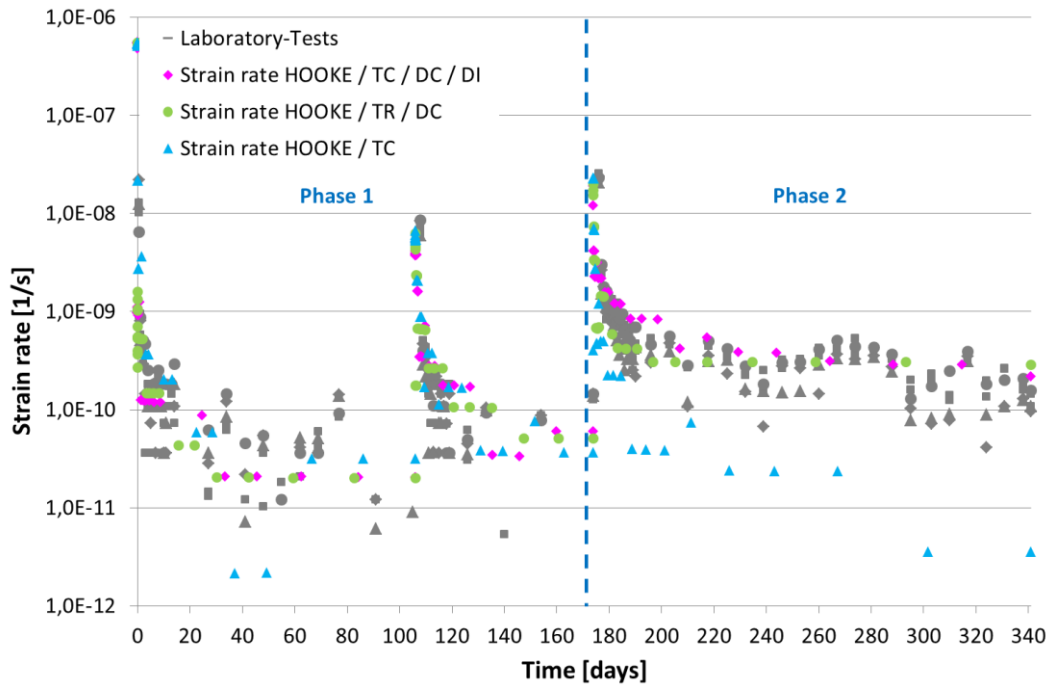


Fig. 4.36 Exercise UCc5 - Comparison between strain rates of laboratory tests and calculation results

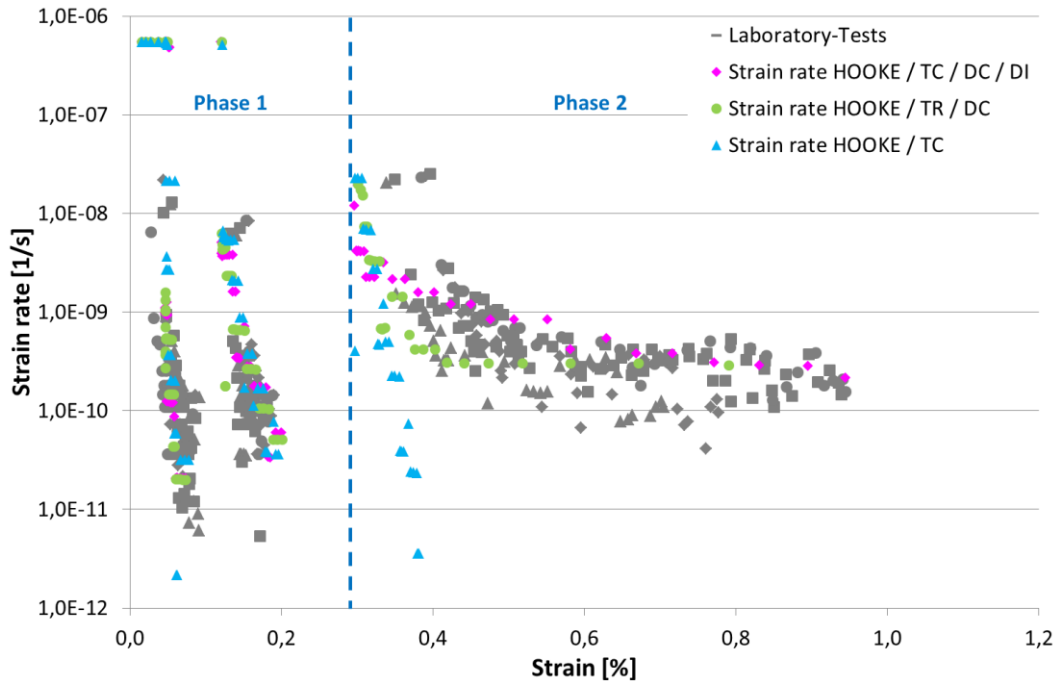


Fig. 4.37 Exercise UCc 5 - Comparison between strain rates versus axial strain of laboratory tests and calculation results

If DC was used additionally to HOOKE and VP (with parameters for phase 1), the development of strain rates is similar as before in phase 1 in Fig. 4.35 and Fig. 4.36. The different steps of iteration can explain the small differences between the calculated strain rates. The deviation of strain rates in the first stress level from calculation before was extinct, which supports the assumption, that the process of iteration can explain the aberrations. Hence, stationary creep has less influence to phase 1. In phase 2 strain rates show a different development versus the calculation without DC. Fig. 4.35 and Fig. 4.36 shows that strain rates are higher than before. They adapted much better to the laboratory results. Only in the beginning they decrease to fast, probably.

Finally strain rates by using DC, HOOKE and VP with combined parameters for phase 1 and phase 2 were considered. Strain rates are in a good range for second and third stress level in both figures. Strain rates decrease more slowly in phase 2 because of the shear thickening material behavior. In the first stress level strains are a little bit too small in the second part (Fig. 4.36) as expected from consideration of Fig. 4.35. The depiction of strain rates versus strains shows, that strains develop rarely at a stress level of 5 MPa and become higher in the second stress level. A clear development of strains is shown in third stress level. This development corresponds to the laboratory results. So the consideration of the development of strain rates supports, that the time dependent deformation behavior of salt concrete is well simulated by using HOOKE, DC and VP with individual parameters for phase 1 and phase 2.

5 Preliminary conclusions and outlook

This report presents the status of the work performed during the first 24 months by GRS as part of the European project DOPAS to improve the way how geotechnical sealings are represented in integrated performance assessment models for radioactive waste repositories in salt.

The deformation behaviour of salt concrete was investigated by laboratory testing and numerical modelling. In the laboratory, two types of tests were carried out: Triaxial compression tests and uniaxial creep tests. The tests were simulated using CODE_BRIGHT and the calculation results were compared to the laboratory results. The simulation of the triaxial tests aimed at the investigation of the material changes between the second and third stress level in the uniaxial tests. The results were useful, because the onset of dilatancy could be pinpointed. In all the simulations, the onset of dilatancy occurred before the load limit was reached. The perceptions from the uniaxial tests in combination with the results from the triaxial tests showed that the material behaviour of salt concrete at an axial stress up to 10 MPa is different to the material behaviour at 20 MPa. Strains and strain rates clearly increase at higher stresses. The simulations showed that an adaptation to laboratory results was only possible if two different sets of parameters were used at the lower stress levels (phase 1) and the higher stress level (phase 2). The main problem of simulating the deformation behaviour of salt concrete is the description of the viscoplastic (transient creep) material behaviour. Elastic deformations and stationary creep can be adapted by the available material properties. For a better description of transient material behaviour a constitutive model should be adapted or developed. The constitutive model used here allowed only a mathematical adaptation. Salt concrete consists of the cement matrix and the grains of salt concrete. This structure and its changes could not really be considered yet. If the structure of salt concrete could be considered in detail, description of the deformation behaviour at different stress levels would become easier and clearer. Further investigations and developments in this direction are necessary.

The report at hand is an interim version. The report will be superseded by a final report to be issued in February 2016.

6 Acknowledgements

The authors gratefully acknowledge the funding of the European Commission under FP7 framework programme, contract no. FP7-323273 the DOPAS project, and the funding received by the Federal Ministry for Economics and Energy (BMWi), represented by the Project Management Agency Karlsruhe (PTKA-WTE), contract no. 02E11132.

Special thanks go to Kyra Jantschik, former master student of the Technical University of Braunschweig, for the great commitment and the necessary persistence in parameter variation for modelling practice.

7 References

- [BGR03] BGR
Thermomechanisches Verhalten von Salzgestein, Projekt Gorleben, Abschlussbericht, Bundesanstalt für Geowissenschaften und Rohstoffe (BGR), Deutschland 2003
- [Mül10] Müller-Hoeppe, N.
Untersuchungen der Kontaktzone am ASSE-Vordamm – Gesamtinterpretation, Deutsche Gesellschaft zum Bau und Betrieb von Endlagern (DBE), Deutschland 2010
- [Sto94] Stockmann, N., Beinlich, A., Droste, J., Flach, D., Gläß, F., Jockwer, N., Krogmann, P., Miehe, R., Möller, J., Schwägermann, F., Wallmüller, R., Walter, F., Yaramanci, U.
Dammbau im Salzgebirge, Abschlussbericht Projektphase II - Berichtszeitraum 01.07.1998 – 31.12.1992, Institut für Tiefenlagerung – Abteilung für Endlagertechnologie, GSF-Bericht 18/94, Forschungszentrum für Umwelt und Gesundheit (GSF), Deutschland 1994
- [UPC14] Technische Universität Barcelona (UPC)
CODE_BRIGHT User's Guide, Department d'Enginyeria del Terreny, Cartogràfica i Geofísica, Universitat Politècnica de Catalunya, Spanien 2014
- [Wie10] Wieczorek, K., Förster, B., Rothfuchs, T., Zhang, C.-L., Olivella, S., Kamlot, P., Günther, R.-M., Lerch, C.
THERESA Subproject MOLDAU, Coupled Thermal-Hydrological-Mechanical-Chemical Process in Repository Safety Assessment, Deutsche Gesellschaft zum Bau und Betrieb von Endlagern Technology (DBE Tec), Gesellschaft für Anlagen- und Reaktorsicherheit (GRS), Institut für Gebirgsmechanik (IfG), GRS-262, ISBN: 978-3-939355-37-3, Deutschland 2010